

Editor-in-Chief B.E.Paton

Editorial board:

Yu.S.Borisov	V.F.Khorunov
A.Ya.Ishchenko	I.V.Krivtsun
B.V.Khitrovskaya	L.M.Lobanov
V.I.Kyrian	A.A.Mazur
S.I.Kuchuk	Yatsenko
Yu.N.Lankin	I.K.Pokhodnya
V.N.Lipodaev	V.D.Poznyakov
V.I.Makhnenko	K.A.Yushchenko
O.K.Nazarenko	A.T.Zelnichenko
I.A.Ryabtsev	

International editorial council:

N.P.Alyoshin	(Russia)
U.Diltey	(Germany)
Guan Qiao	(China)
D. von Hofe	(Germany)
V.I.Lysak	(Russia)
N.I.Nikiforov	(Russia)
B.E.Paton	(Ukraine)
Ya.Pilarczyk	(Poland)
G.A.Turichin	(Russia)
Zhang Yanmin	(China)
A.S.Zubchenko	(Russia)

Promotion group:

V.N.Lipodaev, V.I.Lokteva
A.T.Zelnichenko (exec. director)

Translators:

A.A.Fomin, O.S.Kurochko,
I.N.Kutianova, T.K.Vasilenko

Editor:

N.A.Dmitrieva

Electron galley:

D.I.Sereda, T.Yu.Snegiryova

Address:

E.O. Paton Electric Welding Institute,
International Association «Welding»,
11, Bozhenko str., 03680, Kyiv, Ukraine

Tel.: (38044) 200 82 77

Fax: (38044) 200 81 45

E-mail: journal@paton.kiev.ua

URL: www.rucont.ru

State Registration Certificate
KV 4790 of 09.01.2001

Subscriptions:

\$324, 12 issues per year,
postage and packaging included.
Back issues available.

All rights reserved.

This publication and each of the articles
contained herein are protected by copyright.
Permission to reproduce material contained in
this journal must be obtained in writing from
the Publisher.

Copies of individual articles may be obtained
from the Publisher.

CONTENTS

SCIENTIFIC AND TECHNICAL

- Yushchenko K.A., Romanova V.A., Balokhonov R.R., Savchenko V.S., Chervyakov N.O. and Zvyagintseva A.V.*
Experimental study and modelling of thermal-deformation processes occurring in welded joints on nickel superalloys 2
- Kasatkin O.G., Tsaryuk A.K., Skulsky V.Yu., Gavrik A.R., Moravetsky S.I., Nimko M.A., Strizhius G.N., Terovets N.V., Byvalkevich A.I., Nemlej N.V. and Kuran R.I.* Welding from one side of clad piping of nuclear power plants 10
- Kulik V.M., Demchenko E.L., Vasiliev D.V. and Elagin V.P.*
Chromium-manganese consumables for welding of higher-strength steels without preheating and heat treatment 15
- Dmitrik V.V. and Syrenko T.A.* To the mechanism of diffusion of chromium and molybdenum in the metal of welded joints of steam pipelines 20

INDUSTRIAL

- «Binzel Ukraine GmbH» — 15 Years of Development: Interview with Yu.A. Didus, Director General 25
- Kaleko D.M.* Modern methods of welding aluminium alloys to steels (Review) 27
- Lobanov L.M. and Volkov V.S.* Development of the technology of manufacturing double-wall welded transformable-shell structure 34
- Khorunov V.F., Stefaniv B.E., Sabadash O.M. and Voronov V.V.* Peculiarities of wear and criteria of reparability of drill bits with diamond-hard-alloy cutters 39
- Murashov A.P.* Thermal spraying of coatings using tips 44
- Protokovilov I.V. and Porokhonko V.B.* Control of formation of welded joints in ESW (Review) 49

NEWS

- 6 Years Anniversary of Russian-German Regional Laser Centres 55
- International Seminar «Materials Science in EU Projects» 59



EXPERIMENTAL STUDY AND MODELLING OF THERMAL-DEFORMATION PROCESSES OCCURRING IN WELDED JOINTS ON NICKEL SUPERALLOYS

K.A. YUSHCHENKO¹, V.A. ROMANOVA², R.R. BALOKHONOV², V.S. SAVCHENKO¹,
N.O. CHERVYAKOV¹ and A.V. ZVYAGINTSEVA¹

¹E.O. Paton Electric Welding Institute, NASU, Kiev, Ukraine

²Institute of Strength Physics and Materials Science, SB RAS, Tomsk, Russia

Results of experimental and numerical investigations of the processes of deformation and fracture of welded joints on nickel superalloys under conditions of mechanical and thermal loading are presented. Structural transformations were investigated, and thermal-deformation processes in the heat-affected zone (HAZ) during the welding cycle process were evaluated. The mechanisms of initiation and propagation of hot cracks in the HAZ metal near the fusion line were determined, and local plastic strains under the thermal cycle condition were assessed. Evolution of the stress-strain state in the HAZ metal was analysed in terms of physical mesomechanics, and conclusions on the role of grain boundaries in the processes of initiation and propagation of cracks were made.

Keywords: arc welding, nickel superalloys, welded joints, thermal loading, inter-grain boundaries, hot cracks, numerical modelling

Nickel-base superalloys are characterised by high mechanical properties, but low weldability. They exhibit sensitivity to hot cracking under the welding cycle conditions. Experimental data [1–4] indicate that the thermal cycle of welding leads to substantial structural transformations of material in the HAZ adjoining the fusion line. Mostly hot cracks form in this zone.

To find out causes of hot cracking under the welding cycle conditions it is necessary to have a clear idea of the kinetics of the deformation processes and evolution of the stress-strain state in different zones of a welded joint. So far the information available on these phenomena is scanty, as experimental studies are extremely labour-intensive, and money- and time-consuming.

This article describes experimental and numerical studies of the processes of deformation and fracture of welded joints on nickel alloys under conditions of thermal loading. Structural transformations were investigated, thermal-deformation processes in the HAZ metal during the welding cycle were evaluated, the mechanisms of initiation and propagation of hot cracks under the thermal-force effect conditions were determined, and local plastic strains in the HAZ metal in welding of austenitic nickel alloys were assessed by using experimental methods.

Models of the materials under investigation were developed by allowing for the internal

structure, and the deformation processes under the thermal cycling conditions were modelled on the base of the obtained experimental data. Development of the model of a material provides for determination of the explicit temperature dependence of its physical-mechanical properties. At a level of the polycrystalline structure, the sources of the concentration of stresses, initiation of plastic shears and microcracks are grain boundaries.

At the mesoscale level the model described the grained structure in its explicit form, and structural transformations fixed in the HAZ metal during the welding cycle processes were allowed for through phenomenological dependences of mechanical properties upon the temperature. Evolution of the stress-strain state in different regions of HAZ under the heating-cooling thermal cycle conditions was investigated numerically.

Investigation of the deformation processes and peculiarities of structural transformations in the HAZ metal under the welding cycle conditions. Investigations were carried out on nickel alloy IN738LC. As shown experimentally, phase transformations of the $\gamma' + \gamma \rightarrow \gamma \rightarrow \gamma + \gamma'$ type occurs in the HAZ region wherein the propagation of cracks takes place. Precipitation of the fine γ' -phase occurs in the HAZ region adjoining the weld. Size of the γ' -phase particles in the base metal and HAZ is 0.4–0.9 and 0.05–0.15 μm , respectively (Figure 1).

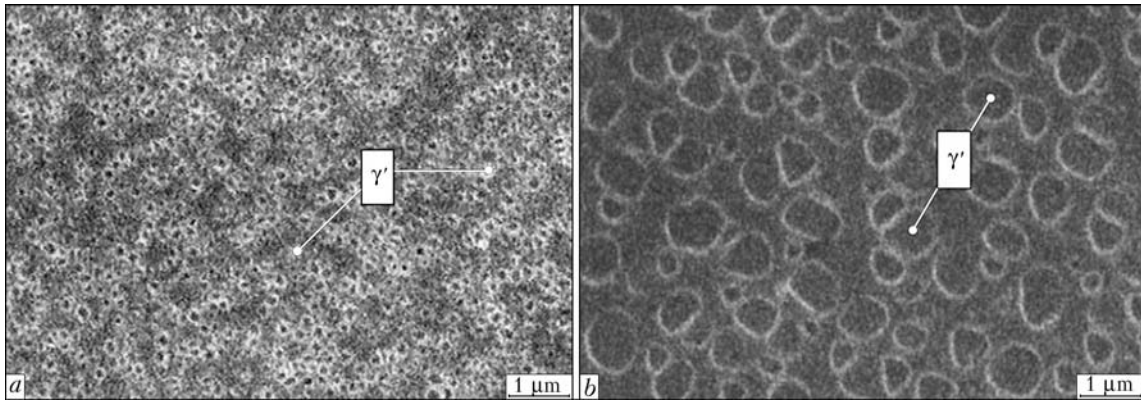


Figure 1. Microstructure with γ' -phase particles in different regions adjoining the weld: *a* – zone of formation of hot cracks; *b* – zone of base metal

Temperature of the beginning of dissolution of the γ' -phase particles ($T = 630\text{ }^\circ\text{C}$) and temperature of complete dissolution of the γ' -phase particles ($T = 1100\text{ }^\circ\text{C}$) were determined by using the contactless laser dilatometer. It was shown that size of the region where structural transformations take place corresponds to the $T_L - T_{Solv}$ temperature range. Statistical investigations of the presence of defects in welded joints showed that the most probable location of cracks is a zone adjoining the weld. In a general form, the scheme of predominant formation of cracks in the near-weld zone of welded joints on nickel alloys with γ' -strengthening, and its relationship to structural transformations in the HAZ metal, is shown in Figure 2.

Propagation of a formed hot crack along the grain boundaries from zone I (see Figure 2) towards the base metal is inhibited by relaxation of local stresses and plastic strains at the crack mouth (Figure 3, *a*). It can be seen from the

scheme shown in Figure 3, *b* that the state of plane deformation takes place in this case. The results obtained are confirmed by optical interference metallography of the surface of the hot crack mouth after welding. It can be seen in Figure 3, *c* showing the interference pattern, as well as in the region of artificial deformation due to a scratch on the section surface that the course of the interference lines in a region of the crack mouth and scratch tends to move upward. As the scratch is a recess in metal, the zone of metal ahead of the crack shifted downward with respect to the section plane, i.e. shrinkage of metal took place due to realisation of the plastic deformation mechanism.

Analysis of distribution of inter-granular deformation in the welded joint was carried out by

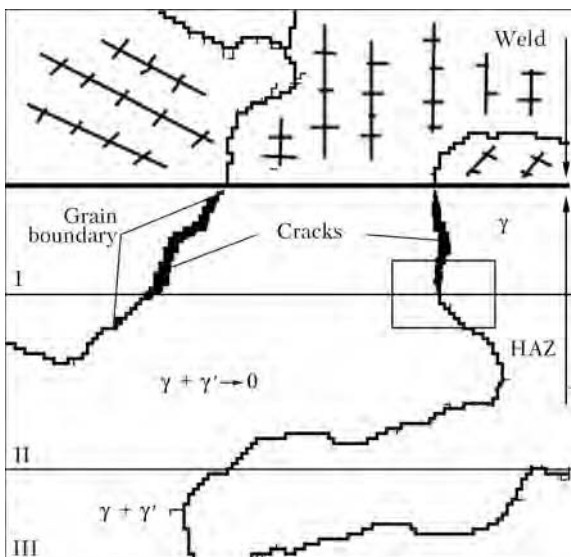


Figure 2. Scheme of predominant formation of cracks in HAZ metal of welded joints on superalloys containing the strengthening γ' -phase: I – zone of complete $\gamma + \gamma' \rightarrow \gamma \rightarrow \gamma + \gamma'$ transformation; II – zone of incomplete transformation; III – zone experiencing no transformations

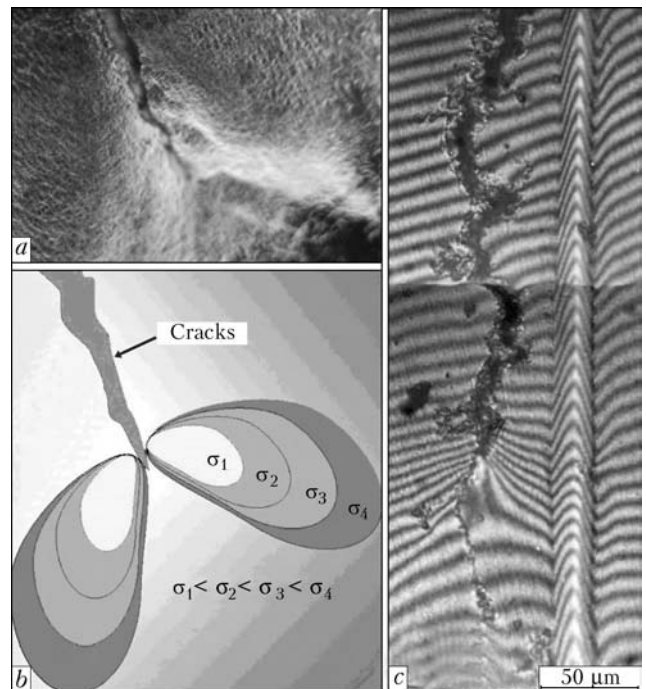


Figure 3. Arresting of hot crack in HAZ metal under the effect of plastic deformation [5]: *a* – surface of metal at the crack mouth ($\times 400$); *b* – scheme of distribution of plastic deformation in stress fields; *c* – plastic strains in the hot crack mouth

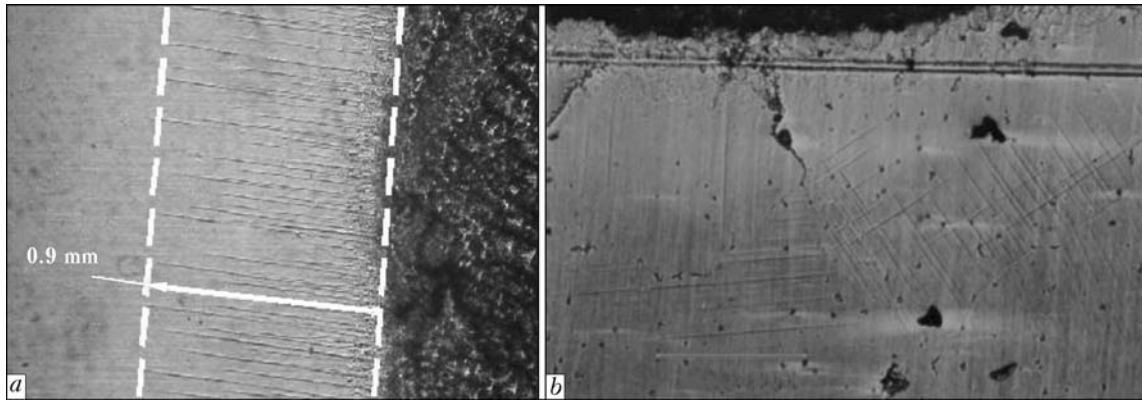


Figure 4. Localisation of plastic strain in HAZ metal near the fusion line (*a*) and development of slip bands inside grains during the welding process (*b* – $\times 125$)

investigation of the geometry of a polished surface of the base metal after welding, the character of fracture of oxide films, as well as the free surface of the electron beam weld metal. Inter-granular strains (displacements) in welding are concentrated near the fusion zone, attenuating with distance from it (Figure 4, *a*). The character of inter-granular strains in metal of the near-weld zone depends to a considerable degree upon its phase composition.

Investigations of deformation processes in the HAZ metal on the nickel alloy under the welding cycle conditions were carried out on preliminarily polished plates with a mesh deposited on it. The mesh was made with a diamond tool in the device based on toolmaker’s microscope BMI-1, providing thickness of a line equal to 0.01–0.02 mm.

Figure 4, *b* shows a fragment of the surface with slip bands formed in plastic deformation of metal in HAZ, which develops along the slip planes within a grain. The slip system changes in transition to the other grain. Plastic deformation causes orientation rotations in grains.

Numerical investigations of thermal-deformation processes occurring in the HAZ metal were

conducted to understand kinetics of initiation of hot cracks. Nickel alloy (9Cr–9Co–1Mo–10W–6Al–1Ti–2Nb–Ni – base) and stable-austenitic steel (20Cr–16Ni–6Mn–Fe – base) that is insensitive to hot cracking were chosen for comparative calculation analysis.

The thermomechanics problem in the two-dimensional statement was solved numerically by using the finite element method. Detailed formulation of the problem and method used to solve it are presented in [6]. In calculation of elasto-plastic strains and stresses, the experimental data, including elasticity modulus E , yield stress $\sigma_{0.2}$ and linear expansion coefficient α , were determined in a temperature range above 1200 °C. Yield stress $\sigma_{0.2}$ was evaluated by using the ALA-TOO machine IMASH 20-75 (of the «Gleeble» type) in vacuum. Linear expansion coefficient α was determined by the contactless method using the laser beam. Numerical modelling was performed for the case of TIG welding. Sizes of plates and welding heat input in modelling of the thermal-deformation processes were assumed to be the same. Calculation of temperature fields in welding was checked by direct measurements of the thermal cycles in the HAZ metal using thermocouples.

It was found that maximal plastic strains form near the fusion line at a distance of up to 2 mm from it. Dependences of thermal stresses on strains at a point located at a distance of 0.5 mm from the fusion line in welding of the nickel alloy and austenitic steel are shown in Figure 5. At a heating stage (from point 0 to point 2) the material experiences compressive stresses and strains. Point 1 determines the moment of reaching the yield stress value of the material. Point 2 corresponds to the maximal temperature in the thermal cycle and maximal compressive thermal strain. After point 2 there begins the cooling process and, hence, unloading, which continues

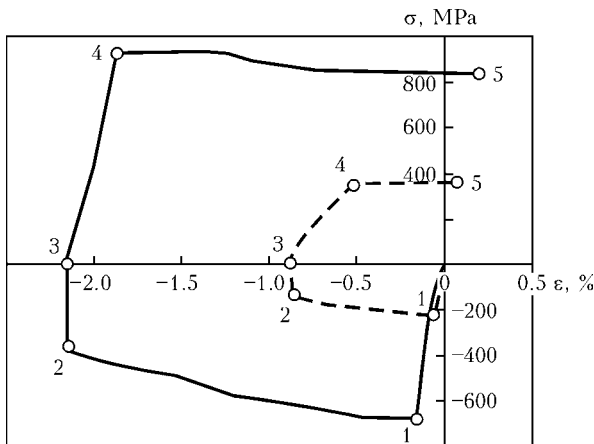


Figure 5. Changes in stresses and strains at a point located at 0.5 mm from the fusion line for nickel alloy (solid line) and for austenitic steel (dashed line): 1–5 – see the text



to point 3, where elastic strains and stresses are equal to zero. Elastic tensile strain grows from point 3 to point 4, and the second plastic strain, but having the opposite sign, starts at point 4. The state at point 5 corresponds to complete cooling of the plate. As shown by calculations, in welding of the nickel alloy at a heat input of more than 350 J/mm, considerable plastic strains (above 3 %) and tensile stresses amounting to yield stress of the material form in the HAZ metal at a distance of up to 2 mm from the fusion line.

Modelling of thermal-deformation processes in the HAZ metal under heating-cooling thermal cycle conditions allowing for the polycrystalline structure. *Mathematical statement of the problem.* In a general case, the stages of modelling include development of a structural-mechanical model of a material, setting of the initial and boundary conditions, and numerical solution of the system of continual mechanics equations allowing for internal interfaces. The general system of the dynamic continual mechanics equations in the Cartesian coordinates system, ignoring the mass forces, includes the following equations:

- equation of motion

$$\rho \dot{U}_i = \sigma_{ij, j}; \tag{1}$$

- equation of continuity

$$\frac{\dot{V}}{V} - U_i, i = 0; \tag{2}$$

- energy balance equation

$$\rho \dot{E} = \sigma_{ij} \dot{\epsilon}_{ij} + \dot{q}^{(e)}; \tag{3}$$

- relationships for components of tensor of total strain rates

$$\dot{\epsilon}_{ij} = \frac{1}{2}(U_{i, j} + U_{j, i}); \tag{4}$$

- defining relationships that specify connection between components of the stress and strain tensors

$$\sigma_{ij} = f(\epsilon_{ij}). \tag{5}$$

Here $U_i = \dot{x}_i$ are the components of the rate vector; x_i are the coordinates; $V = \rho_0/\rho$ is the specific relative volume of the material; ρ_0 and ρ are the initial and current densities, respectively; E is the internal energy; $\dot{q}^{(e)}$ is the vector of the inflow of heat from external sources; and ϵ_{ij} are the components of the total strain tensor. The spot under a symbol means the time derivative, and coma after an index – the correspond-

ing coordinate derivative, summation being made on repeating indices $i, j, k = 1-3$.

It is convenient to present the stress tensor in the form of a sum of the spherical and deviator parts:

$$\sigma_{ij} = -P\delta_{ij} + S_{ij}, \tag{6}$$

where P is the pressure; S_{ij} are the components of the stress deviator; and δ_{ij} are the Kronecker symbols.

The Duhamel–Neumann equation, which allows for thermal expansion, is used to describe the spherical part of the stress tensor:

$$P = -3K\epsilon_{kk} + \alpha_t(T - T_0), \tag{7}$$

where ϵ_{kk} is the volumetric strain; K is the volumetric compression modulus; α_t is the thermal expansion coefficient; and T_0, T are the initial and final temperatures.

Relationships that connect components of the stress and strain deviator tensors in the elastic loading region are written down in terms of rates in the following form:

$$\dot{S}_{ij} = 2\mu \left(\dot{\epsilon}_{ij} - \frac{1}{3} \delta_{ij} \dot{\epsilon}_{kk} \right), \tag{8}$$

where μ is the shear modulus.

Elasto-plastic transition was described by using the Mises yield criterion, according to which the material transforms into a plastic state providing that

$$S_{ij}S_{ij} > \frac{2}{3} \sigma_0^2. \tag{9}$$

In this case, the stress deviator components are reduced to the yield surface through multiplying S_{ij} by the $\frac{\sigma_0}{\sqrt{3} S_{ij}S_{ij}}$ value, where σ_0 is the yield stress of the material allowing for strain hardening.

The experimental data prove that the elasto-plastic characteristics of nickel-base superalloys demonstrate non-linear dependences on the temperature and size of the γ' -phase. The experimental data for alloy IN738LC [3, 4] were used as a base for determination of approximation dependences for the elasticity modulus and yield stress as functions of temperature, volume content and size of the γ' -phase particles (Figure 6, b).

The model sample with a periodic polycrystalline structure (Figure 6, a) was generated by the method of stepwise filling [7] on the $100 \times 150 \times 100$ mesh with a spacing of 2 μm . Periodicity suggests an infinite translation of structure in corresponding directions. For the subsequent solution of the mechanics problem the

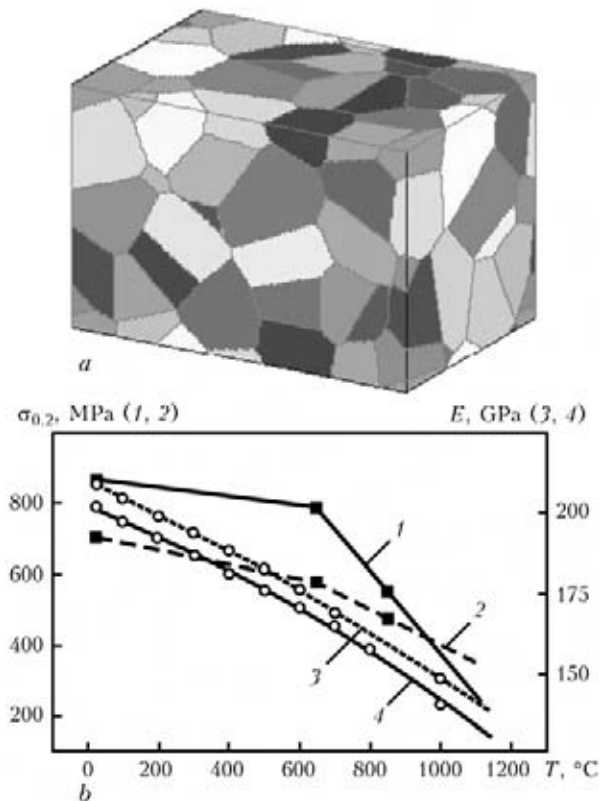


Figure 6. Model polycrystalline structure (a) and approximation calculation dependences of mechanical characteristics of alloy IN738LC on temperature and size of the γ' -phase (b): 1, 4 – 50–150 nm; 2, 3 – 400–900 nm; points – experiment [3]

periodic boundary conditions can be set on the corresponding surfaces, which are required for more realistic modelling of the restricted deformation conditions.

The effect of crystallographic orientation on the mechanical response of grains was taken into account through scattering of elastic moduli and yield characteristics with respect to the average values within 20 %.

At the same time, mechanical characteristics inside a grain remain constant, although they change in crossing the boundary between the grains.

The equation (1) through (9) system supplemented with the initial and boundary conditions was solved by the numerical finite difference method [8]. The boundary conditions on six surfaces of the calculation sample in the mechanics problem corresponded to the restricted deformation conditions in adiabatic heating. Normal components of the displacement vector on each surface were assumed to be equal to zero. Tangential displacements corresponded to the conditions of absence of the external forces.

Modelling results. According to the experimental data the volume content and size of the γ' -phase particles change during the heating–

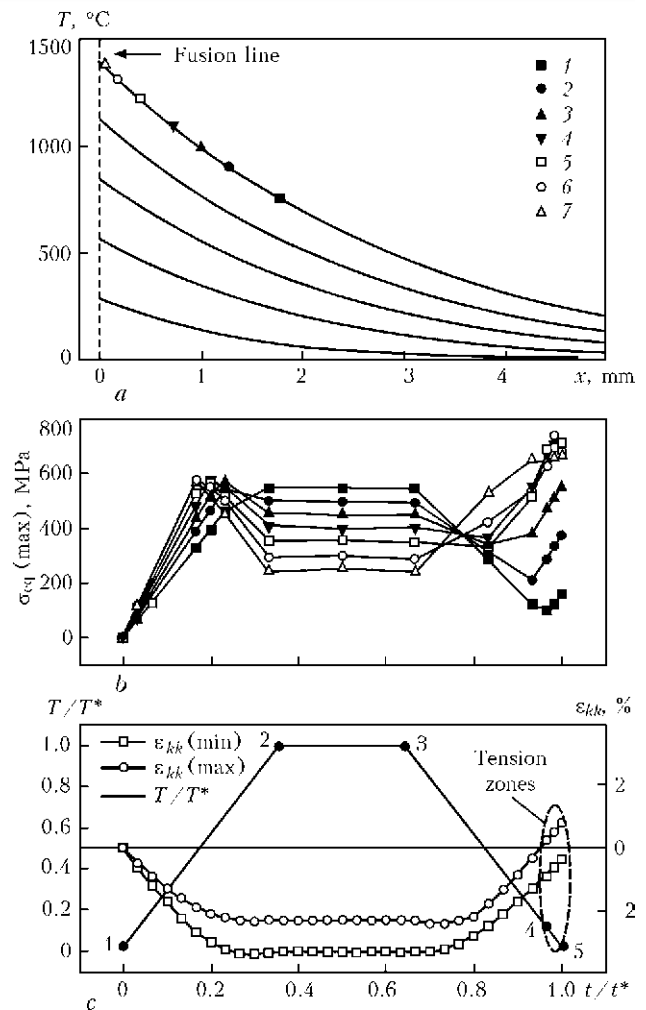


Figure 7. Calculated dependences derived for model polycrystalline grain under the heating–cooling thermal cycle conditions: a – distribution of temperature in HAZ metal during heating (1–7 – regions for which calculations of behaviour of polycrystalline structure were made); b – evolution of maximal stress intensity in polycrystalline structure of regions 1–7 at different distances from the fusion line; c – variation of temperature and growth of volumetric strain ϵ_{kk} (1–5 – see in the text)

cooling thermal process. In the base metal the size of the γ' -phase particles is 0.4–0.9 μm . Dissolution of the γ' -phase begins at a temperature of 630 °C, completely terminating at a temperature of 1100 °C. In cooling the reverse $\gamma \rightarrow \gamma + \gamma'$ transformation takes place. In this case the forming γ' -phase particles are approximately 50–150 nm in size, this causing a change in the mechanical response of the material (Figure 6, b). The obtained experimental data were introduced into the model of the mechanical response of grains under thermal loading performed by the heating–cooling scheme shown in Figure 7, c on dimensionless coordinates (here T^* and t^* are the maximal temperature of heating and time of the complete cycle, respectively).

Maximal heating temperature T^* was varied in numerical experiments to investigate the

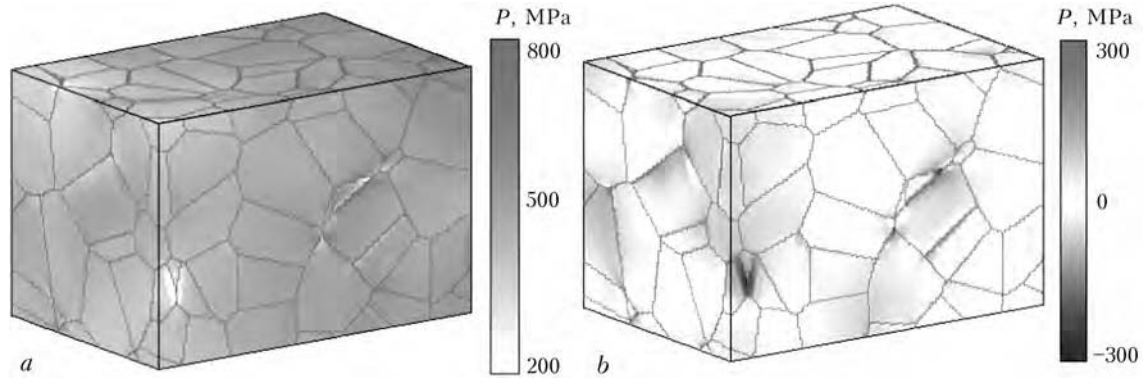


Figure 8. Pressure in HAZ metal at distance of 0.65 mm from the fusion line ($T^* = 1100\text{ }^\circ\text{C}$) at points 4 (a) and 5 (b) of the thermal cycle (see Figure 7, c)

stress-strain state occurring at different distances from the fusion line. Variations in temperature through depth of HAZ were determined from the solution of the one-dimensional equation of thermal conductivity

$$\frac{\partial T}{\partial t} = a \frac{\partial^2 T}{\partial x^2}, \quad T(0, t) = f(t), \quad T(L, t) = T_0, \quad (10)$$

where $a = 2.6\text{ mm}^2\cdot\text{s}^{-1}$ is the thermal diffusivity, and $f(t)$ is the linear function of temperature changing from $T_0 = 20\text{ }^\circ\text{C}$ to $T_{\text{melt}} = 1470\text{ }^\circ\text{C}$.

The calculations showed that width of the zone of the complete $\gamma' + \gamma \rightarrow \gamma$ transformation with subsequent precipitation of the fine γ' -phase corresponds to the experimentally determined width of HAZ in welding of the samples with the initial temperature of $20\text{ }^\circ\text{C}$. The maximal temperature gradient within $300\text{ }\mu\text{m}$ (size of the polycrystalline fragment under consideration) was fixed in HAZ near the fusion line, and it was not in excess of $100\text{ }^\circ\text{C}$.

Let us analyse the stress-strain state forming in the polycrystalline structure at a distance of 0.65 mm from the fusion line. Assuming that temperature in the weld zone amounts to melting point $T_{\text{melt}} = 1470\text{ }^\circ\text{C}$, at a distance of 0.45–0.65 mm from the fusion line the temperature gradient at boundaries of the polycrystalline mesovolume was about $90\text{ }^\circ\text{C}$ (see Figure 7, a).

Compressive stresses form in the polycrystalline material in the restricted deformation state (Figure 8, a) during adiabatic heating (regions 1–2, Figure 7, c). Grain boundaries act as sources of a clearly defined concentration of stresses from the very beginning of thermal loading (Figure 9, a). The maximal level of stresses is fixed near the triple junction of grains with the most different characteristics. It is here that initiation and propagation of plastic shears take place in subsequent loading (Figure 9, c, d). The first plastic shears are observed near the fusion line.

More and more distant (from the weld) regions of the HAZ metal are involved into plastic deformation during heating.

At a stage of cooling to room temperature (regions 3–5, Figure 7, c) the mean level of stresses falls. However, residual stresses at a distance of 0.65 mm from the fusion line amount to 700 MPa in the local regions of a polycrystalline grain near the grain boundaries that experienced plastic deformation (see Figure 7, b).

Modelling of fracture in the problems of mechanics of media with a structure involves certain difficulties, as such a statement imposes extremely high requirements to resolution of the calculation mesh. At the same time, some conclusions on initiation of hot cracks in the HAZ metal can be made on the basis of analysis of evolution of the stress-strain state within the frames of non-equilibrium thermodynamics and physical mesomechanics given in [9, 10]. These studies show experimentally and substantiate theoretically that pores and microcracks in a loaded material initiate in the volumetric tension zones. In this connection, consider now a growth of volumetric strain in the process of the heating-cooling thermal cycle. Figure 7, c shows the temperature dependences of growth of maximal and minimal volumetric strains ε_{kk} . Scatter of the relative mean level is caused by a heterogeneous stress-strain state occurring near the grain boundaries. At a stage of heating (regions 1–2, Figure 7, c), the volumetric compressive strain grows with growth of temperature, and the scatter related to localisation of strain near the grain boundaries also grows. At a stage of cooling (regions 3–5, Figure 7, c), the material tends to return back to the initial state, and volumetric compression decreases. However, the scatter of local strains with respect to the mean level persists, which is associated with development of plastic strain during the previous loading process.

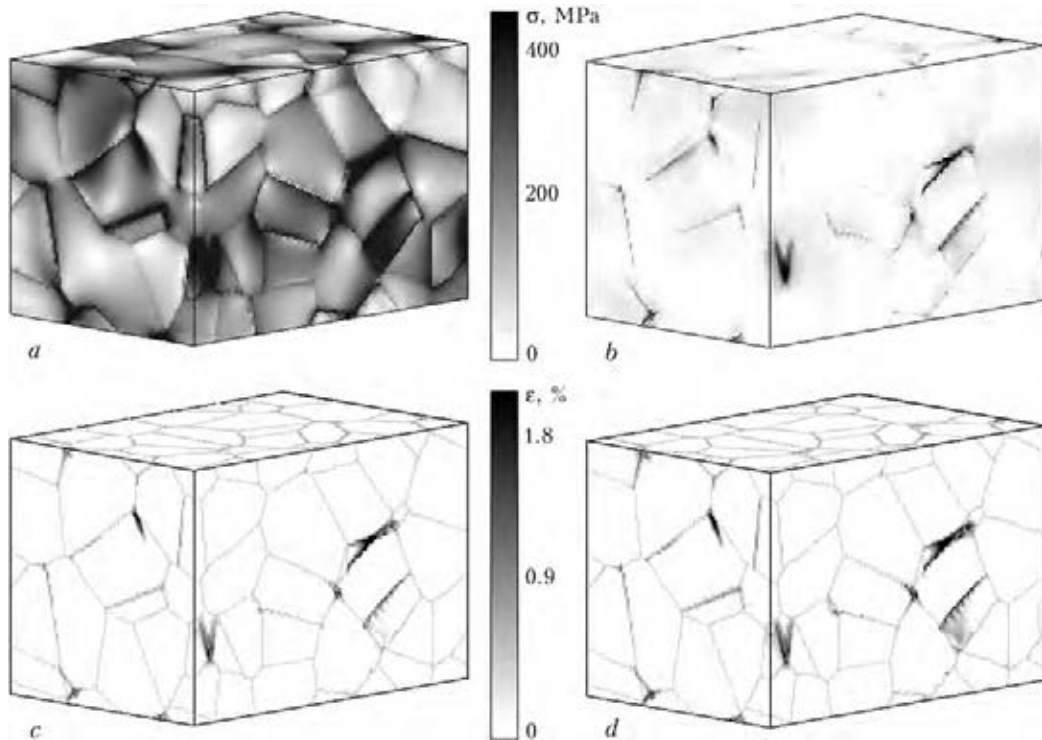


Figure 9. Intensity of stresses (*a, b*) and plastic strains (*c, d*) in HAZ metal at distance of 0.7 mm from the fusion line ($T = 1100\text{ }^{\circ}\text{C}$) at points 2 (*a, c*) and 5 (*b, d*) of the thermal cycle (see Figure 7, *c*)

Finally, at stages 4–5 (Figure 7, *b*), the local volumetric strain propagates into the positive region, which means formation of the local volumetric tension zones (Figure 8, *b*). These zones located near the boundaries of plastically deformed grains (compare Figures 8, *b* and 9, *d*) are potential sources of initiation of hot cracks, providing that the intensity of stresses here amounts to the tensile strength value. As shown by the calculations made for the polycrystalline grains located in different regions of the HAZ metal, such conditions take place within approximately 0.7 mm from the fusion line.

Evolution of the stress-strain state in the HAZ metal is an extremely complicated process, this being related both to the non-linear dependence of mechanical properties on the temperature, and to the structural transformations near the fusion line.

Analyse now variations in the intensity of stresses in the HAZ metal during the process of the heating–cooling thermal cycle. Curves of the maximal intensity of stresses in different regions of the HAZ metal are shown in Figure 7, *b*. Compare them with variations in temperature during the thermal cycle (see Figure 7, *c*). At the initial stage of heating a linear growth of stresses at a rate corresponding to that of growth of temperature in the corresponding regions of the HAZ metal was fixed in all the HAZ regions considered. A break of all the curves was observed with the beginning of development of plastic shears.

After this break, curves 1–6 in Figure 7, *b* demonstrate a drop of stresses, whereas stresses in a region that is most distant from the fusion line continue growing (curve 7). This character of evolution of the stress-strain state in different regions of the HAZ metal is determined by two competing processes, i.e. increase in stresses related to further heating, and fall of yield stress in a region of high temperatures. Upon reaching the maximal heating temperature, all the curves go to a stationary level corresponding to region 2–3 (see Figure 7, *c*) of the thermal cycle, after which cooling begins. At the beginning of cooling, the course of the curves is also determined by two competing processes. On the one hand, recovery of yield stress takes place with decrease in temperature, and the material starts showing increase in the compression deformation resistance. On the other hand, there occurs unloading related both to cooling and propagation of plastic shears. Therefore, increase or decrease of local stresses is fixed in different regions of the HAZ metal depending on the distance to the fusion line (compare curves 1–7, Figure 7, *b*). At the end of the cooling stage all the curves demonstrate a rise related to formation of tensile stresses.

The highest level of residual stresses was fixed near the boundaries of plastically deformed grains within 0.7 mm from the fusion line (curves 4–7, Figure 7, *b*). These regions are potential zones of development of hot cracks, which then



propagate along the grain boundaries towards the base metal.

CONCLUSIONS

Evolution of the stress-strain state in the HAZ metal of the nickel superalloy under the welding cycle conditions was investigated experimentally and numerically. Special consideration was given to evaluation of local stresses and strains at the mesolevel, where the grain boundaries play an important role. As shown by the experimental and numerical investigations, heterogeneous compressive stresses form at the mesolevel in a polycrystalline structure of the HAZ metal during heating. The sources of a high concentration of stresses are inter-grain boundaries, the maximal level of stresses being fixed at the triple junctions of grains near the fusion line. Plastic shears initiate in these regions. The local zones of volumetric compression, where hot cracks initiate and develop, appear at the cooling stage near the boundaries of plastically deformed grains. Microcracks that initiated at the fusion line propagate along the grain boundaries towards the base metal. The growth of cracks stops at such a distance from the fusion line where the level of local stresses is insufficient to provide their further propagation.

The models considered allow for by no means all the effects related to the most complicated processes occurring under the welding cycle conditions. Fracture in the HAZ metal occurs under conditions of high-temperature creep and under the effect of couple stresses. These processes can be modelled by the excitable cellular automaton method allowing for the forming couple stresses. In this case the flows of local structural transformations along the fusion line in the HAZ me-

tal, as well as along the grain boundaries within the complete $\gamma' + \gamma \rightarrow \gamma \rightarrow \gamma' + \gamma'$ transformation zone are the driving deformation mechanism. These problems will be considered in the future.

The study was performed under the collaborative project between the Russian Foundation for Fundamental Research and the National Academy of Sciences of Ukraine (No. 10-01-90403-Ukr).

1. Yushchenko, K.A., Savchenko, V.S., Zvyagintseva, A.V. (2004) Effect of heat treatment and degree of alloying on structural changes in nickel alloys. *The Paton Welding J.*, **7**, 12–14.
2. Zvyagintseva, A.V., Yushchenko, K.A., Savchenko, V.S. (2001) Effect of structural changes in high-temperature heating on ductile characteristics of nickel alloys. *Ibid.*, **4**, 13–17.
3. Ibekwe, S.R., Gabb, T. (2005) Impulse excitation study of elasticity of different precipitated microstructures in IN738LC at high temperatures. *J. Materials Eng. and Performance*, **14**, 188–193.
4. Balikci, E., Mirshams, R.A., Raman, A. (2000) Tensile strengthening in the nickel-base superalloy IN738LC. *Ibid.*, **9(3)**, 324–329.
5. Yushchenko, K.A., Savchenko, V.S., Chervyakov, N.O. et al. (2004) Character of formation of hot cracks in welding cast heat-resistant nickel alloys. *The Paton Welding J.*, **8**, 34–38.
6. Makhnenko, V.I. (1976) *Computational methods of study of kinetics of welding stresses and strains*. Kiev: Naukova Dumka.
7. Romanova, V.A., Balokhonov, R.R. (2009) Numerical study of deformation processes on the surface and in the bulk of three-dimensional polycrystalline grains. *Fiz. Mezomekhanika*, **12(2)**, 5–16.
8. Wilkins, M. (1999) *Computer simulation of dynamic phenomena*. Berlin: Springer.
9. Panin, V.E., Egorushkin, V.E. (2009) Physical mesomechanics and non-equilibrium thermodynamics as a methodological basis of nanomaterials science. *Fiz. Mezomekhanika*, **12(4)**, 7–26.
10. Panin, V.E., Egorushkin, V.E., Panin, A.V. (2010) Effect of plastic shear channeling and non-linear waves of localised plastic deformation and fracture. *Ibid.*, **13(5)**, 7–26.



WELDING FROM ONE SIDE OF CLAD PIPING OF NUCLEAR POWER PLANTS

O.G. KASATKIN¹, A.K. TSARYUK¹, V.Yu. SKULSKY¹, A.R. GAVRIK¹, S.I. MORAVETSKY¹
M.A. NIMKO¹, G.N. STRIZHIUS¹, N.V. TEROVETS¹, A.I. BYVALKEVICH²
N.V. NEMLEJ³ and R.I. KURAN⁴

¹E.O. Paton Electric Welding Institute, NASU, Kiev, Ukraine

²OC «Atomremontservis of NAEC «Energoatom», Slavutich, Ukraine

³OC «South-Ukrainian NPP of NAEC «Energoatom», Yuzhno-Ukrainsk, Ukraine

⁴YUTEM-Engineering, Bucha, Ukraine

Regularities of structure formation in bimetal material welded joints are generalized. Causes for deterioration of toughness, ductility and technological strength of weld metal are considered. Technological measures to ensure the required service properties and crack resistance of weld metal are specified. Initial data are determined to develop the basic process of welding from one side the NPP piping from clad sheets.

Keywords: arc welding, clad steels, welded joints, brittleness, cracks, carbon diffusion, brittle interlayers, welding technologies

Clad pipes in critical structures are used, in particular, in the main circulating pipeline of NPPs. The main metal of the pipe is higher-strength low-alloyed steel which is coated with corrosion-resistant austenitic steel inside.

At replacement of steam generators it is necessary to make a butt joint of the main circulating pipeline and steam generator nozzle. Abutted elements are made from 10GN2MFA steel. Pipe inner diameter is 850 mm at 70 mm thickness.

In keeping with the standard technology, the edges of the made joints of low-alloyed steel have V-shaped groove opening outside; 10 mm wide

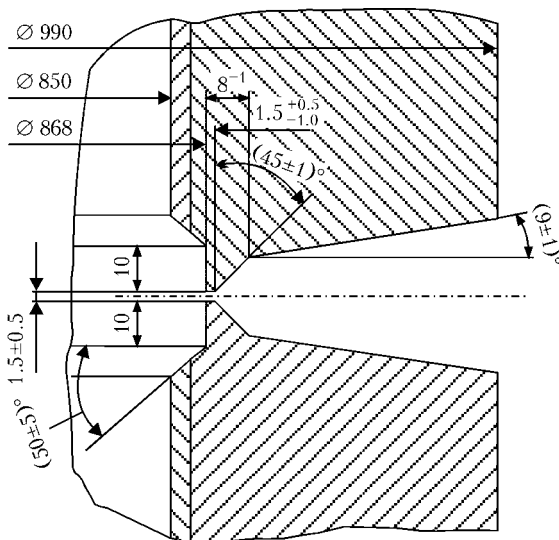


Figure 1. Schematic of edge preparation of pipe butt joint from clad steel welded by the standard technology

cladding layer has been removed on each edge (Figure 1). Cladding removal is associated with elimination of the possibility of cracking at austenite metal penetration into the low-alloyed pearlitic root weld. Such joints are made in two stages. First heat-resistant steel 10GN2MFA is welded across the entire thickness from the outside and NDT of the joint is performed as follows: 100 % X-ray structural (RI), 100 % ultrasonic (UT), 100 % liquid-penetrant inspection (LPI). Then deposition of a double anticorrosion layer is performed in the section of milling the pipe inner surface. After deposition, the deposited layer reinforcement is ground flush with the cladding surface and NDT (100 % visual-measurement, 100 % UT to detect cladding delamination, and 100 % LPI) are performed.

However, as a result of an increased radiation background in the zone of steam generator and piping, it became necessary to develop a welding technology, ensuring a lowering of welder exposure and eliminating their working inside the made pipe joint.

The objective of this work was development of the technology of welding from one side from the outside of clad pipelines of the primary coolant circuit of NPPs that allows lowering both the radiation load on personnel, and labour consumption of repair-welding operations.

Welded joints from bimetal steels are a complex system in terms of metallurgy that forms at joining of metal with different alloying and belonging to different structural classes. Proceeding from alloying and structure, distinction can be made between weld sections on the cladding



layer level, in the zone of transition from the cladding layer to the weld of the base low-alloyed layer and the base weld. Joint sections of both the base and cladding layers can be included into the category of similar steel joints. Transition sections, where layers with markedly different alloying levels, structure and properties are joined, belong to the category of joints of dissimilar metals (steels). Therefore, when making welded joints from two-layer steel, the regularities of formation of structure and properties should be taken into account, as well as possible problems, characteristic for welding similar low-alloyed or carbon steels, high-alloyed steels and dissimilar steel joints.

In welding of cladding layers from austenitic steels, a possible problem is formation of hot (primarily, solidification) cracks. A high technological strength is achieved by weld metal alloying with molybdenum and manganese at limitation of the concentration of easily liquating impurity elements (sulphur, phosphorus and silicon) in the deposited metal. A highly efficient measure for prevention of solidification crack development in austenitic welds is producing deposited metal with such Cr_{eq}/Ni_{eq} ratio, which ensures primary solidification with formation of δ -ferrite. A criterion for realization of the mechanism of primary solidification with δ -ferrite formation is controlling its residual fraction in the weld metal at room temperature. However, excessive growth of the fraction of ferrite at increase of ferritizer concentration relative to austenizers, may lead to a reverse effect — crack resistance lowering. In [1] it is shown that for Cr–Ni welds with 20–22 % Cr lowering of solidification crack resistance is observed at δ -ferrite content of more than 40–50 %. 2–8 % of δ -ferrite is optimum in terms of ensuring a high resistance to solidification cracking. To prevent formation of chromium carbides at sensitizing heating and development of intercrystalline corrosion in operation, the deposited metal is further alloyed by active carbide-formers. The above principles of deposited metal alloying are applied in practice when making a corrosion-resistant facing layer on the inner surface of clad pipes and nuclear reactor case. For this purpose, welding consumables of alloying systems of 25 % Cr–13 % Ni type are used to make the first layer of cladding over low-alloyed steel, and those with stabilization by niobium of 20 % Cr–10 % Ni–2 % Mn–Nb type are used for the second layer.

Transition sections between the high-alloyed and low-alloyed metal can be a special problem in clad steel welding. Depending on welding con-

sumable alloying and degree of its mixing in the weld metal with the melt of high-alloyed and low-alloyed metals (that depends on the welding mode), a martensite-containing structure can form [2, 3]. Such welds can demonstrate brittle fracture susceptibility. Possibility of solidification or cold cracking is not ruled out, either. In addition, at differences in the alloying system and structural class of the base and consumable materials brittle interlayers can form at the weld pool walls in the section of incomplete mixing [3, 4]. Such interlayers form, for instance, in welding of carbon or low-alloyed steel using high-alloyed welding consumables.

Diffusion redistribution of carbon also affects formation of structural inhomogeneity in the transition sections of joints from steels of various structural classes. This phenomenon is visible on the boundary between the low-alloyed or carbon base metal and weld with a higher content of alloying elements and active carbide-formers [3–5]. Carbon diffusion towards the more alloyed weld metal results in base metal forming a zone depleted in carbon and having a lower hardness, and the weld developing an interlayer with a high carbon concentration and high hardness (here carbon accumulation promotes an increase of hardness of martensite interlayer, forming as a result of inhomogeneous mixing of the deposited and base metal). Thus, it is experimentally established that in the transition section between steel 20–austenitic weld, hardness in the martensite interlayer in the zone with higher carbon concentration was HV 500–650, in steel 20 in the depletion zone adjacent to the weld it was HV 180–200, and at a distance from the weld it was HV 200–250. Carbon redistribution can occur in welding and at postweld heat treatment. It is supposed that this process also affects the stress-strain state of the metal [4]. Phase inhomogeneity in the fusion zone results, first, in the risk of brittle fracture development in the low-ductility metal, secondly, the zone of base metal with a variable carbon content can be subjected to a special kind of stress corrosion fracture in service [5]. As an illustration of nonuniform redistribution of carbon between pearlitic steel and high-alloyed steel, Figure 2 shows the microstructure of the transition section of bimetal between the cladding and load-carrying layers. In the Figure a region with carbon accumulation in the austenitic layer has a dark colouring. In the adjacent low-alloyed metal in the carbon depletion zone a coarse-grained purely ferritic structure, having a low hardness, formed.

Prevention of martensite formation in the structure of intermediate welds (similar to welding of austenitic and low-alloyed steels) is

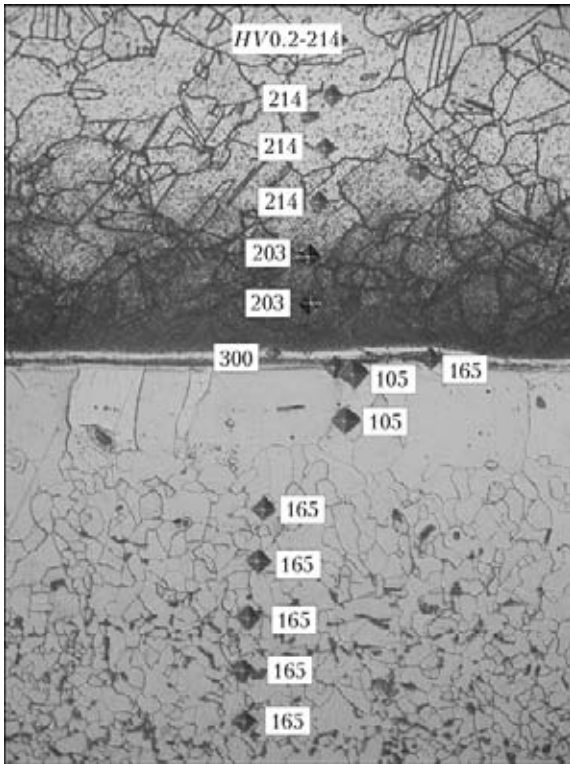


Figure 2. Microstructure ($\times 100$) of bimetal in the section of transition from boiler pearlitic steel (*below*) to austenitic cladding layer (*above*)

achieved through application of welding consumables with «higher austeniticity», providing the resultant, purely austenitic or austenitic-ferritic primary crystallization. Reducing the width of variable composition zone at the weld pool walls and martensitic interlayers in them requires ensuring an increased gradient of concentrations of austenizers in this zone. The latter is also achieved by application of welding consumables with increased nickel content. These measures, however, based on application of welding consumables of Cr–Ni or Cr–Ni–Mo systems do not eliminate diffusion displacement of carbon from low-alloyed metal into the high-alloyed weld. This problem can be solved by application of Ni-based welding consumables or facing the low-carbon steel edge by metal with low carbon content.

Welding of the base layer from low-carbon quenching steel of the bainitic class involves the need to prevent delayed fracture. This requires application of preliminary and concurrent pre-heating. To eliminate stresses and ensure the required mechanical properties of weld metal, welded joints are subjected to high-temperature tempering after welding.

Considered special features of making clad steel welded joints were taken into account in this work.

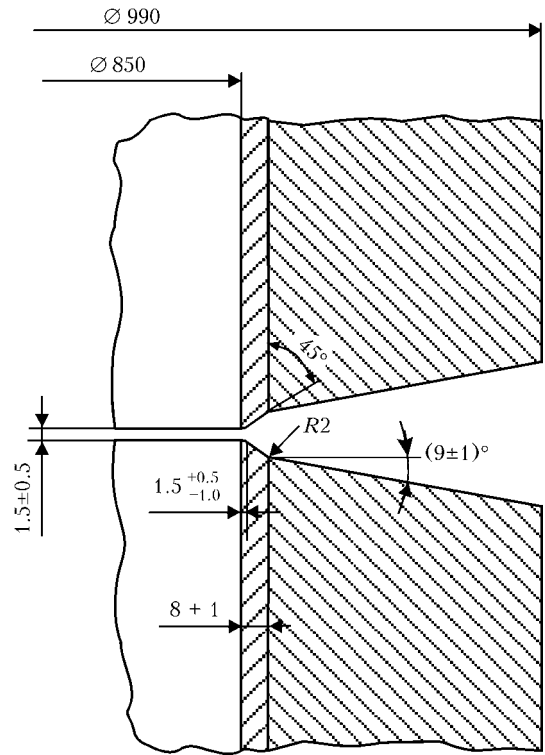


Figure 3. Schematic of edge preparation for welding from one side of pipe joint from clad low-alloyed steel

Selected configuration of the groove for welding from one side (Figure 3) ensures the possibility of sound performance of the root weld in the cladding layer zone. When making the joints both manual welding processes (coated electrode arc welding or nonconsumable electrode argon-arc welding), and automatic argon-arc welding can be applied using the currently available welding equipment.

For welding the root pass and filling the groove in the cladding layer filler wire of 04Kh20N9G2B type should be used, which is envisaged by the rules and norms in nuclear power engineering (PNAE G-7-01–89) for argon-arc welding of corrosion-resistant Cr–Ni steels. The above wire ensures the required corrosion resistance of the weld metal and its high hot cracking resistance due to formation of δ -ferrite. For coated electrode manual arc welding electrodes ensuring similar alloying of the deposited metal, namely TsT-15K, EA-898/21B should be applied.

Groove filling in the base layer can be performed using welding consumables envisaged in PNAE G-7-01–89 for welding 10GN2MFA steel: manual arc welding with coated electrodes PT-30, argon-arc welding with Sv-10GNMA filler wire. For argon-arc welding Sv-08G1NMA wire was also certified and allowed for application [6]. Under the repair conditions it is rational to use the automated welding process, eliminating



long-term staying of welders at the pipe joint. Therefore, automatic nonconsumable electrode argon-arc welding using Sv-08G1NMA wire was selected in this study. Checking the groove filling with the above wire, starting with austenitic metal of the cladding without making an intermediate weld with special alloying showed that metal with a martensitic structure with high hardness (approximately *HV* 450) forms in the first passes of such a weld. At the same time, hardness of weld metal of 08G1NMA type and 10GN2MFA steel after the thermal cycle of welding is on the level of *HV* 260–270 and *HV* 280–303, respectively.

To avoid the risk of embrittlement of sections of low-alloyed weld metal of 08G1NMA type deposited on the austenitic underlayer of 18-10 type, the technology of welding with a transition layer was optimized. Transition layers were made using Ni-based (Ni–20Cr, Ni–3Ti) welding wires, low-carbon wire of Armco-iron type and austenitic Cr–Ni–Mo wire Sv-10Kh16N25AM6, traditionally applied for welding dissimilar steels.

It should be noted that the advantage of Ni-based consumables is, first of all, prevention of brittle structure formation in the weld metal, also at the fusion zones, secondly, formation of lower stresses in the joint zone in connection with values of linear expansion coefficient close to those of steels with δ -lattice. In austenitic Cr–Ni steels this coefficient is approximately 1.5 times higher than that of ferritic ones. Application of Sv-10Kh16N25AM6 wire allows lowering the risk of martensite formation in welds, because of an increased content of nickel. It, however, does not prevent formation of diffusion carbon interlayers between the low-alloyed steel and intermediate weld, because of its high content of active carbidizers, namely chromium and molybdenum.

The Table gives the results of measurement of distribution of hardness values in the sections of cladding austenitic layer–intermediate layer–load-carrying weld. Tempering of test samples (650 °C, 2 h) was conducted at the temperature recommended for welded joints of 10GN2MFA steel. Results show that mixing of load-carrying weld metal with the intermediate layer of 10Kh16N25AM6 type leads to formation of a harder and, accordingly, more brittle intermediate structure. The used tempering temperature practically does not influence the hardness in the zone of transition to weld metal of 08G1NMA type. At the same time, a certain increase of hardness in the austenitic metal is in place, that is, probably, due to development of dispersion hard-

ness values *HV*50 in the zones of weld metal with different alloying of intermediate layers

Joint section, material	After welding	After tempering
Cladding – 18Cr–10Ni Intermediate weld – Ni–20Cr Weld – 08G1NMA	200 214 175–232	225 200–215 160–180
Cladding – 18Cr–10Ni Intermediate weld – Ni–3Ti Weld – 08G1NMA	185–200 152–161 286–293	223–250 150–200 300
Cladding – 18Cr–10Ni Intermediate weld – Armco-iron Weld – 08G1NMA	200 237–396 254–262	216 230–300 250–260
Cladding – 18Cr–10Ni Intermediate weld – 10Kh16N25AM6 Weld – 08G1NMA	190–200 210 330–450	206 175–206 300–400

ening at precipitation of carbide (in the case of Cr–Ni steel of 18-10 type), and intermetallic phases (in the region of Ni–3Ti alloy).

More uniform, proceeding from hardness values, are joint sections with an intermediate layer from nickel alloys, as well as with a layer of Armco-iron. In the layer of Armco-iron-base weld metal, hardness is somewhat higher; these values, however, are on the level of hardness characteristic for welds of 08G1NMA type.

Welding of technological samples showed that hot microcracks are found in the sections of transition from the nickel intermediate layer to the weld, made with low-alloyed wire 08G1NMA. They form in the metal, produced at mixing of the nickel layer with low-alloyed deposited metal and can partially propagate into the lower-lying high-nickel layer. Weld in these sections has a columnar structure characteristic for the cast metal. Sites of crack initiation and propagation are intercrystalline zones, which are characterized by accumulation of liquated impurity elements, as well as boundaries of austenitic grains containing chains of discrete phases, which coincide with intercrystalline regions (Figure 4).

Proceeding from the conducted experiments welding wire from Armco-iron was selected for performance of the intermediate layer.

Further filling of the groove in the base layer was performed by manual arc welding with PT-30 electrodes. Used preheating and concurrent heating was 170–200 °C. Welding was followed by high-temperature tempering at the temperature of 650 °C. Weld metal had a bainitic structure with isolated microregions of ferrite. The joint has no defects (Figure 5). Mechanical properties of base weld metal correspond to the level of properties characteristic for 10GN2MFA steel joints ($\sigma_t \approx 640$ MPa, $\sigma_{0.2} \approx 550$ MPa, $\delta \approx 17.6$ %,

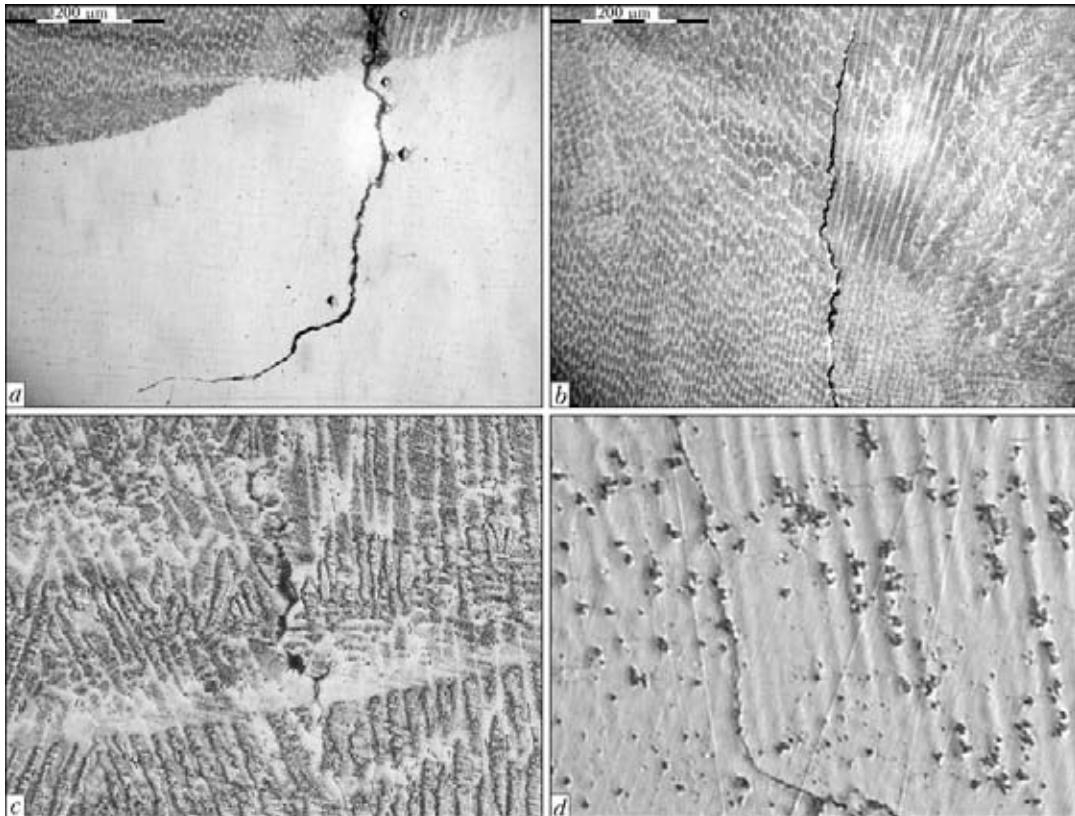


Figure 4. Microstructures ($\times 200$) in the section of transition from nickel intermediate layer to weld metal of 08G1NM type: *a, b* – cracks in the fusion zone of Ni-3Ti sublayer and load-carrying weld (*a* – in nickel metal, *b* – in the section of fusion of nickel layer and load-carrying weld metal); *c* – microcrack in the section of fusion of Ni-20Cr type layer with the load-carrying weld; *d* – secondary boundary, coinciding with intercrystalline zone, with precipitations of dispersed phases in the transition layer of Ni-20Cr type (potential path of crack formation)

$\psi \approx 69 \%$, $KCV \approx 160\text{--}200 \text{ J/cm}^2$). At application of automatic argon-arc welding with Sv-08G1NMA filler wire the following properties of weld metal are provided [6]: $\sigma_t \approx 690 \text{ MPa}$, $\sigma_{0.2} \approx 600 \text{ MPa}$, $\delta \approx 24.2 \%$, $\psi \approx 73 \%$, $KCV \approx 270 \text{ J/cm}^2$.

Welding from one side is also used in welding of joints of clad pipes of up to 500 mm diameter from heat-resistant steels. In this case welding up the entire section of the joint is conducted with austenitic welding electrodes, used for welding dissimilar steels (EA-395/9). However, such joints have an increased level of residual

welding stresses due to shrinkage of the austenitic weld, and also formation of brittle interlayers in the fusion zone and partial softening of the adjacent layers of base metal due to hydrogen diffusion into the weld are observed. As was noted, non-uniform structure and high stresses in the HAZ metal adversely affect performance of joints welded with austenitic consumables. It is rational to apply instead of such a technology, the above-described process of welding with a transition layer between the austenitic root weld and pearlitic filling weld. Welding (for instance, for pipes from 10GN2MFA steel) should be performed in

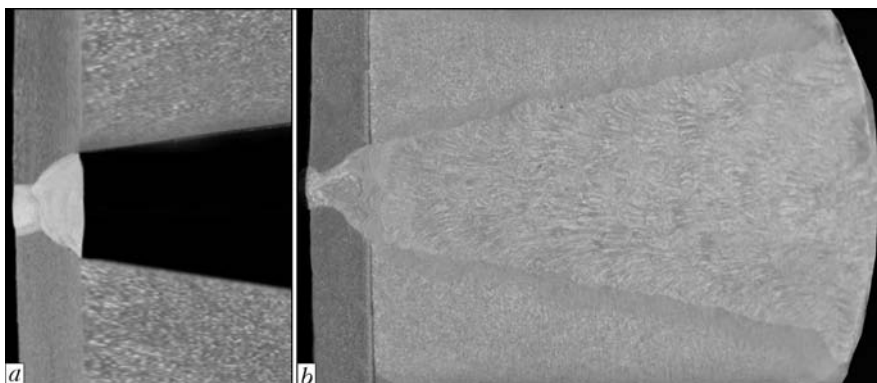


Figure 5. Weld macrostructure in the cladding layer (*a*) made in the welded joint of clad pipe steel by the developed technology (*b*)



the following sequence: welding up the root pass and groove root in the area of the cladding layer — by austenitic material of 04Kh20N9G2B type; making the transition weld from low-carbon ferrite metal (Armco-iron); filling the groove with electrode material, designed for welding the base weld (Sv-08G1NMA, Sv-10GNMA in argon-arc welding, PT-30 electrodes in manual arc welding) with compulsory preheating and concurrent heating; performance of local high-temperature tempering of the joint. Such an approach ensures a uniform structure and low level of residual (after tempering) stresses in the zone of welded joint of the base low-alloyed layer that should improve the service reliability of the joint as a whole.

Thus, the result of the performed work is confirmation of basic possibility of performance of welding from one side of pipe butt joints of clad 10GN2MFA steel. A feature of the proposed development is making the transition weld with low-carbon ferritic metal to eliminate formation of brittle interlayers. Application of the devel-

oped technology allows considerably lowering the labour cost, and improving the sanitary-hygienic working conditions of personnel. The proposed approach also allows replacing the traditional technology of welding the clad pipes using austenitic weld metal by making a ferritic weld that enables improvement of welded joint strength.

1. Kakhovsky, N.I. (1975) *Welding of high alloy steels*. Kiev: Tekhnika.
2. Fartushny, V.G., Evsyukov, Yu.G. (1977) Transition welds in welding of two-layer steels. *Avtomatich. Svarka*, **10**, 30–33.
3. Zemzin, V.N. (1966) *Welded joints of dissimilar steels*. Moscow; Leningrad: Mashinostroenie.
4. Gotalsky, Yu.N. (1981) *Welding of dissimilar steels*. Kiev: Tekhnika.
5. Kasatkin, O.G., Tsaryuk, A.K., Skulsky, V.Yu. et al. (2007) Method for improving local damage resistance of welded joints in NPP pipelines. *The Paton Welding J.*, **3**, 27–30.
6. Tsaryuk, A.K., Skulsky, V.Yu., Kasperovich, I.L. et al. (2006) Development and certification of automatic narrow-gap argon-arc welding technology of MPC Dn 850 elements at NPP. *Ibid.*, **5**, 19–25.

CHROMIUM-MANGANESE CONSUMABLES FOR WELDING OF HIGHER-STRENGTH STEELS WITHOUT PREHEATING AND HEAT TREATMENT

V.M. KULIK, E.L. DEMCHENKO, D.V. VASILIEV and V.P. ELAGIN
E.O. Paton Electric Welding Institute, NASU, Kiev, Ukraine

Data on new chromium-manganese electrodes of grades ANVM-2, ANVM-3 and flux-cored wire PP-ANVM-3, designed for welding and surfacing of higher strength steels, are given. The paper presents the results of the evaluation of the structure and mechanical properties of welded joint metal made with new welding consumables, as well as areas of their application.

Keywords: arc welding, chromium-manganese electrodes, flux-cored wire, alloyed carbon steel, austenitic weld metal, fusion zone, mechanical properties, area of application

Current mining, metallurgical and other branches of machine building provide for a manufacture of different parts and assemblies from alloyed steels 40Kh, 30KhGSA and others of high strength $\sigma_t = 600\text{--}800$ MPa and higher. The necessity of application of preheating and post-weld tempering is caused by the cold cracks that can be formed in welding of such hardenable steel. This complicates a technological process and can be impossible during manufacture of massive large dimension parts.

High-alloy nickel welding consumables Sv-08Kh20N25G8M6, Sv-08Kh20N9G7T and others providing formation of austenite weld metal structure are as a rule used for welding of the hardenable steels in order to avoid performance of labor-consuming thermal operations. Low strength of the austenitic weld metal provides a necessity of its performance with high reinforcement in order to increase strength of the welded joint. Labor-intensiveness of welding and consumption of expensive welding consumables dramatically increase due to this. At that rising of concentration of stresses in the places of transfer from thickened weld to base metal results in reduction of working capacity of the welded joint.

Application of Cr–Mn alloying system ($\sigma_t = 590\text{--}690$ and 980 MPa) at 0.2 and 0.4 wt.% C

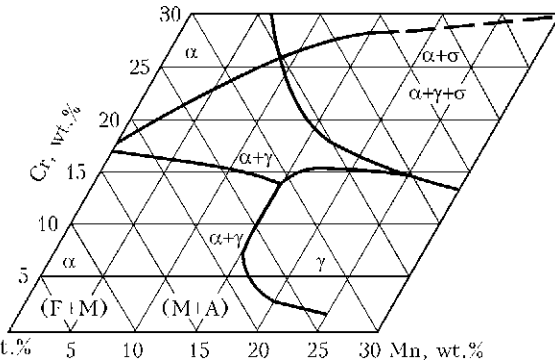


Figure 1. Constitutional diagram of steels of Fe–Cr–Mn system [1, 3]

[1] provides increased strength of the austenite steels and welds. For comparison [2] σ_t of Cr–Ni steels and welds makes 485–580 MPa. Increase of C + N up to 1.6 % promotes linear rise of the strength properties of Cr–Mn metal up to $\sigma_t = 1220$ and $\sigma_{0.2} = 800$ MPa [3–5].

Aim of the present work is a development of welding consumables providing the austenitic Cr–Mn weld metal with increased strength and working capacity of welded joints from hardenable steels being welded without preheating and heat treatment.

Austenite structure of low-carbon steel is formed at content of more than 3–7 wt.% Cr and not less than 15 wt.% Mn in it in accordance with the constitutional diagram of steels of Fe–

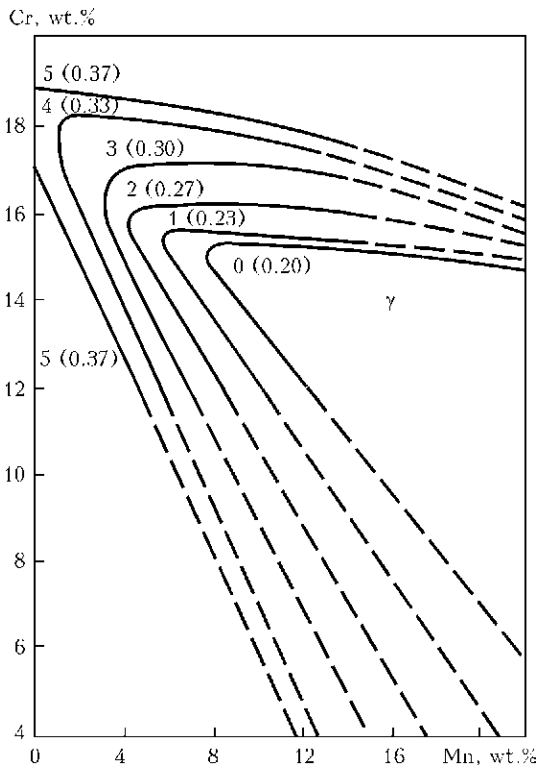


Figure 2. Extension of boundaries of γ -area of Cr–Mn steels containing 0.10–0.12 wt.% C and 0.08–0.15 wt.% N at their alloying by nickel (figures – content in weight percents) [2, 3] or in increase of total C + N content (figures in the brackets): dashed lines – data extrapolation

Cr–Mn system (Figure 1) [1, 3]. Minimum content of manganese necessary for obtaining of the austenitic metal with 0.10–0.12 wt.% C and 0.08–0.15 wt.% N can be reduced up to 8 wt.% rising the chromium content up to 15 wt.% (Figure 2) [2, 3]. Additional alloying by nickel up to 5 wt.% provides a reduction of manganese and chromium. Increase of the total content of carbon and nitrogen by $5/30 = 0.17$ wt.% corresponds to the mentioned above (as for equivalent influence on the structure). Rise of concentration of the latter from 0.20 up to 0.37 wt.% gives the possibility for reduction of the total content of chromium and manganese from 22.5–28.0 up to 16.5–17.0 wt.% (extrapolated in area of small values of chromium given in Figure 2). Crack formation (Table 1) was experimentally detected in the welds with 16.9 wt.% total content of chromium and manganese and less and 0.08–0.11 wt.% C due to occurrence of martensite constituent and increase of metal hardness.

Batches of Cr–Mn electrodes of 3–5 mm diameter with coefficient of coating weight 0.9–1.0 and flux-cored wire of 2.8 mm diameter with coefficient of filling 0.42 were manufactured considering mentioned above. The rods and strips Sv-08, Sv-08A, Sv-08kp (rimmed) of 0.4×12.0 mm cross section from low-carbon steel were used at that. Alloying of the weld metal (deposition) was provided by the components in composition of the electrodes and core of the flux-cored wire, i.e. metal chromium and manganese, nitrated manganese, ferrovanadium, electrode graphite (crystalline), as well as ferrotitanium, preventing manganese oxidation. Dolomite or marble, fluorite and feldspar, forming basic slag [$(CaO + MgO/SiO_2 > 5)$], carbon oxide and carbon dioxide during melting and dissociation, provide the gas-slag shielding of welding zone. Stable arcing at that is provided through introduction of alkali and alkali-earth elements in the arc atmosphere. Interaction of CaF_2 and SiO_2 with formation of gaseous SiF_4 is accompanied by bounding of hydrogen into insoluble in liquid metal HF that promotes the

Table 1. Effect of chemical composition (wt.%) on crack resistance of Cr–Mn weld metal

C	Cr	Mn	Si	Ti	Cr + Mn	Presence of cracks
0.10	8.9	18.4	0.22	0.07	27.3	Not
0.08	6.3	16.4	0.20	0.09	22.7	Same
0.08	8.8	12.4	0.21	0.17	21.2	»
0.08	6.8	10.1	0.22	0.18	16.9	Yes
0.11	3.5	4.8	0.21	0.16	8.3	Same

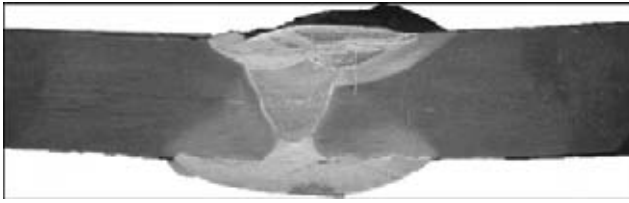


Figure 3. Macrostructure of 30KhGSA steel butt joint with austenitic Cr-Mn weld obtained using pilot consumables

rapid reduction of porosity [6] in combination with the increased solubility of hydrogen in austenitic weld metal. A rutile was introduced in the flux-cored wire instead of feldspar.

Application of clean charge materials with regard to sulfur (≤ 0.02 wt.%) and phosphorus (≤ 0.03 wt.%), small content of silicon with maintaining of $Si/C \ll 5$, replacement of nickel by manganese in combination with introduction of nitrogen in the metal, and high basicity of formed slag are the basis for preventing of formation of the hot cracks in austenitic welds [2]. Crack resistance of the austenitic welds possibly increases as a result of the additional refining and disorientation of metal structure through its alloying by vanadium and modification using present dispersed chromium and titanium oxides [2].

Manual and mechanized welding (surfacing) of 40Kh, 30KhGSA, 18G2AF, 15Kh5M, 20, 09G2S and 110Kh13L steels (in similar and dissimilar combinations) by Cr-Mn electrodes and self-shielded flux-cored wire in keeping of $I_w = 90-180$ and $250-350$ A and $U_a = 28-32$ V are characterized by stable arcing, moderate spattering of electrode metal, acceptable separability of slag crust and satisfactory formation of the welded joint without cracks and pores (Figure 3). However, increase of diameter of coating of the electrodes with 4 and 5 mm core up to 8.3–9.8 mm complicates their operation at small edge opening that can result in defect formation in the root part of the joint. Defect-free joints are obtained in performance of the root weld using the electrodes with 3 mm diameter core and 6.6–6.8 mm diameter coating.

Chemical composition of the weld metal (deposit) made using developed electrodes and flux-cored wire changes in the following limits, wt.%: 0.10–0.39 C; 7.5–10.2 Cr; 16.5–25.8 Mn; 0.42–0.56 Si; 0.05–0.12 Ti; ≤ 0.4 V; ≤ 0.2 N; 0.010–0.025 S and 0.02 and 0.03 P at $Cr + Mn = 26.5-35.9$. Weld metal has mainly austenite structure (Figure 4, a). Hardness HV 180–260 in the weld metal of 15Kh9G19AT type is commensurable with the hardness of austenitic Cr-Ni weld (HV 190–280) performed by LO-1 electrodes [7], and weld metal of 35Kh9G22FT type has HV 260–306, higher values of which correspond

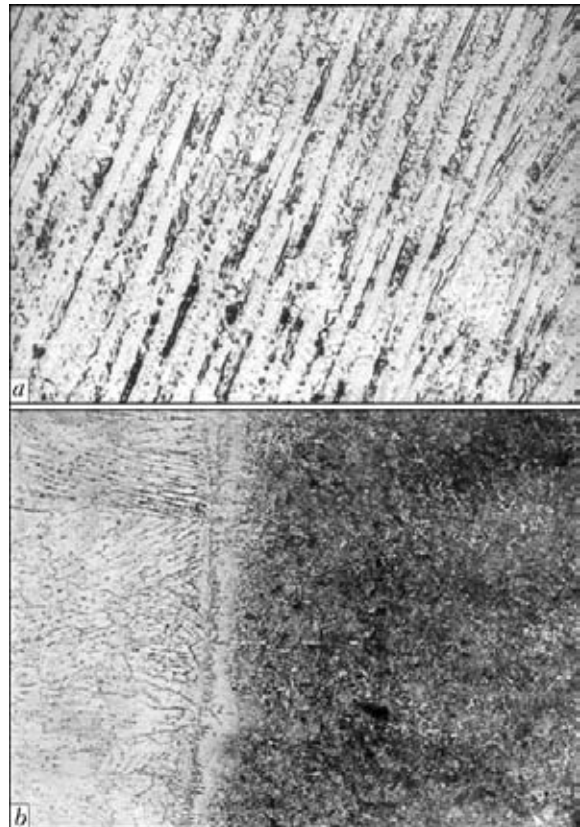


Figure 4. Microstructures ($\times 400$) of weld metal of 35Kh9G22FT type (a) and its fusion zone with alloyed steel 30KhGSA (b)

to its root part with increased portion of the base metal (Figure 5).

More intensive mixing of a weld pool and possibility of reduction of thickness of transition layer of the weld near the base metal are caused by decreased toughness and surface tension of manganous melt with respect to chromium-nickel one [8]. Martensitic Cr-Mn interlayer (Figure 4, b) formed in the transition layer is comparable with the Cr-Ni one on thickness and hardness. Thickness of the transition layer and martensitic interlayer as well as hardness of the latter reduce with the increase of total content of chromium and manganese and, thus, resource of austenite

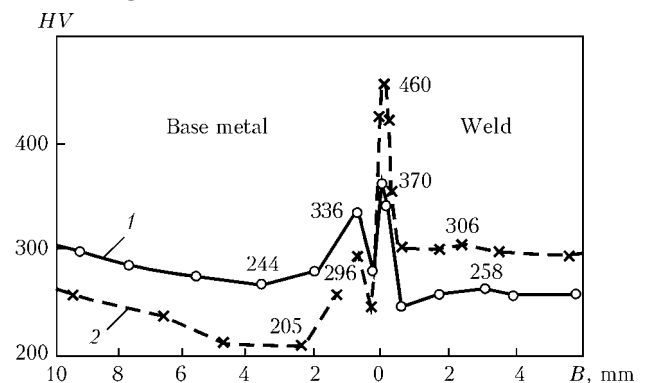


Figure 5. Distribution of hardness in cross section of the heat hardened steel 30KhGSA welded joint with weld metal of 35Kh9G22F type in the upper (1) and root (2) part



Table 2. Influence of type of weld metal alloying on transition layer parameters

Type of alloying	Thickness, μm		Hardness <i>HV</i>
	Transition layer	Martensitic interlayer	
10Kh9G19AT	10–22	4–10	288–415
10Kh9G14AT	14–26	6–15	440–600
08Kh20N9G7T	12–24	4–15	325–415
08Kh20N9T	18–29	6–18	415–512

level of the weld metal (Table 2). Nitrogen in the weld metal provides reduction of the specified parameters of the fusion zone, structural-and-mechanical inhomogeneities in it, tendency to hardening of transition zone metal, and promotes increase of portion of residual austenite with significant refinement of structural components of the martensitic interlayer [9, 10]. Additional increase of content of Cr + Mn and carbon in the weld metal without nitrogen introduction (type of alloying 35Kh9G19FT) does not promote significant change of hardness (*HV* 370) of the martensitic interlayer. Larger rise of its hardness up to *HV* 460 takes place in the root part of the joint with increased portion of base metal in the weld metal.

Smaller local rises of hardness of the hardenable steel welded joint are also observed in a short distance from the weld (0.6–0.8 mm) where the metal experienced the phase transformations in a process of welding (Figure 5). Hydrogen diffusion from the base metal in the weld pool levels such a rise and provokes a local decrease of hardness of HAZ metal in areas of 0.1–0.3 mm width close to the weld. Heating up to tempering temperature in welding provides softening of HAZ metal in several millimeters distance from the weld. Its larger softening takes place in the root part of multilayer joint subjected to repeated welding heating.

Investigations of stressed state of the welded joints of 30KhGSA steel and resistance of metal of fusion zone to cold crack formation were car-

Table 3. Influence of type of electrode metal alloying on stresses in welded joints

Type of alloying	Welding speed, m/h	Stresses, MPa, at temperature, $^{\circ}\text{C}$	
		450	20
35Kh9G22FT	8	65	160
	12	30	105
08Kh16N25M3	8	60	150
	12	35	100
08Kh20N9G7T	8	60	145
	12	40	110

Table 4. Effect of chromium and manganese in weld metal (0.15 wt.% C) on temporary and residual stresses in welded joints

Weight fraction of elements, %			Stresses, MPa, at temperature, $^{\circ}\text{C}$	
Cr	Mn	Cr + Mn	450	20
7.5	19.5	27.0	30	110
9.0	19.8	28.8	47	140
10.2	19.3	29.5	60	155
9.2	16.5	25.7	42	90
9.0	19.5	28.5	50	150
9.4	22.0	31.4	75	160

ried out on the procedure [11] developed at the E.O. Paton Electric Welding Institute. It was determined that the temporary (at 450 $^{\circ}\text{C}$) and residual stresses made 30–65 and 105–160 MPa, respectively, in welding by 35Kh9G22FT type flux-cored wire with formation of austenitic weld metal. They are virtually the same as in welding using austenite wires Sv-08Kh16N25M3 and Sv-08Kh20N9G7T (Table 3), and welding speed decrease promotes their increase. High values of the temporary (30–75 MPa) and residual (90–160 MPa) stresses are also found at 0.15 wt.% C and the total content of chromium and manganese 25.7–31.4 wt.% (Table 4). Increase of temperature interval of transformations of supercooled austenite in the metal of near-weld zone of hardenable steel is observed, tempering and reduction of tetragonal structure of formed martensite with rise of possibility of its crystals to microplastic deformation and relaxation of local microstresses take place, resistance to delayed fracture of the welded joints [12] significantly rises under the effect of increased temporary welding stresses in a presence of high-alloyed weld metal. No fracture of the samples after welding without preheating is found in delayed fracture testing after cooling up to 50–20 $^{\circ}\text{C}$.

Table 5 shows the mechanical properties of metal of the welds. Increase of strength with rise of carbon content is accompanied by reduction of ductility and toughness of Cr–Mn weld. Austenitic weld metal has hardness *HRC* 21–22 in as-welded condition and *HRC* 39–50 after cold plastic deformation.

Table 5. Mechanical properties of Cr–Mn weld metal

Type of metal	$\sigma_{0.2}$, MPa	σ_t , MPa	δ , %	ψ , %	<i>KCU</i> , J/cm ²
15Kh9G19AT	380–540	610–720	20–46	38–46	95–140
35Kh9G22FT	420–610	670–760	21–28	34–36	110–190



Fracture of the 30KhGSA steel welded joints in as-delivery condition and after heat strengthening (from $\sigma_{0.2} = 830$ and $\sigma_t = 935$ MPa) with $\sigma_t = 725$ –730 and 910 MPa, respectively, takes place along the base metal or area of softening. Fracture of special cylinder sample with cavity (stress concentrator) in the fusion zone takes place along the weld near the fusion zone at $\sigma_t = 795$ MPa. Obviously, that the martensitic interlayer in the fusion zone of Cr–Mn weld with alloyed steel provides no limitation of working capacity of the welded joint at static loading. Impact toughness of the samples with notch along the fusion zone of the welded joints of hardenable steel makes $KCU_{+20} = 63$ –124 and $KCU_{-40} = 17.5$ –23.6 J/cm². The fractures take place along the near-weld zone or more distant from the weld areas of HAZ metal without detection of influence of martensitic interlayer.

Specific emissions of solid constituent of the welding fumes containing, wt. %: 27 Fe, 21 Mn, 2.3 Cr, 2 silicon oxide, 5 fluoride 5, make 29 g/kg of consumed electrodes, as was determined in a course of hygiene and sanitary investigations. Cr–Mn electrodes are close to high-alloyed Cr–Ni–Mn electrodes on indices of emission of harmful substances. New consumables are permitted for application with a local exhaust ventilation. Application of individual facilities for defense of respiratory organs is possible, if necessary.

Developed electrodes ANVM-2 and ANVM-3 (deposited metal of 15Kh9G19AT and 35Kh9G22FT type) as well as self-shielded flux-cored wire PP-ANVM-3 were industrially tested at PJSC «Krivoy Rog Mining Equipment Plant» in welding without preheating and heat treatment of the butt joints of 20Kh2NM and 30KhGSA steels, welding-in of cast defects and welding of bucket teeth. It was also determined that the Cr–Mn electrodes can be used for welding of steel saturated with sulfur and other sur-

face and internal impurities. This allows performing quick welding repair without cleaning of difficult-to-access areas damaged during operation of parts. It is not reasonable to use the Cr–Ni electrodes for that due to bad formation of the welds and development of the hot cracks. The Research Center «Consumables for Welding and Surfacing» of the E.O. Paton Electric Welding Institute mastered manufacture of the Cr–Mn consumables. They are 2–3 times cheaper than the Cr–Ni welding consumables.

1. Khimushin, F.F. (1962) *Alloying, heat treatment and properties of heat-resistant steels and alloys*. Moscow: GNTIO.
2. Kakhovsky, N.I. (1975) *Welding of high-alloy steels*. Kiev: Naukova Dumka.
3. Pridantsev, M.V., Talov, N.P., Levin, F.L. (1969) *High-strength austenitic steels*. Moscow: Metallurgiya.
4. Pikerling, F.B. (1982) *Physical materials science and development of steel*. Moscow: Metallurgiya.
5. Sagaradze, V.V., Uvarov, A.I. (1989) *Strengthening of austenitic steels*. Moscow: Nauka.
6. Pidgaetsky, V.V. (1970) *Pores, inclusions and cracks in welds*. Kyiv: Tekhnika.
7. Snisar, V.V., Demchenko, E.L., Gajvoronsky, A.A. (1993) Influence of structure on properties of heat-affected zone of 30Kh2N2M steel welded joint. *Avtomatich. Svarka*, **9**, 43–45.
8. Ershov, G.S., Bychkov, Yu.G. (1983) *Properties of metallurgical melts and their interaction in steelmaking processes*. Moscow: Metallurgiya.
9. Elagin, V.P., Snisar, V.V., Savitsky, M.M. et al. (2001) Chemical and structural inhomogeneity in the zone of fusion of low-carbon steel with austenitic weld during shielded-gas welding. *The Paton Welding J.*, **4**, 7–12.
10. Snisar, V.V., Elagin, V.P., Grabin, V.F. et al. (1999) Effect of nitrogen and oxygen in shielding atmosphere on structure and properties of fusion zone of austenitic metal with low-alloy steel. *Avtomatich. Svarka*, **7**, 15–19, 48.
11. Sterenbogen, Yu.A., Vasiliev, D.V. (1998) New procedure and energy criteria in evaluation of resistance of welded joint metal fusion zone to cold cracking. *Ibid.*, **6**, 2–8.
12. Gordonny, V.G., Gajvoronsky, A.A., Sarzhevsky, V.A. (1992) Influence of weld metal type on structure, properties and resistance of high-strength hardenable steels to cold cracking. *Ibid.*, **11/12**, 13–18.



TO THE MECHANISM OF DIFFUSION OF CHROMIUM AND MOLYBDENUM IN THE METAL OF WELDED JOINTS OF STEAM PIPELINES

V.V. DMITRIK¹ and T.A. SYRENKO²

¹Kharkov Polytechnic Institute, Kharkov, Ukraine

²Kharkov Engineering College, Kharkov, Ukraine

The concepts of the mechanism of diffusion of chromium and molybdenum in the metal of welded joints of steam pipelines from heat-resistant pearlite steels in long-term operation were widened. It is shown that diffusion movement of atoms of chromium and molybdenum occurs by vacancy and dumbbell mechanisms.

Keywords: arc welding, heat-resistant pearlite steels, welded joints of steam pipelines, solid-phase reactions, activation energy, adhesion forces, diffusion movement

During long service the physical-chemical processes occur in the metal of welded joints of elements of steam pipelines of heat-resistant pearlite steels (12Kh1MF, 15Kh1M1F) under the conditions of creep ($T_{op} = 545-585$ °C, $P_{op} = 20-25$ MPa), accompanying with development of structure, chemical and mechanical heterogeneities. The latter lead to degradation of metal and damage of welded joints. The similar processes occur as well in base metal of steam pipelines [1-5], however their intensity and, respectively, damage of steam pipelines is considerably lower than that of welded joints, the service life of which amounts 0.6-0.8 of life of the base metal.

In the process of long service the initial bainite-ferrite structure of welded joints, meet-

ing the requirements of standard documents TU 14-3R-55-2001, is transformed to different-grain ferrite-carbide mixture without bainite component. The carbide reactions $M_3C \rightarrow M_7C_3 \rightarrow M_{23}C_6 \rightarrow M_6C$ and also coagulation of carbide phases occur which cause the formation of creep micropores at their interfaces with crystals of α -phase (Figure 1). The rate of presented solid-phase reactions is controlled by the level of segregation of atoms of chromium and molybdenum in the near-boundary zones of crystals of α -phase [6], which is limited by quantity of diffusion-moving atoms of chromium and molybdenum to the place of reactions running.

The purpose of this work is specification of mechanism of diffusion in metal of welded joints of steam pipelines, operated during long time under the creep conditions. The fundamentals of the theory of diffusion processes [7-12] as-applied to welded joints of heat-resistant steels with long-term operation (>250,000 h) under the creep conditions require further development.

The mechanism of diffusion movement of atoms of chromium and molybdenum at combined action of elastic and chemical forces in the crystals of α -phase under the creep conditions is connected with simultaneous formation and displacement of vacancies and interstitial atoms. In the crystal of α -phase the exchange of place between atom and vacancy, located in the initial neighboring sites, occurs at transmitting the proper activation energy to the atom, required for loosening the crystal lattice for displacement of atom (ion) from nodal position to the site or occupation of the vacant place. The activation energy can be determined considering the potentials of interaction between the atoms.

During determination of minimum activation energy of displacement of vacancies the charac-

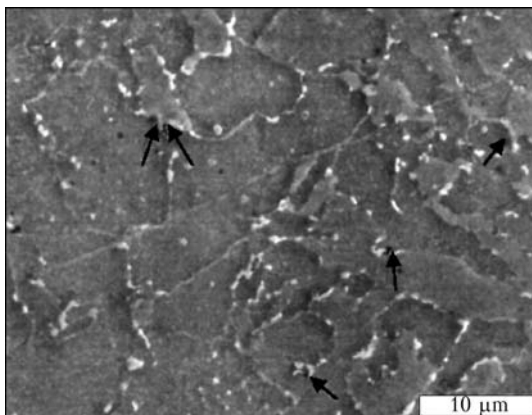


Figure 1. Microstructure of area of partial recrystallization of HAZ metal of welded joints of live steam — steel 12Kh1MF, service life — 170,000 h; pores are marked with arrows)



teristics of field of alternated elastic stresses and relaxation of structure, adjacent directly to the vacancy, were taken into consideration. It was established that activation energy is close to 0.4–0.5 of the energy of crystal lattice of α -phase related to one atom. The least is the activation energy for the area of incomplete recrystallization of HAZ of welded joints characterized by the presence of significant structural and chemical heterogeneity, the level of which is higher than that of analogue levels of activation energy of other regions of HAZ metal and also the weld metal and base metal. The most intensive energy is required for base metal not subjected to welding heating.

Let us represent the frequency of displacement of vacancies using migration as-applied to the crystal of α -phase in the form of known expression

$$v_v = Cv \exp(-E_A/RT), \quad (1)$$

where E_A is the activation energy of migration, J/(g·atom); v is the pre-exponential multiplier, close to 10^{13} s^{-1} ; C is the eight-coordination number; $R = 8.3 \text{ J/(g·atom)}$ is the gas constant; T is the temperature, °C.

The directed displacement of vacancies to the place of atoms of the first coordination sphere was taken as the effect of stressed state of the system.

The coefficient of self-diffusion of vacancies under the creep conditions can be determined by separation in crystal of two parallel planes of 1 mm^2 area, located at the distance close to the parameter of crystal lattice of α -phase ($a = 0.25 \text{ nm}$). It was assumed that concentration of vacancies at one plate K_1 is larger than K_2 concentration of vacancies in another one. Then, the directed flow of vacancies from their higher concentration to lower one can be represented in the form of specified expression [7]

$$J = -\frac{1}{6} v' b^2 \frac{dK_V}{dx}, \quad (2)$$

where v' is the frequency of migration of vacancies; b is the parameter of crystal lattice; K_V is the surface concentration of vacancies; symbol « \rightarrow » is the direction of displacement of vacancies to the side of their lower concentration.

Considering the coefficients, close by their values, of diffusion movement (migration) of vacancies and atoms [11], and also their similar activation mechanism in the crystals of α -phase, depending on the temperature, the activation energy of displacement of vacancies for the given creep conditions can correspond to activation energy of movement of atoms of chromium, i.e.

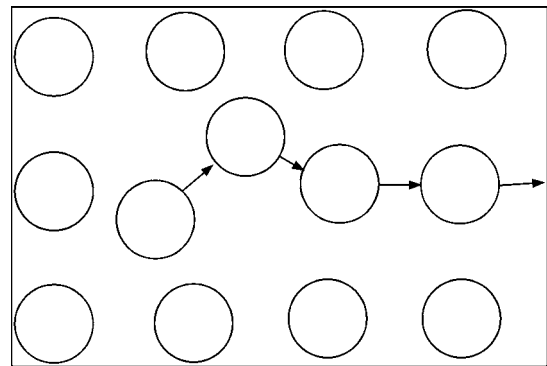


Figure 2. Scheme of dumbbell mechanism of movement of atoms in the crystal of α -phase

2.5–2.9 eV, which is close to the data of work [12].

During testing period of welded joints under the creep conditions above 250,000 h and the presence of partial degradation of their metal the intensity of movement of atoms of chromium and molybdenum will be provided due to a larger extent to the dumbbell mechanism, and to a lower extent – to vacancy mechanism. This movement is promoted by the slipping of dislocations under the conditions of gradient of chemical potential [13]. The movement occurs by the formation of configurations of the type of moving dumbbells by interstitial atoms with each of neighboring atoms (Figure 2). The dumbbell mechanism of movement is realized in the presence in α -phase crystals of creep pores of $0.5\text{--}1.7 \mu\text{m}$ size (Figure 3), and also polygonal structure of crystals (Figure 4).

We find the coefficient of diffusion D depending on the temperature from Arrhenius equation

$$D = D_0 \exp(E_D/RT), \quad (3)$$

where D_0 is the pre-exponential multiplier characterized according to Frenkel by the distance between atoms in the lattice of α -phase and also by period of oscillation or frequency of atom oscillations; E_D is the dependence of coefficient of diffusion on temperature determined as a sum of

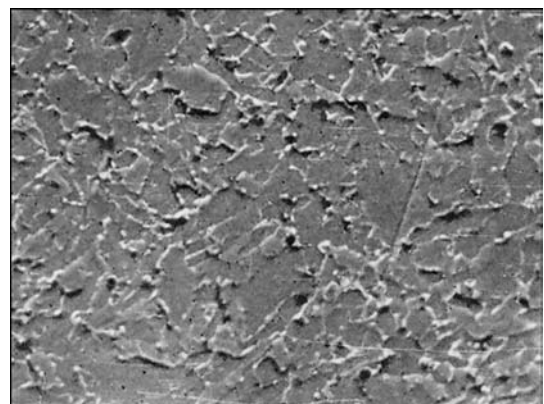


Figure 3. Microstructure ($\times 2500$) of weld metal with creep pores (alloy 08KhMF, service life – 190,000 h)

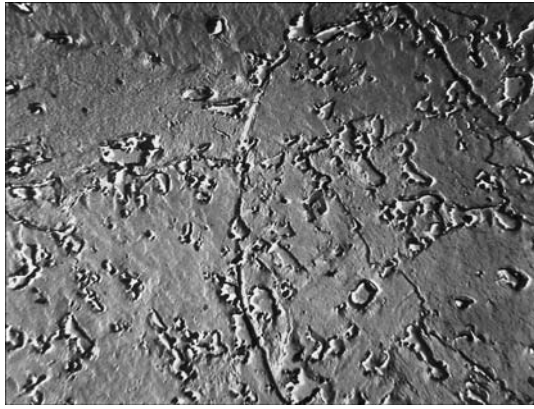


Figure 4. Polygonal structure ($\times 6000$) of crystal of α -phase of the area of partial recrystallization of HAZ metal of welded joint of steel 15Kh1M1F (service life – 186,000 h)

enthalpies of formation of vacancies E_{f1} and activation energy of jump of atom E_{v1} , i.e. $E_{f1} + E_{v1}$ (vacation mechanism) and as a sum of enthalpies of formation of vacancies and movement of atom (dumbbell mechanism) $E_{f2} + E_{v2}$. The values D_0 for chromium in the structure of welded joints of steel 15Kh1M1F amount to $(14.2-17.1) \cdot 10^{-3} \text{ cm}^2/\text{s}$, which corresponds to the length of ordinate, cut off by Arrhenius straight line at $1/T = 0$ (or $\ln D_0$).

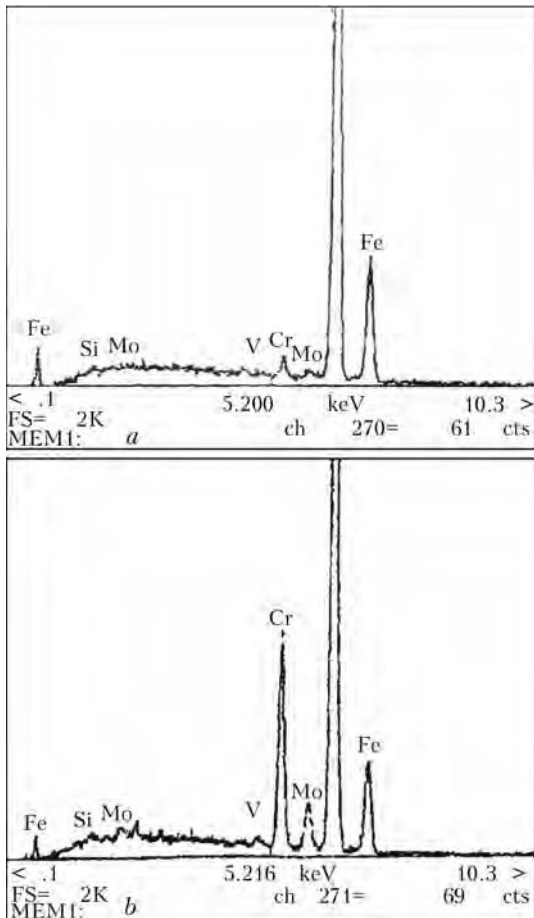


Figure 5. Spectrum of α -phase crystal of 08KhMF alloy weld metal: *a* – initial; *b* – after 276,000 h service (welded joint of steel 15Kh1M1F)

Let us suppose that $E_D = (E_{f1} + E_{v1}) + (E_{f2} + E_{v2})$. For the metal of welded joints of steels 15Kh1M1F and 12Kh1MF in long-term operation under the creep conditions, $E_D = 220-270 \text{ kJ/mol}$, that greatly depends on their structural and chemical heterogeneity.

The diffusion movement of atoms is mostly provided by elastic forces and chemical potential $\mu = \mu_0 + kT \ln C_m$, where C_m is the concentration of diffusive atoms of chromium and molybdenum. Let us write the chemical force as a change of chemical potential and concentration (symbol « \rightarrow » shows that force is directed to the equalizing of chemical potential and concentration):

$$f_{ch} = \left(\frac{\partial \mu}{\partial x} \right) T = - \frac{kT}{C_m} \left(\frac{\partial C_m}{\partial x} \right) T. \quad (4)$$

Under the influence of chemical force f_{ch} the diffusive movement of flows of atoms of chromium and molybdenum occurs. Let us write $f_{ch} = f_{ch, Cr} + f_{ch, Mo}$ for the crystal of α -phase. In the metal of welded joints as a non-stationary system the processes of diffusion are expressed by the Fick second law:

$$\begin{cases} \frac{\partial Cr}{\partial t} = \frac{\partial}{\partial x} D \frac{\partial Cr}{\partial x}, \\ \frac{\partial Mo}{\partial t} = \frac{\partial}{\partial x} D \frac{\partial Mo}{\partial x}, \end{cases} \quad (5)$$

where x is the average displacement of diffusive atoms of chromium and molybdenum, determined experimentally.

We will find, respectively, the approximate value of coefficient of diffusion D for chromium and molybdenum through the square of average displacement:

$$D = x^2 / 2t. \quad (6)$$

The values of average drift velocities and also coefficients of diffusion of chromium and molybdenum in the metal of welded joints, long time operated under creep conditions, are significantly different. This is proved by the presence of segregations along the boundaries of grains of α -phase (Figures 5 and 6) which promotes the transition of chromium and molybdenum into carbides and formation of new carbides [6]. The average value of segregation of chromium is considerably higher than similar segregation of molybdenum (Figure 7). It is known that diffusion mobility of atoms of molybdenum is higher than diffusion mobility of atoms of chromium [14]. However, in the presence of atoms of chromium, vanadium, silicon and manganese and also possibility of molybdenum to form new carbides



(Mo₂C) the intensity of formation of its segregation along the boundaries of grains of α-phase is significantly decreased.

In α-phase crystals of area of incomplete recrystallization of HAZ metal of welded joints of steel 15Kh1M1F after their testing under the creep conditions during 270,000 h, the carbide phases contained about 64 % V, 82 % Mo, 49 % Cr. The amount of VC carbides increased approximately by 10–15 % as compared to initial ones. In the coagulating carbides (mainly) M₂₃C₆ (*a* = 1.05722 nm) the slow substitution of atoms of chromium by atoms of molybdenum occurs [1, 8].

Diffusion movement of atoms of molybdenum, chromium and iron with atomic radii 0.139, 0.127 and 0.126 nm, respectively [15] is different. This difference is provided by different level of activation energy, that is due to the force of bond between atoms in the lattice (lattice energy). In the presence of significant structural and chemical heterogeneity, there is a sense to determine separately the diffusion movement of atoms for each area of HAZ metal and also separately for weld and base metal.

It was established that activation energy of chromium, diffusion mobility of which is the most significant in the crystals of α-phase, is differed from the activation energy of other elements. The chemical coefficients of diffusion *D*_{Cr} and *D*_{Mo} considering the data of work [10] were determined through the coefficients of self-diffusion *D*^{*}_{Cr} and *D*^{*}_{Mo} which were found experimentally (Figure 6):

$$\begin{cases} D_{Cr} = D_{Cr}^* \left(1 + \frac{d \ln f_{Cr}}{d \ln \gamma_{Cr}} \right) = D_{Cr}^* \frac{d \ln a_{Cr}}{d \ln \gamma_{Cr}}, \\ D_{Mo} = D_{Mo}^* \left(1 + \frac{d \ln f_{Mo}}{d \ln \gamma_{Mo}} \right) = D_{Mo}^* \frac{d \ln a_{Mo}}{d \ln \gamma_{Mo}}, \end{cases} \quad (7)$$

where *a*_{Cr}, *a*_{Mo} is the activity of components of chromium and molybdenum; *f* = *a*/*γ* is the coefficient of activity; *γ* is the molar concentration of chromium and molybdenum; $1 + \frac{d \ln f}{d \ln \gamma}$ is the thermodynamic factor.

The parameters *a* and *f* were found basing on the data of segregation of chromium and molybdenum (see Figures 5 and 6) the level of which considerably changed with time.

It was assumed that temperature dependence of coefficients of self-diffusion of chromium and molybdenum can be described for given steels using the following equation [14]:

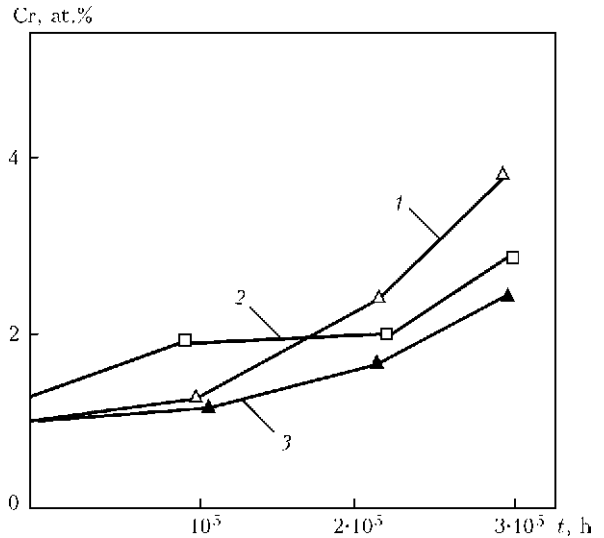


Figure 6. Dependence of local segregation of chromium in near-boundary zone of α-phase crystal on time *t* at the area of partial recrystallization (1), overheat of HAZ metal (2) of steel 15Kh1M1F welded joint of live steam pipeline, and in the area of weld metal (3)

$$D = 0.2 \exp \left(- \frac{33T_{\text{melt}}}{RT} \right) \text{ [cm}^2\text{/s]}.$$

Under the conditions of long operation the values of activation energy will differ, as well as values of pre-exponential multiplier, which can vary within the limits of 0.01–4 cm²/s, the coefficient in numerator will also change, respectively.

It was established that value of averaged coefficient of diffusion *D*_{Cr} in the metal of welded joints of steel 15Kh1M1F (testing period of 276,000 h) amounts approximately from (2.3–2.7)⁻¹² to (3.1–3.3)⁻¹⁴ cm²/s. The value of this coefficient depends greatly on conditions of operation of welded joints (starts/stops of energy units, overheats) and also their structure, chemi-

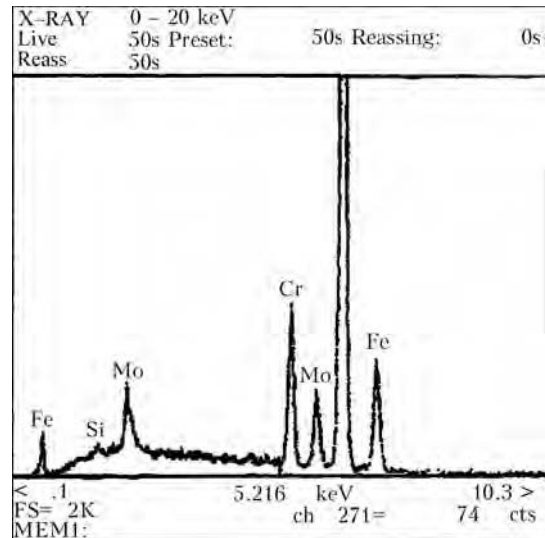


Figure 7. Spectrum of near-boundary zone of α-phase grain for area of partial recrystallization of steel 12Kh1M1F welded joint of steam pipeline (service life – 275 637 h)



cal composition and other factors. The intensity of formation of segregations of molybdenum amounts about 0.3–0.4 of intensity of segregation of chromium (Figure 7). In the metal of welded joints after their test time of about 270,000 h the tendency towards decrease of diffusion mobility of atoms of chromium and increase of diffusion mobility of atoms of molybdenum was observed, that requires additional study. The decrease in mobility of chromium and increase in molybdenum mobility is connected with appropriate changes of gradients of chemical potentials.

During determination of coefficients of diffusion the error was considered predetermined by difference in chemical composition of specimens of diffusion pair, gradient of concentration in the crystal of α -phase where coefficient of diffusion is determined; peculiarities of interface phases; heterogeneity of chemical composition of steel; structural heterogeneity and sizes of grains.

The values of chemical coefficients of diffusion for different structural areas of welded joints are considerably differed. Taking into account the coefficients it was found that the diffusion processes under the creep conditions are most intensive at the area of partial recrystallization of HAZ metal (see Figure 6), which is proved by the data of surface microprobe analysis (see Figure 7).

It should be noted that it is the diffusion movement of atoms of chromium and, at the least extent, of atoms of molybdenum that leads to the formation of near-boundary zones of segregation in the grains of α -phase (see Figures 5 and 6). The increase of concentration of mentioned elements was predetermined by the energy of bonding, average heat energy kT , frequencies of jumps of atoms of chromium and molybdenum, displacement of vacancies, which is, in its turn, determined by the difference of chemical potentials and caused by the presence of significant chemical and structural heterogeneity in the metal of welded joints.

The chemical heterogeneity as segregation, predetermined by diffusion of atoms of chromium and molybdenum, was revealed by electron-probe microanalysis of working surface of sections with application of scanning electron microscope JSM-820 with the Link AN 10185S system of X-ray microanalyzer.

The presence of local zones of segregation, occupying from several atomic layers to approximately 0.1 μm (at shifting of its coherency) along the boundaries of crystals of α -phase does not cause the noticeable changes of properties. The basic effect of segregation zones is the increase

in rate of carbide reactions $M_3C \rightarrow M_7C_3 \rightarrow M_{23}C_6$ and also coagulation of $M_{23}C_6$, which is determined by concentration in the zones of chromium and molybdenum, which leads to degradation and damage of metal of long-time operated elements of steam pipeline systems and mostly their welded joints [2–6, 13, 14, 16]. It is possible to decrease the intensity of considered diffusion processes by producing of welded joints with decreased initial structural and chemical heterogeneity, which will allow increasing the stability of structure of welded joints, decreasing their damageability and increasing the service life by approximately 15–20 % [2, 3].

CONCLUSIONS

1. During determination of parameters of diffusion processes the mechanism of diffusion of chromium and molybdenum in the metal of long-operated welded joints of steam pipelines of heat-resistant pearlite steels was specified.

2. It was established that diffusion movement of atoms of chromium and molybdenum in the metal of welded joints occurs by two integrated mechanisms: vacancy and dumbbell.

1. Khromchenko, F.A. (2002) *Life of welded joints of steam pipelines*. Moscow: Mashinostroenie.
2. Mirkin, L.I. (1968) *Physical principles of strength and plasticity*. Moscow: MGU.
3. Krutasova, E.I. (1981) *Reliability of metal of power equipment*. Moscow: Energoizdat.
4. Kumanin, V.I., Kovalyova, L.A., Alekseev, S.V. (1988) *Life of metal in creep conditions*. Moscow: Metallurgiya.
5. Berezina, T.G. (1986) Structural method for determination of residual life of steam pipeline parts in long-term operation. *Teploenergetika*, **3**, 53–56.
6. Dmitrik, V.V., Baumer, V.N. (2007) Carbide phases and damageability of welded joints in long-term operation. *Metallofizika. Nov. Tekhnologii*, **29(7)**, 937–948.
7. Butyagin, P.Yu. (2006) *Chemical physics of solid*. Moscow: MGU.
8. Tretiakov, Yu.D., Putlyayev, V.I. (2006) *Introduction to chemistry of solid-phase materials*. Moscow: Nauka.
9. Larikov, L.N., Gejchenko, V.V., Falchenko, V.M. (1975) *Diffusion processes in ordered alloys*. Kiev: Naukova Dumka.
10. Gertsriken, S.D., Degtyar, I.Ya. (1960) *Diffusion in metals and alloys in solid phase*. Moscow: Fizmatgiz.
11. Bokshtejn, B.S. (1978) *Diffusion in metals and alloys*. Moscow: Metallurgiya.
12. Gottstain, G. (2011) *Physico-chemical principles of materials science*. Moscow: BINOM.
13. Dmitrik, V.V., Bartash, S.N. (2010) To damageability of welded joints of steam pipelines on creep mechanism. *Metallofizika. Nov. Tekhnologii*, **32(12)**, 1657–1663.
14. Krishtal, M.A. (1972) *Diffusion mechanism in rail road alloys*. Moscow: Metallurgiya.
15. (1976) *Tables of physical values: Refer. Book*. Ed. by I.K. Kikoin. Moscow: Atomizdat.
16. Dmitrik, V.V., Tsaryuk, A.K., Bugaets, A.A. et al. (2006) Evaluation of remaining life of welded joints of pipelines for thermal power plants. *The Paton Welding J.*, **2**, 6–10.

«Binzel Ukraine GmbH» — 15 Years of Development: Interview with Yu.A. Didus, Director General

What was the background of foundation of «Binzel Ukraine GmbH»?

The history of the Company began in the middle of the 1990s. At that time the market of Ukraine was explored by many foreign companies manufacturing welding equipment and components, Company «KURT HAUFE Schweisstechnik/ABICOR BINZEL» being among them. Exhibition «Welding – Ukraine 96» was held in autumn 1996 in the territory of the National Exhibition Centre (Kiev). Being a fourth-year student, I was invited to this Exhibition to work as an interpreter at the «KURT HAUFE Schweisstechnik/ABICOR BINZEL» booth. Eleven months later my duties were widened and transformed into a post of the Director of Company «Binzel Ukraine GmbH».

On September 2, 1997, a Protocol was signed on foundation of the company with foreign investments «Binzel Ukraine GmbH» with the office in Kiev. It should be noted that our enterprise at that time was the thirtieth subsidiary of the «ABICOR BINZEL» group in the world and the first in the CIS territory.

What was the impetus for you to choose this line of activity?

In my making and development I always considered my current activity to be the main one, and was absorbed in the current work element until I found interest in something absolutely new. I wanted to find the job and environment which would become part of my life.

So, my first goal, after mastering profession «Wide-profile machine operator with the right to operate machine tools with CNC» and obtaining the fourth grade, was to become a shop foreman. After serving in the Army in 1989–1991 (Magdeburg, Germany) I joined the Kiev State Institute of Foreign Languages and saw myself at a teacher's table in secondary school.

I don't know whether I have finished my search, but what I have been doing during these 15 years gives me and, hopefully, the people who surround me much pleasure.

What are the main stages of development of the enterprise which you can mark out during these 15 years?



Shortly, this is the stage of formation, to which I devoted the first three difficult and very interesting years to win the trust of the market, and the stage of active development of the enterprise as a key player in the market. This stage is still in progress.

Have you always succeeded in everything? How did you select the staff?

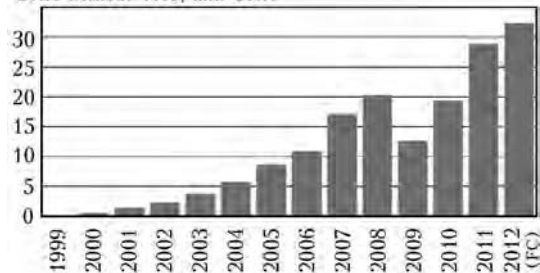
If I had succeeded always and in everything, I think my search for an interesting job would go on. At the moment of foundation of the enterprise we forgot to write scenario of our activities, which would allow us to work without problems. All that we failed to do was always systematically analysed, and corresponding conclusions were made, which helped us to continue our efforts and acquire experience.

The staff of the Company was formed gradually, in accordance with financial indicators of the enterprise and market demands. Mainly, we chose young people, often just from a college, and not yet spoiled specialists, whom we brought





Development of sales of products in 1999–2012
UAH without VAT, mln UAH



up to meet the work style of the «ABICOR BINZEL» group. At present, 12 young, active and goal-seeking people are working at the Company. Graduates of the Kiev Polytechnic Institute make up the base. And what is most important, the staff must be a team and have a goal that is clear for everybody. This helps in any situation.

How did the activities of «Binzel Ukraine GmbH» influence the technological level of welding production in Ukraine?

Our main and most difficult task in the first years of our presence in the welding market of Ukraine was to draw attention to the necessity to change the culture of production and operation of welding equipment.

We were among the first who offered to the market the system of welding torches that comprised models of the entire range of working loads and different geometries. Being a curiosity in 1997, today Binzel-spray and Duesofix-paste are the standard for a welding post. We formed the structure of official distributors with regional stores of components and consumables, which is a guarantee of the failure-free operation with our products. The latest models of welding torches of the ABIMIG® GRIP A LW and ABIMIG® AT LW systems presented to the market in 2010 and 2012, respectively, were developed jointly with research institutes, which were involved in studies of the role of utilisation of new materials in reducing loads on the welders' back muscles and arms. According to professors, here as well we were the first who in production of their torches paid attention to their effect on the health of welders.

What industries are regular customers of the «Binzel Ukraine» products?

Generally, these of course are enterprises of all sectors of machine building, pipeline transport maintenance, and metallurgical enterprises. As of December 2011, the base of our active customers included 593 enterprises from across Ukraine.

You have the system of distribution of your products in Ukraine. What is the efficiency of this system, and are there ways of improving it?

Our purpose in forming the system of official distributors was to promptly and qualitatively respond to inquiries of our customers in the field. Later on the frequent requests from our customers to confirm the status of this or other distributor were a signal for us that the market accepted the given model of delivery and maintenance of our products.

Starting from ten distributors in 1997, now the prompt deliveries to regions are provided by 147 partners of five groups of distributors. As of December 2011, the share of sales through our network of distributors was over 60 %. And we constantly, from year to year, are finding, discussing with our partners and implementing new methods for improving it.

What can you say about the dynamics of sales of products during 15 years?

I think the diagram of the sales of products over a period of 1999–2012 will tell you better about this dynamics.

How did the crisis of the last years affect the activities of your company, and what steps did you make to mitigate it?

It happened so that the time of unpredictable situations and problems began to test us to resistance as early as at the initial stage of our formation, namely in 1998, during the economic crisis in Russia. Subsequent tests made us more creative, serving as an incentive to work at a still higher efficiency. That helped us to remain afloat and sometimes even go against the stream. Of course, this is the achievement of our entire team, as well as of our customers who chose the «ABICOR BINZEL» products.

The conversation was written down by Prof. V.N. Lipodaev, PWI

MODERN METHODS OF WELDING ALUMINIUM ALLOYS TO STEELS (Review)

D.M. KALEKO

E.O. Paton Electric Welding Institute, NASU, Kiev, Ukraine

Modern methods of welding aluminium alloys to steel were analyzed. Techniques of minimizing the thickness of intermetallic interlayer in the joints were noted, which include heating of the joint metal below the steel melting temperature, accelerated cooling of the joint, and application of damping coatings or inserts.

Keywords: *welding processes, aluminium alloys and steels, welded joints, intermetallic interlayer, technological techniques, heat input, hybrid welding, electron beam welding*

Designers and architects in their work continuously face the dilemma of high strength and low weight. It can be solved by a combination of strong and lightweight materials. In particular, joining steel and aluminium elements became widely applied in automotive industry and shipbuilding, in manufacture of passenger railway cars, as well as lightweight building structures and decorative elements of facades. Here such material qualities as strength and corrosion resistance, low weight and good formability are combined.

In automotive industry the tendency of steel replacement by aluminium alloys emerged as far back as 25 years ago. It was calculated [1] that lowering of car weight by 100 kg saves on average 0.3 l of petrol per 100 km of mileage. In addition, at lowering the car weight and respective lowering of energy power input the European norm for 2012 – CO₂ emissions of not more than 130 g/km – can be met [2]. By the data of [3], the potential weight saving when aluminium is used instead of steel is up to 42 %. However, actually, this figure drops to 24 % as a result of application of modern high-strength steels. In mass production of cars, steel ensures a weight saving, and considering its good formability and strength, it remains one of the most important materials in automotive industry.

European car makers undertook to reduce the consumption of pigments that led to a change of design of the body of Audi A2 and A8, in which it is equal to almost 24 % of the car weight [4]. So, in the modern car individual parts, or even whole assemblies, as for instance, engine compartment in BMW, are made of aluminium. In Audi TT only the rear part of the body is steel, the rest is made of aluminium alloy (Figure 1).

In shipbuilding steel replacement by aluminium alloys allows reducing the ship weight and lowering the center of gravity, and further gives such important advantages as nonmagnetization and corrosion resistance. Aluminium alloys are used to make hull structures (predominantly, of lightweight ships), as well as superstructures, deck cabins, bridges, chimney casings, partitions, enclosure, etc. [5]. Aluminium alloys also found broad application in manufacture of railway rolling stock. In Europe aluminium alloys are used to make about 80 % of railway cars [6].

Automotive industry mostly uses alloys of Al–Mg–Si system of 6000 series with good hot painting properties (preserve strength properties at heating up to 300 °C) [6]. In Europe readily formable EN AW 6016 alloy (%: 1.0–1.5 Si; ≤ 0.25–0.60 Mg; ≤ 0.2 Mn; ≤ 0.5 Fe; ≤ 1.15 Ti; balance being Al) is mostly used for body outer parts, in the USA these are alloys ANSI 6111 (0.9 Si; 0.7 Cu; 0.2 Mn; 0.7 Mg; balance being Al) and 6061 (0.6 Si; 0.23 Cu; 0.15 Mn; 1.0 Mg; 0.2 Cr; balance being Al) [6]. Alloys of Al–Mg system with 2–3 % Mg are now used for support frames of cars and other parts made with application of arc welding [7].

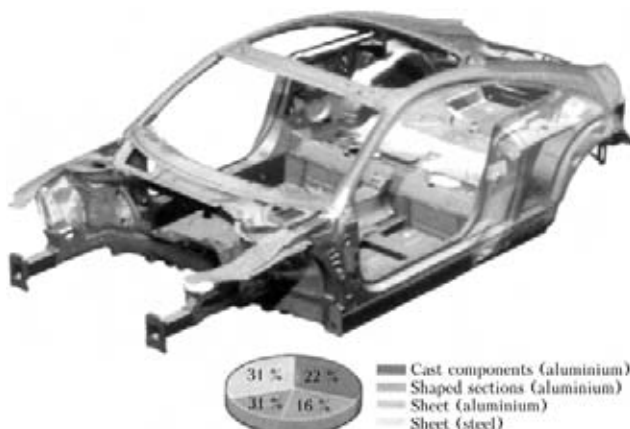


Figure 1. Structure of Audi TT body from dissimilar materials [4]

It is known that the main obstacle in joining steels to aluminium alloys is a negligible (0.025 at.%) solubility of iron in aluminium. The problem arises at formation of brittle intermetallic phases of various composition, both at interaction of liquid metals, and as a result of element diffusion at joint heating up to temperatures of 350–400 °C, i.e. below aluminium melting temperature. Noticeable thickness of intermetallic layer has a negative role already at joint cooling because of a considerable difference in the coefficient of thermal expansion (1.2 and 2.3 mm/100 °C for steel and aluminium, respectively), leading to appearance of significant inner stresses and quite often to formation of cracks. High hardness of intermetallic layer (up to *HV* 1200) and low viscosity of chemical compound of metals prevents relaxation of thermal stresses.

Most of the problems, related to welding of aluminium alloys to other metals, and methods of their solution are described in [8]. However, over the 30 years, which have passed since the moment of its writing, welding science and technology proposed a number of technological processes, which took us closer to satisfying industry requirements when making hybrid joints of steel and aluminium. Some of them are described in this review.

It was already mentioned above that the influence of brittle intermetallic zone is the smaller, the thinner it is. In keeping with [9, 10], the thickness of this zone should not be greater than 10 µm. It is obvious that such a thickness can only be ensured by limiting the heating of the joint butt. All the modern processes are based on observing this condition.

Arc welding. In manufacture of steel-aluminium parts great attention is given to traditional welding processes in their new implementation.

Nonconsumable electrode welding of joints of steel with aluminium alloys is currently seldom applied, although there are reports [11] about good results at application of DC05 steel ($C \leq 0.06$, $Mn \leq 0.35$) 0.8 mm thick with EN AW 6016 alloy 1.15 mm thick. Blanks of 9.5 mm diameter demonstrated reduction ratio of 7.9. At greater deformation ratio, cracks develop, which initiate in aluminium.

Considerable progress has been made in consumable electrode inert-gas arc braze-welding (MIG). Braze-welding of steel to aluminium, based on a significant difference of melting temperatures of aluminium (~660 °C) and steel (~1500 °C), allows making from aluminium alloy

side a welded joint with solidified filler metal, and a brazed joint from the steel side. Here the process, naturally, should be conducted so that the part was heated above the aluminium alloy melting temperature but below steel melting temperature.

The simplest form of joints made by consumable electrode braze-welding are overlap joints. Here the aluminium alloy part is located from the consumable electrode side, and the steel part is predominantly heated due to heat removal from the aluminium part. In [11] it is shown that at removal of the arc axis for 3 mm from the aluminium part edge, it is possible to reduce intermetallic phase formation to the thickness of 2–3 µm in the weld central part and to less than 1 µm on the boundary. To achieve optimum properties of butt and overlap joints weld reinforcement, as well as the extension should correspond to 2.5 times thickness of the sheet. Static strength of such a joint is on the level of the weakest partner. Steel wettability by aluminium is improved by applying zinc coating on steel that was noted already by V.R. Ryabov in 1969 [12]. Liquid aluminium dissolves zinc [13].

Influence of filler material composition on characteristics of braze-welded joint of aluminium and steel was studied by many experimenters. These investigations included testing wires from Zn- and Al-based material [10]. It is shown that application of wire from a zinc alloy makes more complicated the task of filler feed and controlling welded joint geometry, because of low hardness and melting temperature of the material. At the same time, with this filler wire type, thickness of intermetallic phase layer decreased and corrosion resistance of the joint increased. As a result, AlSi3Mn1 wire was recognized to be the best composition. The same metal was used also in investigations [11], the results of which are given above. Earlier [14] high-silicon wire from AlSi12 eutectic alloy was used as filler material. However, the small difference between AlSi12 melting temperature (577 °C) and zinc evaporation temperature (907 °C) requires an extremely accurate heat input into the weld, in order to avoid zinc evaporation from the steel surface and joining pure steel to aluminium with formation of Fe_2Al_5 or $FeAl_3$. Silicon ability to slow down intermetallic phase formation was also taken into account here [12, 13].

At present AlSi3Mn1 filler material is applied in cold metal transfer (CMT) welding developed by Fronius Company [2, 15, 16]. System of control of short-arc process ensures an almost no-current transition of filler material to the base

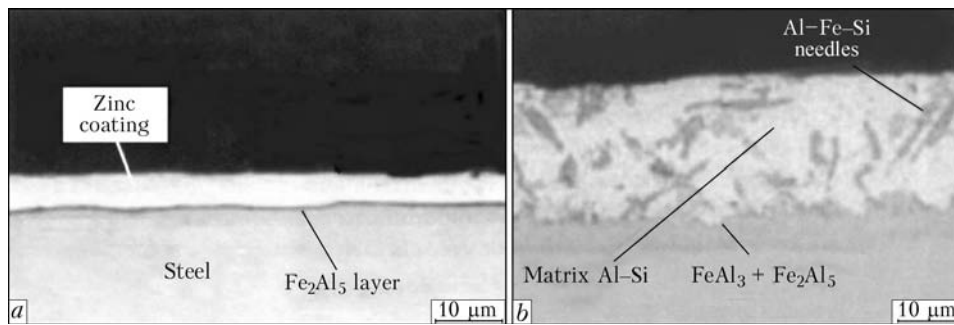


Figure 2. Microstructures of joints of aluminium to steel with zinc (a) and aluminosilicate (b) coatings

aluminium alloy, and the melt wets the Zn-plated steel. This process is innovative not only in that owing to highly accurate control of short-circuiting current, heat input can be lowered, but also in that a good drop transfer of molten metal takes place due to a periodical change of the direction of consumable wire motion, and welding without spatter can be implemented.

Braze-welded joints from DC05 steel with zinc coating of 140 g/cm^2 0.8 and 1.0 mm thick and AW 6061-T4 alloy, the thickness of which varied from 1.15 up to 1.20 mm, were tested. AlSi5 alloy was used as filler material and welding was performed in pure argon. Both the sheets were located in one plane, and misalignment by height was not more than 0.35 mm along the butt. Static strength of the joint was equal to base metal strength, and at steel thickness of 0.8 mm the joint failed in steel, whereas at steel thickness of 1.0 mm it failed in the aluminium alloy HAZ. In the first case calculated rupture strength was 190 MPa (base metal ultimate strength was 210 MPa in aluminium alloy and 280 MPa in steel), and in the second case – 210 MPa. In the produced joints average thickness of the intermetallic fringe on top, bottom and along the end face of the sheets was not more than $5 \mu\text{m}$, which the paper authors believe to be not critical.

Coating of steel sheet surface has an essential influence on weld geometry. Five different coatings were checked, namely zinc, nickel, titanium, aluminosilicon and aluminosilicon [3]. Heat-resistant coatings from titanium and nickel are partially or completely preserved after joining. Titanium alloy completely prevents formation of brittle Fe–Al phases [17], but requires an increased heat input, thus creating high weld reinforcement above the steel surface, impairing the conditions of item formability.

Nickel coating also prevents intermetallic phase growth. Application of fluxing means enabled improvement of wettability of the steel part surface and obtaining a flat geometry of the weld. All the joints with nickel coating failed in the base material of aluminium sheet at testing.

In case of aluminosilicate coating, which allows working without the fluxing means, a highly uniform intermetallic phase forms of average thickness of $5 \mu\text{m}$. As noted by the authors of [3], such a coating has no advantages over hot galvanizing; it, however, creates readily wettable surfaces and smooth transition from the weld to the steel sheet that markedly improves the mechanical indices.

Microphotographs of the joints of aluminium to steel and different coatings obtained by CMT method [10] (Figure 2) reveal the diffusion nature of intermetallic layer formation.

One of the methods to produce a satisfactory steel-to-aluminium joint can be steel coating by copper so that aluminium bronze was produced from the aluminium side at pulsed welding in inert atmosphere [18].

Lowering of heat power density applied to the butt was achieved in inert-gas arc butt welding at the pressure of 600–1000 Pa, when joining steel-aluminium pipe transition pieces in cryogenic mechanical engineering [19, 20]. A feature of this process is the diffuse shape of the arc, as well as relatively low temperature of the cathode and its intensive evaporation at temperatures not exceeding than the melting temperature at atmospheric pressure by more than 100–300 °C. This enables making joints by braze-welding schematic without any significant manifestation of diffusion of the metals being joined.

In many structures, where arc welding cannot be successfully replaced by more «delicate» processes, steel and aluminium are joined using bi-metal transition pieces, produced by various processes, which are considered below.

Laser welding. At present this process is becoming ever wider applied in mass and batch production not only when making miniature joints, but also extended welds in automotive industry. Considering the possibility of fine control of thermal power of pulsed laser radiation, researchers have also given their attention to this fusion welding process for joining steel to aluminium.

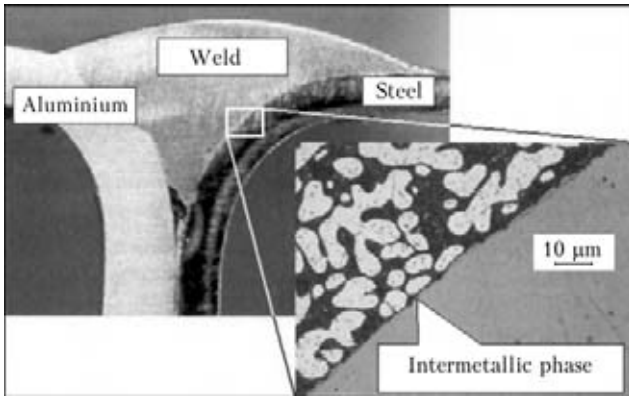


Figure 3. Schematic of laser braze-welding in car manufacture [23]

When making overlap joints, heating by neodymium laser is performed from the steel side [21]. The steel sheet is heated up to aluminium melting temperature, while remaining solid. Static strength of such joints reaches 70–90 % of aluminium strength. Similar to consumable electrode welding, the joint is of braze-welded nature.

Strength of laser braze-welded joints can be increased through application of Al-based filler metal and preheating of the steel Zn-plated sheet by the second laser beam to improve the wettability of the surface by molten filler [22]. At static tensile testing, the overlap joint failed through the aluminium sheet. Thickness of intermetallic fringe on the steel sheet did not exceed the critical value (Figure 3). Corus RD & T Company (The Netherlands) called such a process Fluxless Laser Brazing [23].

Developers of the technology of joining steel to aluminium can see great advantages of hybrid laser-arc welding (Figure 4). Increase of the speed of CMT process at leading laser heating allows minimizing intermetallic phase formation and joint zone embrittlement [4]. However, in this case the need for good heating of steel for its sufficient wettability and lowering of heat input to avoid the growth of intermetallic phase

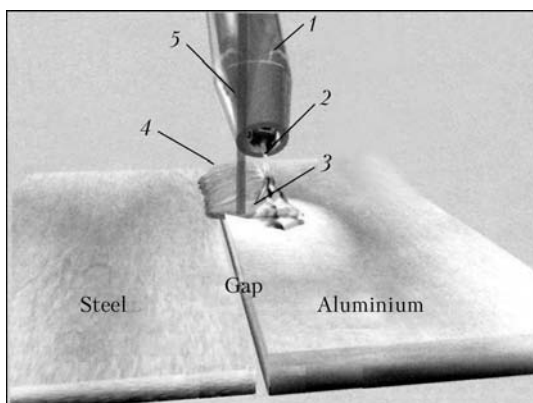


Figure 4. Schematic of hybrid laser-arc welding [17]: 1 – welding torch; 2 – filler wire; 3 – weld pool; 4 – weld; 5 – laser beam

come into a conflict. Bremen Institute for Applied Beam Technology (BIAM) managed producing butt joints of up to 3 mm sheets with 140 MPa strength by selection of modes of CO₂ laser radiation and MIG welding [24].

Speed of welding 1 mm thick butt joint at 4 kW laser power was more than 100 mm/s [25].

Process of hybrid laser-arc welding became accepted in manufacture of special bimetal tanks and items in automotive industry and shipbuilding [17]. At simple bending the characteristics of such joints are not critical, but at deep drawing they are not quite satisfactory so far.

Another kind of hybrid welding, namely laser welding with pressure application (Figure 5) has a special place, combining the advantages of fusion welding and pressure welding [26]. In particular, interface temperature can be controlled by scanning with the beam. The joint forms during strip compression by rollers.

In the experiment with 1 mm strips of A6061 alloy (wt. %: 0.8–1.2 Mg, 0.4–0.8 Si, balance being Al) with more than 295 MPa ultimate strength and cold-rolled sheet steel SPCC (< 0.12 C, 0.5 Mn, < 0.04 P, < 0.045 S) with 270 MPa ultimate strength the laser beam was guided between the strips being welded, which were taken through rollers, and scanned from one surface to another or just over one surface parallel to the joint line. This technique allowed controlling the butt metal composition and largely suppressing formation of brittle intermetallic compounds using the thermal cycle of fast beam heating and abrupt cooling at pressing to-

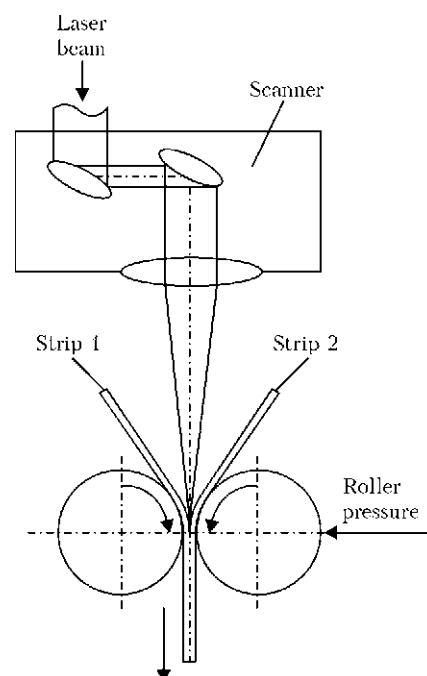


Figure 5. Schematic of laser-press welding

gether by rollers [27, 28]. At irradiation of sheet joint from the ferrous metal side melting of aluminium alloy occurs by heat transfer [26]. Investigation of the above joints [29] showed that they have sufficient strength, and can be used in manufacture of the car bonnet and roof.

Overlap joint of galvanized steel and aluminium alloy, made by roller laser welding at beam power of 1200–1400 W and roller pressure of about 3 kN [30], failed in the aluminium sheet at shear testing. Thickness of intermediate layer between steel and aluminium was from 7 up to 20 μm . During electron microscopy examination [31] it was established that the main phase in the intermediate layer was Al–Zn solid solution. Intermetallic compounds FeAl, Fe₂Al, Fe₄Al₁₃ and Fe₂Al₅Zn_{0.4} were found in it by electron diffraction. The authors came to the conclusion about heating of the strips being welded above the melting temperature, while strength of the joint with relatively thick intermetallic layer is determined by formation of Al + Zn phase with finely-dispersed intermetallic inclusions.

Electron beam welding. Sound joints of aluminium and steel parts were achieved at application of buffer coatings of titanium [18], nickel and zirconium [32] on steel.

Resistance spot welding. In resistance spot welding, similar to all the above-considered processes, joining occurs at simultaneous solidification of molten metal of the parts being joined. Generally known and earlier mentioned causes do not allow producing a satisfactory spot joint of steel and aluminium alloys even in welding in capacitor-type machines with stiff discharge mode [33].

The solution was found due to application of an intermediate bimetal strip produced by simultaneous rolling of steel and aluminium [34]. In welding two separate nuggets form on aluminium-aluminium and steel–steel interface. Limitation of heat input allows avoiding diffusion formation of the intermetallic layer on the inner boundary of bimetal insert. Static and dynamic testing of such joints showed that the strength of spot joints is comparable with riveted joints.

Press welding. This welding process was studied for the case of joining aluminium buses with steel elements of electrolyzer current conduit for aluminium production [35]. To reduce the probability of intermetallic compound formation, the authors used additives of finely dispersed powders of silicon, copper or zinc, which ensured development of an eutectic phase with melting temperature below that of aluminium melting.

The lowest thickness of intermetallic interlayer was achieved at application of silicon powder. The highest breaking stress was also observed in this case — 55–60 MPa.

Diffusion welding. Despite the fact that the joining process proceeds without melting of the parts being joined, because of the long time of contact of materials being welded at a high temperature, aluminium diffusion into steel leads to formation of brittle intermetallic phases rich in aluminium (FeAl₃ and Fe₂Al₅) [36].

Explosion welding. Bimetal joints produced by explosion welding are used extensively in the shipbuilding yards of Japan, Poland, USA, Great Britain, France and other countries, as was already mentioned above, as an intermediate element welded by the known processes (already in the similar combination) to the base material of the structure. The state-of-the-art limits application of steel-aluminium sections of a simple shape with 120 MPa strength [24].

12Kh18N10T stainless steel (wt.%: ≤ 0.12 C; 17–19 Cr; ≤ 0.8 Si; 1–2 Mn; 9–11 Ni; up to 0.02 S; up to 0.035 P) was successfully welded to AMg6 alloy (5.8–6.8 Mg) by explosion through an intermediate AD1 commercial alloy layer [37, 38]. The boundary between AD1 and stainless steel did not have any typical indications of intermetallics, although FeAl₃ and Fe₂Al₅ phases were actually found. Tearing stress was also equal to 120 MPa.

Results of testing welding of steel-aluminium hull structures with application of bimetal transition pieces allowed RSI of Structural Materials «Prometey» (St.-Petersburg) developing technological recommendations on welding butt, tee and overlap joints in manufacture of small displacement surface vessels, satisfying the requirements made of ship-hull materials [5].

Friction welding. Friction welding of pure aluminium A0 to St.3 (0.14–0.22 C; 0.3–0.6 Mn) and 1Kh18N9T (≈ 18 Cr; ≈ 9 Ni) steels of 16 and 20 mm diameter already 50 years ago [39] demonstrated the possibility of producing satisfactory welded joints owing to forging, which leads to pressing out of possible reactive phases of aluminium and steel (during welding the rubbing surface of aluminium is in the molten state) and bonding of pure surfaces of base metals. This was also shown by observations in electron and X-ray radiation [40].

Weldability of aluminium alloys with steel by friction directly depends on the alloy hardness. So, AMg6 alloy practically does not weld to steel by friction, whereas AMg3 alloy forms quite satisfactory joints with steel [41].

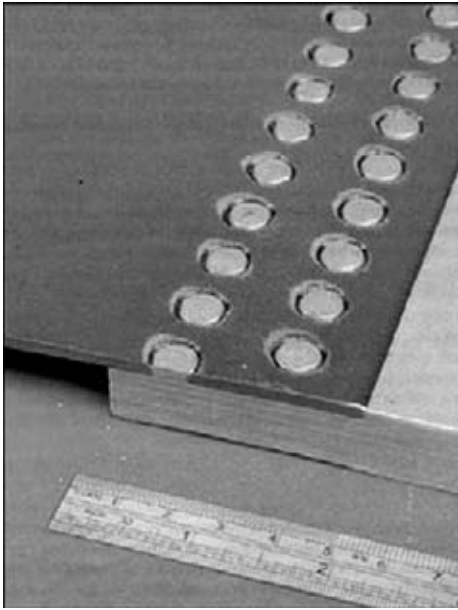


Figure 6. Example of joining steel and aluminium sheets by stir-lock process

The limitations of traditional friction welding also include the requirement of cylindrical shape of at least one of the parts.

Now, friction stir welding (FSW) process turned out to be quite suitable for welding sheets [42].

In FSW of spot welds of A5052 aluminium alloy and low-carbon steel, despite the relatively low temperature of steel heating (below aluminium alloy melting temperature) a layer of intermetallics was found between the metals been joined [43]. However, the shear strength of the joint was relatively high. Steel coating by zinc increased the strength, if the latter was pressed out of the joint zone [44].

A good result was obtained in FSW of aluminium alloy to stainless steel [45]. In the transition zone a layer of intermetallics was also found, but its thickness was limited to just several micrometers.

FSW and CMT processes were compared under JOIN B1 project [46] in welding aluminium to steel. Examination of metallographic sections by energy-dispersive X-ray spectroscopy showed that in all the spot welds, similar to welds made by CMT, joining takes place through an intermetallic phase. In welding by Fronius method this phase had a very non-uniform thickness, while in FSW the thickness was almost unchanged. It, actually, greatly depends on position relative to tool axis. Near the tip the intermetallic phase thickness is relatively small (2.5 μm) and at a distance it reaches 12 μm . FSW process was patented by TWI in 1991. Over the recent years they also developed stir-lock process [47], the principle of which is clear from Figure 6.

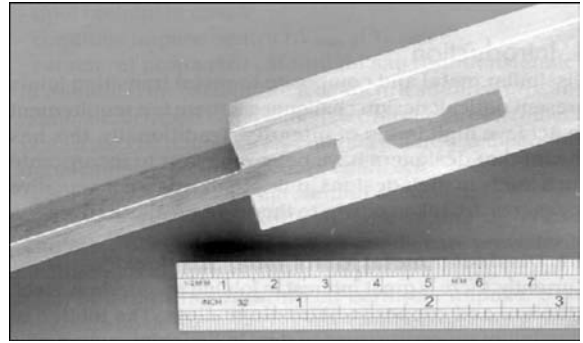


Figure 7. Locking a perforated steel sheet in the aluminium one by stir-lock process

In the harder material (this is steel in our review, but the process was successfully tried out for joining aluminium to magnesium, titanium and copper) a counterbored hole is made, through which the soft metal is heated by a rotating tool. Heated metal is pressed into the hole under pressure, creating a head in the free cavity of the steel sheet, similar to a rivet head.

With stir-lock process the joint can also be made using perforated inserts, as shown in Figure 7.

This review did not cover the processes of joining steel to aluminium by simultaneous deformation, namely rolling, extrusion, drawing, etc., as they are quite traditional and well-known to the reader.

CONCLUSION

As shown by this review of modern processes of welding aluminium alloys to steel it is not possible to completely avoid formation of an intermetallic interlayer between the metals being joined with the processes using thermal transformation of metals. However, in technological terms it is possible to create conditions, under which the thickness of this interlayer will be minimum, and its influence on joint characteristics will, thus, be noncritical. Such welding techniques include joint heating below the steel melting temperature (brazing), accelerated cooling of the joint and application of intermediate damping coatings or inserts. Finally everything is determined by the value of heat input, or, in other words, heating temperature and time during which the parts are staying at high temperature.

Percussion capacitor-type welding can be an example of successful welding of aluminium wire to steel plates [48]. With this process metal of materials being joined, heated up to melting temperature, is removed at upsetting, and at cooling rate reaching 10^6 K/s, joint temperature decreases so fast that interdiffusion of metal through the joint boundary is practically absent.

1. Reisgen, U., Stein, L., Steiners, M. et al. (2010) Schwingverhalten von mit modifiziertem MSG-Kurzlichtbogenprozess gefuegten Stahl-Aluminium-Mischverbindungen. *Schweissen und Schneiden*, 62(7/8), 396–399.
2. (2011) Realisierte Vision: Schweißen, was nicht zu Schweißen. *Schweiss- und Prueftechnik*, 11, 155.
3. Reisgen, U., Stein, L., Steiners, M. (2010) Stahl-Aluminium-Mischverbindungen: Schweißen oder Loeten? Die Kombination zweier etablierter Fuegetechnologien macht Unmoegliches moeglich. *Schweissen und Schneiden*, 62(5), 278–284.
4. Staubach, M., Juettner, S., Fuessel, U. et al. (2007) Fuegen von Stahl-Aluminium-Mischverbindungen MSG-Verfahren und Zusatzwerkstoffen auf Aluminium- und Zinkbasis. *Ibid.*, 59(6), 302–313.
5. Oryshchenko, A.S., Osokin, E.P., Pavlova, V.I. et al. (2009) Bimetal steel-aluminium joints in ship-building hull structures. *The Paton Welding J.*, 10, 35–38.
6. Fridlyander, I.N., Sister, V.G., Grushko, O.E. et al. (2002) Aluminium alloys – promising material in automobile production. *Metallovedenie i Termich. Obrab. Metallov*, 9, 3–9.
7. Sasabe, S. (2004) Welding properties of aluminium alloys for automotive structures. *Welding in the World*, 48(Spec. Issue), 53–64.
8. Ryabov, V.R. (1983) *Welding of aluminium and its alloys to other metals*. Kiev: Naukova Dumka.
9. Bruckner, J. (2005) Der Cold Metal Transfer (CMT) – Prozess von Stahl-Alu Verbindungen und seine Moeglichkeiten. *Schweiss- und Prueftechnik*, 10, 147–149.
10. Guengoer, O., Gerritsen, C. (2008) Effect of filler wire composition and metallic coating on the joint performance of aluminium/steel braze welds. *Welding and Cutting*, 7(5), 303–312.
11. Diltthey, U., Brandenburg, A., Hoecker, F. (2006) Lichtbogenfuegen und Umformen von Verbindungen aus Stahl und Aluminium. *Schweissen und Schneiden*, 58(1), 23–28.
12. Ryabov, V.R. (1969) *Fusion welding of aluminium to steel*. Kiev: Naukova Dumka.
13. Fuessel, U., Zschetsche, J., Juettner, S. (2003) Warum nicht Aluminium mit Stahl durch Metall-Inertgasloeten verbinden? *Praktiker*, 4, 120–121.
14. Kiesche, M., Prietzel, H., Thomas, W. (1973) Verbindungsschweißen von Stahl mit Aluminium. *ZIS-Mitteilungen*, 5, 536–545.
15. Bruckner, J. (2005) Cold metal transfer has a future joining steel to aluminium. *Welding J.*, 84(6), 38–40.
16. Trommer, G. (2012) Das Beste aus zwei Werkstoffen. *Praktiker*, 3, 58–61.
17. Esser-Ayertey, C. (2011) Hamburg ganz in Zeichen der Fuege-, Trenn- und Beschichtungstechnik. *Schweissen und Schneiden*, 63(12), 728–737.
18. Heinz, E. (2009) Zwei Konkurrenten verbinden sich. *Ibid.*, 4, 214–215.
19. Sidiyakin, V.A., Arbuzov, V.M., Khorstov, V.S. (2009) Butt welding of dissimilar metals in low pressure inert medium. *Mir Tekhniki i Tekhnol.*, 10, 40–45.
20. Muravejnik, A.N., Dzykovich, I.Ya., Veselov, V.A. et al. (1990) Structure of transition zone of joints of 12Kh18N10T steel to AD1 aluminium alloy in low pressure arc welding. In: *Welding of dissimilar, composite and multilayer materials*: Transact. Kiev: PWI.
21. (2005) Schweißtechnische Einflussfaktoren bei Festigkeitsnachweisen von Druckbechtaltung. *Schweissen und Schneiden*, 57(3), 71–94.
22. Heinz, E. (2010) Laserstrahlschweiß-Loeten von Stahl-Aluminium-Mischverbindungen: mechanisch-technologisches Eigenschaftsprofil und mikrostrukturelle Charakterisierung. *Ibid.*, 62(11), 649–650.
23. (2007) Corus develops new steel-to-aluminium welding technique. *Welding and Cutting*, 6(2), 64.
24. Kubanek, M., Janssen, A. (2008) Die Verbindungsspezialisten 2007 – Bericht ueber die Vortraege der Grossen Schweißtechnischen Tagung des DVS im September 2007 in Basel. Teil 2. *Praktiker*, 1, 32–44.
25. Vollersten, F., Thomy, C. (2009) Laser-MIG hybrid welding of aluminium to steel. A straight-forward analytical model for wetting length. *IIW Doc. 2041–09*.
26. Nishimoto, K., Fujii, H., Katoyama, S. (2004) Laser pressure welding of aluminium alloy and low carbon steel. *Quart. J. JWS*, 22(4), 572–579.
27. Kutsuma, M., Rathod, M., Ammar, A. (2002) A laser roll bonding of mild steel to aluminium and control of intermetallic compound layer. In: *Proc. of ICALEO*.
28. Rathod, M., Kutsuma, M. (2003) Laser roll bonding of A5052 aluminium alloy and SPCC steel. *Quart. J. JWS*, 2, 282–294.
29. Kutsuma, M., Yamagami, N., Rathod, M. et al. (2006) A laser roll welding for joining of low-carbon steels to aluminium alloys. *Welding Int.*, 20(6), 446–450.
30. Nishimoto, K., Harano, T., Okumoto, Y. et al. (2009) Mechanical properties of laser-pressure-welded joint between dissimilar galvanized steel and pure aluminium. *Ibid.*, 23(11), 817–823.
31. Nishimoto, K., Okumoto, Y., Harano, T. et al. (2008) HR-TEM observation of laser pressure weld of galvanized steel and pure aluminium. *Ibid.*, 23(11), 824–829.
32. Bondarev, A.A., Ishchenko, A.Ya. (2006) Technology of EBW of the stainless steel-aluminium alloy welded joints. *The Paton Welding J.*, 12, 27–30.
33. Moravsky, V.E., Vorona, D.S. (1985) *Technology and equipment for spot and capacitor-discharge projection welding*. Kiev: Naukova Dumka.
34. Sun, X., Stephens, E.V., Khaleel, M.A. et al. (2004) Resistance spot welding of aluminium alloy to steel with transition material – from process to performance. Pt 1: Experimental study. *Welding J.*, 6, 188–195.
35. Korinets, I.P., Sakhatsky, V.A., Nakonechny, A.A. (2011) Resistance welding of aluminium to steel using composite interlayer. In: *Proc. of Conf. on Welding and Related Processes and Technologies* (Kiev).. Kiev: NTU KPI. 2011.
36. Rathod, M.J., Kutsuma, M. (2004) Joining of aluminium alloy 5052 and low-carbon steel by laser roll welding. *Welding J.*, 1, 16–26.
37. Mangur, S.I., Shapovalova, O.M., Dzhur, E.A. (2003) Interaction of stainless steel and aluminium alloys in explosion welding. *Kosmichna Nauka i Tekhnologiya*, 9(1), 48–49.
38. Gulbin, V.N., Nikolaev, V.B. (1990) Study of structure and properties of explosion welded bimetallic joints. In: *Welding of dissimilar, composite and multilayer materials*: Transact. Kiev: PWI.
39. Ginzburg, S.K., Prokofiev, S.N., Shternin, L.A. (1962) Conditions of formation of strong joint in friction welding of aluminium with steel. *Svarochn. Proizvodstvo*, 12, 12–14.
40. Scott, M.H., Squires, I.F., Met, B. (1966) Metallurgical examination of aluminium-stainless steel friction welds. *British Welding J.*, 13(3), 151–164.
41. Vill, V.I. (1970) *Friction welding of metals*. Moscow: Mashinostroenie.
42. Tretyak, N.G. (2002) Friction stir welding of aluminium alloys (Review). *The Paton Welding J.*, 7, 10–18.
43. Miyagawa, K., Tsubaki, M., Yasui, T. et al. (2009) Spot welding between aluminium alloy and low-carbon steel by friction stirring. *Welding Int.*, 23(8), 559–564.
44. Miyagawa, K., Tsubaki, T., Yasui, T. et al. (2009) Spot welding between aluminium alloy and Zn-coated steel by friction welding. *Ibid.*, 23(9), 648–653.
45. Anders, J. (2010) Verbindungen Al-Al, Al-Ti und Al-Stahl mittels Rührreisschweißen. *Schweissen und Schneiden*, 62(7/8), 440–441.
46. (2009) Schweiß- und Prueftechnik. *JOIN Sonderband*, 25–29.
47. Thomas, W.M., Staines, D.J., Norris, I.M. et al. (2006) Transition joints between dissimilar materials. *Sudura*, 16(4), 17–21.
48. Kaleko, D.M., Moravsky, V.E., Chvertko, N.A. (1984) *Capacitor-discharge percussion welding*. Kiev: Naukova Dumka.

DEVELOPMENT OF THE TECHNOLOGY OF MANUFACTURING DOUBLE-WALL WELDED TRANSFORMABLE-SHELL STRUCTURE

L.M. LOBANOV and V.S. VOLKOV

E.O. Paton Electric Welding Institute, NASU, Kiev, Ukraine

Transformable-shell structures (TSS) of a conical type are considered, which are a unique development of PWI, and have no foreign analogs. Engineering solutions are proposed which allow improvement of reliability of shell TSS, as well as technological approaches to their realization. A brief description of the technology of producing permanent joints on sheets of austenitic stainless steel, capable of ensuring the leak-tightness of deformed shells, is given.

Keywords: transformable-shell structures, load-carrying shells, double-wall transformable shells

At development of shell structures one of the most urgent problems is ensuring their service properties – leak-tightness and fatigue life, strength and corrosion resistance of welded joints. In transformable-shell structures (TSS) developed at PWI, the reliability of welds and material of the shell are particularly important, as they undergo considerable bending during transformation, reaching 150° in the vortices of technological corrugations [1]. Promising applications of TSS as storage tanks for bulk and liquid materials, including substances with increased reactivity, require looking for effective methods to improve the shell reliability. The most rational solution can be development of a two-layer struc-

ture, in which outer wall duplication with separation of its enclosing and load-carrying functions can prevent the consequences of possible loss of tightness.

In most of the cases, technology of TSS manufacturing by forming corrugated discs from thin-walled conical shells is preferable, allowing fabrication of structures of a broad range of typesizes and parameters. Isometric transformation of a closed shell in the form of a truncated cone can be realized by dissection of its surface by a family of planes, normal to cone axis, and successive mirror reflection of the parts of the surface relative to the respective planes $\gamma_n, \gamma_{n+1}, \dots, \gamma_k$ (Figure 1). At crossing of the transformed Q_{n+1} and untransformed Q_n parts of the surface a rib is formed in the crossing region, which lies in plane γ_n and moves together with it during transformation. The essence of the method developed at PWI consists in successive, close to an isometric one, bending of a smooth conical blank and forming a corrugated disc by local impact of the forming tool on a rotating shell [2]. The bent circular area of the blank encloses the tool working surface, moves from the outer part of its side surface to the inner side, and takes a position, which is a mirror reflection of the initial one, forming the inner wall of the circular corrugation. The corrugation outer wall is formed by an undeformed section of the shell, which moves along its axis of rotation. During forming of each subsequent corrugation of depth k the height of the conical shell decreases by a value equal to $2k$. Simultaneous forming of two conical shells Q and \bar{Q} in one technological process allows creating topologically equivalent corrugated surfaces Q_1, \bar{Q}_1 , superposable by moving along the axis of symmetry.

Optimum modes of forming two-layer corrugated discs by bending shells of 12Kh18N10T stainless steel with outer diameter $D = 150$ mm

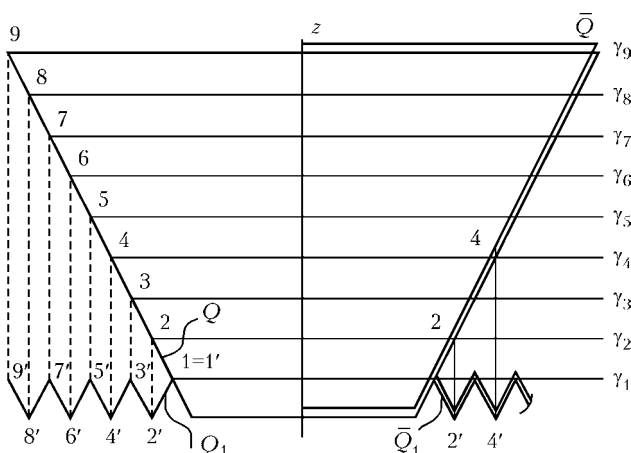


Figure 1. Schematic of isometric transformation of closed conical shells: γ_1 – γ_9 – parallel secant planes; 1–9 – points of intersection of secant plane traces with side generatrix of the conical surface; 1'–9' – points of reflected part of the surface corresponding to points 1–9; Q, Q_1 and \bar{Q}, \bar{Q}_1 – untransformed and transformed parts of the circular cone surface

Strip thickness, mm	Welding current, A	Welding voltage, V	Welding speed, cm/s	Shielding atmosphere	Results		
					Weld width, mm	Lack-of-penetration	Deplanation, mm
0.15	3.5	10	0.14	Helium	1.35–1.40	Complete	0.45–0.50
0.15	5	10	0.28		1.2–1.3		0.5–0.6
0.15	7	10	0.42		1.4–1.5		0.30–0.35
0.15	8.5	10	0.55		1.3–1.4		0.2–0.3

and wall thickness of 0.15 mm were determined experimentally; one of the conical shells is tightly inserted into the other, which is followed by fixing both the blanks in the centering conical opening of the die-mold. At optimum technological parameters of the process, the produced discs do not have any surface defects with a close contact between the shell layers without any tendency to their subsequent separation: range of speeds of blank rotation at rotational extrusion in the mould is within 50–250 rpm, the speed of forward feed of the forming tool being from 0.3 up to 2.0 mm/rev.

Anticipated applications of conical TSS require paying special attention to working-out the problems of reliability and fatigue life of thin shells, the assembly of which implies presence of extended precise welds. Certain difficulties arise at subsequent welding of two-layer shells around circular contours. Despite tight contact of shell edges in assembly, the gap between the layers increases under the impact of welding heat, that may lead to their lack-of-fusion. Analysis of the currently available welding processes and evaluation of their adaptability to fabrication show that:

- in overlap welding by roll-seam welding machine the joints are 2 times thicker than the base metal. The weld has low ductility properties, its making requires complex fixtures, and the rollers burn on longer welds, thus leading to an increase of contact resistance and deterioration of welded joint quality;
- in microplasma fusion welding uniform high-quality joints are made, no sophisticated equipment or devices are required. With this process a molten metal pool of 0.12–0.17 mm³ volume forms in sheet welding. The smallest disturbances lead to its rupture, i.e. burning-through; this can be avoided by an accurate following of the conditions of assembly and welding; studied parameters of welding modes are given in the Table. Proceeding from investigation results, it is possible to select a mode for specific conditions;
- laser welding requires sophisticated and costly equipment and precision assembly of the

shell sections being welded, that involves considerable difficulties; more over, provision of protection of the molten zone and cooling weld zone is complicated. Nonetheless, this process allows achieving a high quality of welds at their minimum width that is important for sound formation of corrugated discs from the welded shells. In welding by a fiber-optic laser with laser beam power $P = 65$ W of blanks from a steel strip of 12Kh18N10T grade, similar to samples from the Table, at speed $v_w = 2$ cm/s, weld width was equal to $w_w = 0.6$ –0.7 mm at complete penetration and deplanation within 0.15–0.25 mm (shielding atmospheres: helium on top and argon from below the weld) [3].

Duration of welding the butt joints in fabrication of TSS of a conical type and relatively high fraction of intermediate assembly operations at other conditions being equal, do not allow regarding welding process speed as the decisive factor, determining the advantage of one of the considered processes. Under the conditions of difficult access to the weld root and complexity of butt aligning at assembly of two shells on load-carrying elements, microplasma process is preferable in most of the cases. Laser welding can be regarded as optimum at the stage of manufacturing the initial conical blanks of corrugated discs, requiring minimum distortions of the surface, when making narrow linear welds with low specific heat input.

At mechanical testing of the studied samples, the nature of deformations of each type of welds, used in TSS linear and circumferential joints, was simulated. To check the strength and ductility characteristics of microplasma welded joints, three standard samples for tensile and bend testing were prepared from each weld. Test results showed that none of the samples failed in the welded joint; rupture passed through the base metal at an angle to sample axis. Sample tension diagram is standard, with a pronounced yield plateau, characteristic for the used steel grade. Produced characteristics (12Kh18N10T steel), depending on thickness h , have the following form:

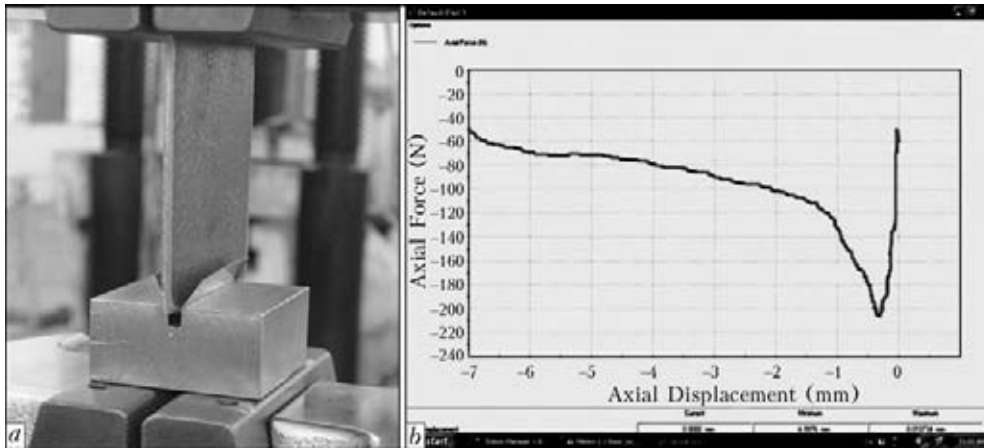


Figure 2. Segment of forming matrix for bend testing of weld fragment (a), and diagram of deformation of 0.15 mm thick sample (b): along ordinate axis – forming force $P_{max} = 230$ N

- for $h = 0.15$ mm
 $\sigma_y = 320\text{--}330$ MPa; $\sigma_t = 68\text{--}71$ MPa;
 $\delta = 40\text{--}42$ %; $\psi = 50\text{--}52$ %;
- for $h = 0.1$ mm
 $\sigma_y = 350\text{--}370$ MPa; $\sigma_t = 70\text{--}72$ MPa;
 $\delta = 39\text{--}41$ %; $\psi = 48\text{--}51$ %.

All the samples were tested for bending up to the angle of 180° in a mandrel with a radius equal to two base metal thicknesses, and no failures or cracks were found. To make testing conditions more complicated, the flattening method was used, in which bending of the rectangular sample was conducted up to touching of its opposite edges; in this case, slight plastic deformation was observed on the weld surface without any indications of welded joint fracture. Thus, strength and ductility of the produced welded joints are not inferior to similar characteristics of the base metal and allow performing the form change of the transformable shells, envisaged by the technology, without violation of their leak-tightness.

Strength tests of butt welded joints of 12Kh18N10T strip, made by laser welding, were conducted in MTS 318.25 testing system in a device, which is a segment of the rotational moulding equipment (matrix) in the area of forming the corrugation with maximum diameter and die with the working edge shape corresponding to the profile of forming roller for this material thickness (Figure 2, a). Figure 2, b shows the deformation diagram obtained at back bending of 0.15 mm thick sample along an axis normal to the weld line. At repeated deformation of each of the three tested samples the curves of $P(l)$ dependence are characterized by shifting of point P_{max} towards the initial values of axial displacements l . After three complete cycles of bending through 180° angle all the samples were examined by liquid-penetrant testing using MR[®] 68 penetrant and MR[®] 70 developer produced by MR[®]

Chemie GmbH with no crack opening or cracks found.

Sealing of the formed corrugated discs was performed by their welding to flat covers of 12Kh18N10T steel around the butt of the small circular contour in the profiled mandrel, ensuring a tight contact of the edges of aligned sections of conical surfaces of the blanks and heat removal in welding of the circumferential weld (Figure 3, a). Technology was verified on shells of larger diameter $D = 140$ mm, smaller diameter $d = 90$ mm, and 0.15 mm thickness as-assembled with covers of design thickness 0.3 mm, and welding was performed without filler material in the automatic mode using microplasma torch with a system of positioning along weld axis and with quality control of welded joint. Welding mode was as follows: $I_w = 3.5$ A, $U = 10$ V, $v_w = 0.33$ cm/s.

Speed of welding by the microplasma torch at disc joining was set by structure rotation in a special fixture. Welded joint quality was controlled visually, and also excess pressure $P = (0.2\text{--}0.3) \cdot 10^{-2}$ MPa was created in the shell inner cavity, with subsequent monitoring of its drop during the next 60 min.

At assembly of corrugated discs on circular load-carrying elements (frame rings) it will be necessary to maintain the relationships of their reciprocal geometrical parameters at all the stages of transformation, which ensure free movement of the inner shell with air compression in the interwall space (caisson) up to a certain pressure, which, in its turn, allows performing complete transformation of the outer shell to design dimensions. Width g of horizontal rims of a frame ring of Π -shaped configuration (Figure 3, c) is determined by the technology of welding along the edge flanges of circumferential contours of the two shells, and is in the range of $g = 40\text{--}50\Delta$, where Δ is the thickness of structural material

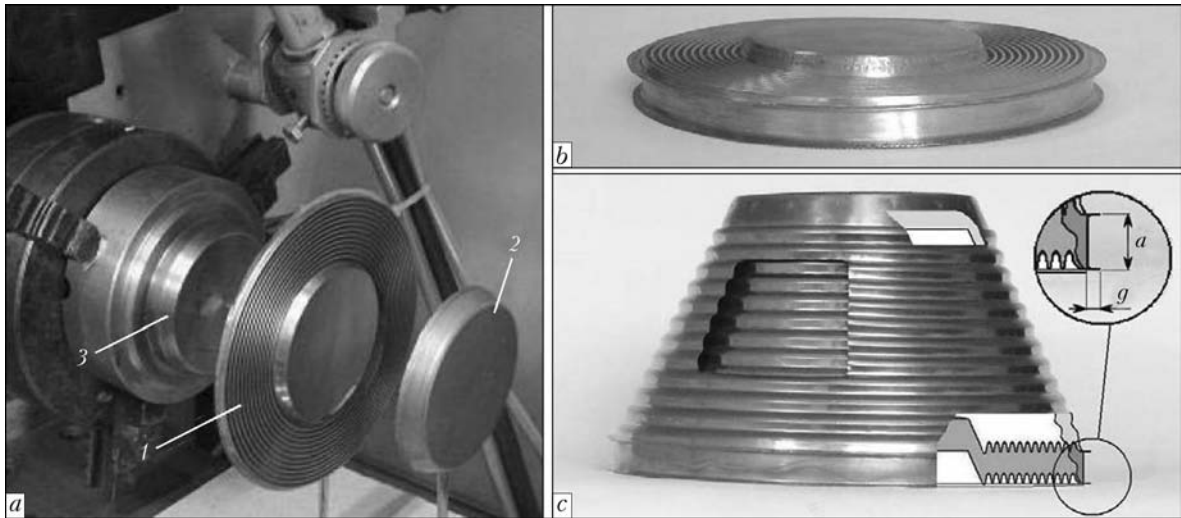


Figure 3. Assembly of initial corrugated discs of double-wall conical shell (a) (1 – corrugated disc; 2 – sealing cover; 3 – profiled mandrel), double-wall TSS with base radii $R = 70$ mm, $r = 49$ mm and angle of conicity $\alpha = 25^\circ$ in the compact (folded) state (b), and the same structure in the deployed state (c); the initial and final phases of transformation are shown in the sectional view on the right (a – frame ring height; g – width of frame ring horizontal rims)

shells; frame ring wall thickness is calculated allowing for process and service loads applied to the structure. Frame ring height a should provide the possibility of simultaneous motion of the shells without contact of any points of their surface.

The process of shell deployment starts with the maximum diameter corrugation. Experimentally derived value of excess pressure, which is necessary for complete deployment of single-wall shell of the studied structure, is equal to 10^5 Pa [4], and is approximately equal to the value of normal atmospheric pressure. Thus, a mandatory condition of complete deployment of the outer shell is 2 times increase of initial air pressure P_1 in the interwall caisson at drawing together of shells at all the transformation stages $P_2 = 2P_1$. Therefore, at isothermal compression of air $V_2 = V_1/2$, where V_1, V_2 are the caisson volumes at the initial moment of deployment of inner shell corrugation and at the initial moment of deployment of the corresponding outer corrugation. However, as follows from the condition of pres-

ervation of isometricity S_1 and S_2 , at the final stage of transformation volumes V_1, V_2 and pressures P_1 and P_2 , respectively, are equal, that means the impossibility of complete deployment of the last corrugation n_i of minimum diameter. In addition, required $P_2 = 2P_1$ ratio at forming of corrugation n_1 of maximum diameter corresponds to condition $l = a/2$, and for the next corrugations parameter l grows because of the change of the volume ratio of transformed and untransformed sections of interwall caisson that may lead to mechanical contact of the shells in the region of minimum diameter corrugations, local loss of stability and distortion of their surfaces. Therefore, frame ring height a is selected proceeding from the condition $a \geq k$, where k is the depth of corrugation forming; maximum a values are limited by the requirements of structure compactness, and, therefore increase of its transformation coefficient.

Figure 4, b gives a schematic of transformation of the last corrugation of the shells, which is of

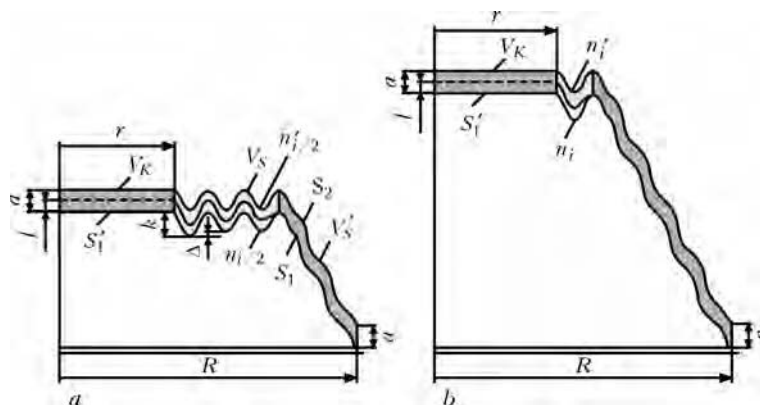


Figure 4. Schematic of transformation of corrugations of double-wall TSS with medium $n_{i/2}$ (a) and minimum n_i (b) diameters

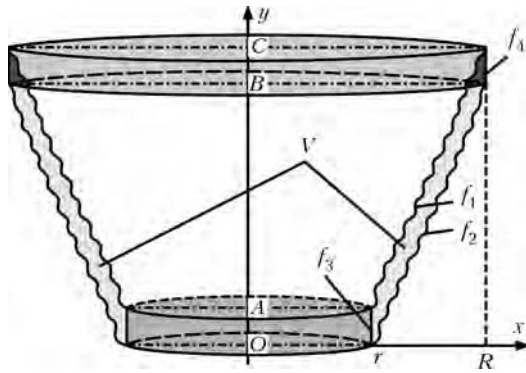


Figure 5. Schematic of double-wall TSS

minimum diameter. Interwall space V is divided into three conditional volumes, with their ratios changing continuously during structure deployment: V_K , limited by sealing covers; V'_S and V_S , limited by transformed and untransformed sections of side corrugated surfaces, respectively. At $l \approx a$ pressure of deployment of corrugation $n_i P_2 = P_1 V_1 / V_2$ and $V_1 / V_2 = 2$. Further process of deployment of outer corrugation of minimum diameter is possible only at forced increase of depth k of inner corrugation corresponding to it, by $\bar{\Delta} \leq a/2$ at the forming stage. It is obvious that after deployment of corrugation $n_{i/2}$ (Figure 4, a) transformation of undeformed surface of the shell by excess pressure is possible owing to compression of the technological caisson of volume V_K , satisfying the following condition:

$$V_K \geq V'_S. \quad (1)$$

Therefore, a criterion for complete deployment of the structure is r/R ratio meeting the same condition with preservation of shell isometricity at all the stages of transformation.

Figure 5 gives a schematic of a double-wall TSS for determination of ratios of conditional volumes of the interwall space (V_1, V_2, V_3, V_4) of the studied TSS, formed by revolution of ordinates of profiles of generatrices f_1, f_2, f_3, f_4

about the axis. Volume of interwall caisson V can be expressed as $V_2 + V_4 - V_3 - V_1$, or allowing for equality of inner volumes of the transformed shells $V = V_4 - V_3$. Congruence of generatrices of initial corrugated shells in any axial section of the structure at calculation of interwall caisson volumes allows their approximation by expressions for a cylindrical surface. Considering that $OA = BC = a$, one can write: $V = \pi a(R^2 - r^2)$. As condition (1) corresponds to relationship $\pi r^2 a \geq \pi a(R^2 - r^2)$, the ratio of double-wall TSS diameters required for complete deployment, will be expressed as

$$r \geq \frac{R}{\sqrt{2}}. \quad (2)$$

Combining double-wall TSS of a conical type into one structure by the respective bases of radii r and R allows producing a multicone TSS of a periodical profile, capable of deployment section-by-section at creation of excess pressure in the inner volume (Figure 6).

In this case, requirements to configuration of the interwall space and ratios of geometrical parameters expressed by relationships (1) and (2), remain the same. Design solution, which allows tightly joining the outer conical shells along the small radii, while providing the possibility of simultaneous deployment of the conjugated transformable surfaces, is shown in Figure 6, a and b. Leak-tightness and reciprocal mobility of contours K_1 and K_2 formed by the edges of radial holes in technological caisson covers of volume V_K (Figure 6, b) are provided by the compensating circular membrane with a fold, reversibly changing the deployment angle at transformation of each subsequent corrugation of double-wall TSS. Radii of contours K_1 and K_2 (R_{K1} and R_{K2}) are determined by design and technological considerations, whereas relationship (2) for a multicone TSS becomes $r_m = \sqrt{r^2 + R_K^2}$, where $R_K =$

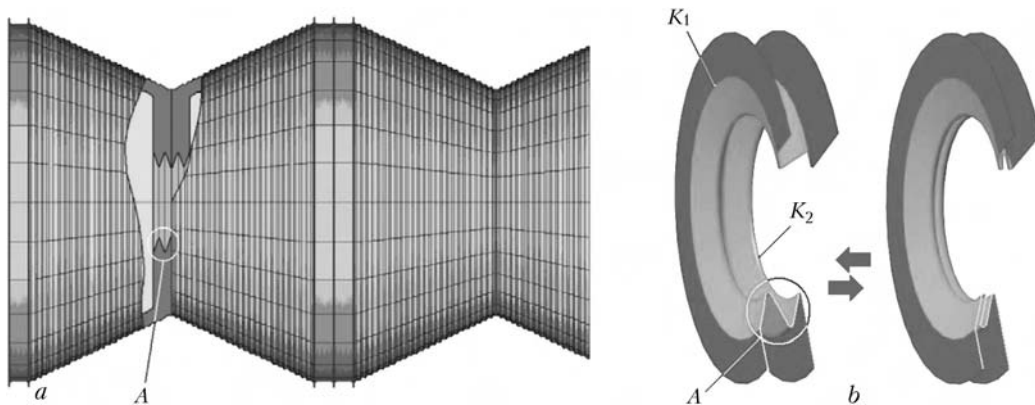


Figure 6. Construction diagram of multicone TSS of periodical profile (a), and compensating circular membrane (b) in the deployed and folded conditions (K_1, K_2 – radial contours associated with the inner and outer transformable shell of the structure, respectively): A – fold of compensating circular membrane

$= \frac{R_{K1} + R_{K2}}{2}$ is the average value of radius of circular membrane fold.

CONCLUSIONS

1. In the studied range of geometrical parameters of double-wall TSS the optimum structure is the one, in which the rectilinear and circumferential joints with different requirements to strength and ductility of welds are made by microplasma and laser welding processes.

2. Studied technology of producing permanent joints of austenitic stainless steel sheets allows ensuring the leak-tightness of deformable shells, both during forming, and at reverse transformation using excess pressure.

3. Complete transformation of double-wall TSS of a conical type up to design dimensions by creating excess pressure in the inner cavity, is possible with following of certain regularities of geometrical parameters on their inner and outer shells. Required ratios of working volumes of air in the structure interwall space are deter-

mined by relative values of radii of its bases, and are independent on the angle of conicity of the side surfaces at fulfillment of the condition of their isometricity.

4. The structure obtained by tight joining of double-wall conical TSS to each other preserves the functional properties of transformable elements included into it. The change of configuration of interwall gaps of each double-wall shell, associated with the need to unite the structure inner space into one volume, should be accompanied by fulfillment of the established dependencies of geometrical parameters in the connections.

1. (2003) *Space: technologies, materials, structures*. Ed. by B.E. Paton. Taylor&Francis.
2. Paton, B.E., Lobanov, L.M., Samilov, V.N. et al. (2006) Design and features of fabrication technology of a large-sized transformable shell structure. *The Paton Welding J.*, **7**, 2–10.
3. Shelyagin, V.D., Lukashenko, A.G., Garashchuk V.P. et al. (2011) Laser welding of thin-sheet stainless steel. *Ibid.*, **4**, 38–42.
4. Paton, B.E., Lobanov, L.M., Volkov, V.S. (2011) Transformable structures (Review). *Ibid.*, **12**, 25–33.

PECULIARITIES OF WEAR AND CRITERIA OF REPAIRABILITY OF DRILL BITS WITH DIAMOND-HARD-ALLOY CUTTERS

V.F. KHORUNOV, B.E. STEFANIV, O.M. SABADASH and V.V. VORONOV

E.O. Paton Electric Welding Institute, NASU, Kiev, Ukraine

The degree of wear and criteria of repairability of drill bits with diamond-hard-alloy cutters were studied. Statistical data on service life of different types of diamond drill bits were analysed.

Keywords: headway, mechanical speed, superhard materials, diamond layer, diamond-hard-alloy cutter (DHAC), wear resistance, drill well, polycrystalline diamond cutter (PCDC)

The rocks making up the well bore hole differ in composition and have different properties, depending on which the rocks can be destructed by cutting, spalling, abrasion or crushing. The character of fracture depends on the hardness and ductility of rock. Hence, drilling of wells is performed by using the certain type of tools. The main tool for mechanical destruction of rock to drill a well is a bit. Different types and kinds of bits are applied currently in practice.

The purpose of this study was to investigate peculiarities of wear and criteria of repairability of drill bits with DHACs.

The objects of the study are rotary drilling tools, such as bits, bores, various crowns and drill heads fitted with diamonds, hard alloys or diamond-hard-alloy materials in the form of cylindrical inserts. The drill bits and heads are made from strong and wear-resistant materials, as during the drilling process a bit is affected by axial loads, including impact ones, torque moment, as well as pressure and reactivity of a drilling mud.

In drilling, the initial shape of working surfaces of inserts changes due to wear, this leading to decrease in technical and economic indicators of the drilling tools. Abnormal wear and formation of circular grooves on the working surfaces of the bits make the tools unserviceable.

Wear of the working surfaces of drilling tools is a complex process caused by many factors,

Table 1. Classification for defining of wear of drill bits

Cutting structure				B	G	Notes	
Inside rows (I)	Outside rows (O)	Character of wear (D)	Location (L)	Compaction of support (B)	Wear on diameter B 1/16 (G)	Other types of wear (O)	Cause of pulling out from well (R)
1	2	3	4	5	6	7	8

including properties of the tool materials and rock at the well bottom, quality of design of the tools, efficiency of cleaning of rock destruction elements and flushing-out of the well.

Much factual data have been accumulated up to now concerning the service life of drills with DHACs and their reparability. To drill oil and gas wells, Ukraine applies mostly the drill bits made in the USA, China and Russia, and to a lesser degree the domestic drill bits. A weak point in drilling hard and superhard rocks of the drill wells is considerable wear of the domestic bits, and to a certain degree of the imported ones. To extend their service life, it is necessary to repair these expensive items. However, no repair and reconditioning of the domestic and imported bits are performed in Ukraine. Bits of the leading companies, such as «Reed Tools», «Smith Tools», «Hughes Christensen» and «Volvabur-mash», the extent of wear of which is not in excess of 30 %, are taken out from Ukraine for repair to the USA, Canada and other countries.

Therefore, investigation of the peculiarities of wear and criteria of reparability of domestic and imported bits is a pressing problem, the solution of which will allow extension of service life of the bits and provide much savings.

The E.O. Paton Electric Welding Institute analysed the peculiarities of wear of DHACs of steel and die drill bits, which had been used for drilling of wells in rock. The work was performed by using the method for description of wear of the bits based on the classification system accepted by the International Association of Drilling Contractors (IADC) [1, 2], according to which eight parameters are used to define wear (Table 1). In our case, to define wear it is enough to use six parameters, except columns 5 and 8 of the Table.

Consider in detail the classification for defining wear of bits given in Table 1.

Wear of inside and outside rows. Columns 1 and 2 are used to define wear of the cutting structure. Column 1 (I – inside row) gives the code of wear of that part of the cutting structure which does not touch the well walls in operation of the bit at the well bottom. As a rule, inside rows make up 2/3 of the entire cutting structure (Figure 1). Characterisation of wear of the cutting structure located at the inside rows allows reducing the quantity of variants of wear and determining its cause in more detail.

Column 2 (O – outside row) gives the code of wear of the cutting structure of a bit, which during the drilling process is in direct contact with the well walls. The outside rows make up 1/3 of the entire cutting structure (see Figure 1). Characterisation of wear of this part of the structure helps to evaluate correctness of op-

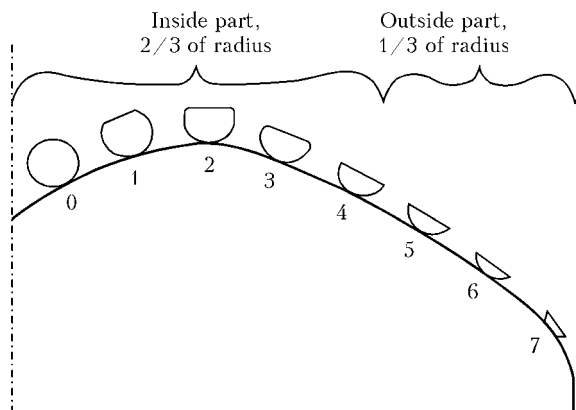


Figure 1. Schematic of wear of cutting structure

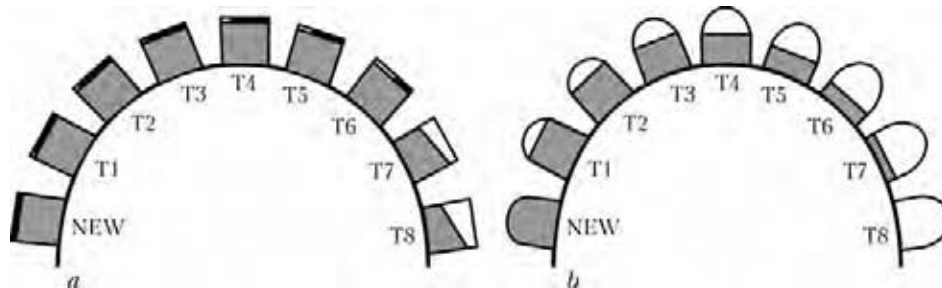


Figure 2. Schematic of wear of DHACs (a) and hard-alloy inserts (b): a: 0 – bit cutter is not worn out; 1–7 – cutter is worn out to 10, 15, 25, 30, 50, 70 and 100 %, respectively; 8 – complete loss of cutting structure; b: 0 – bit insert is not worn out; 2, 4, 6 – insert is worn out to 25, 50 and 75 %, respectively

eration of the gauge part of the cutting structure of a bit in the well.

The linear scale in a range of 0 to 8 is used to describe wear of DHACs or hard-alloy inserts. The number of the degree of wear increases with wear of the PCDC (Figure 2, a) and hard-alloy inserts (Figure 2, b).

Characterisation of wear of a bit. Column 3 (D – character of wear) gives the code indicated in Table 2 to define the main (dominant) character of wear.

Column 4 (L – location) uses the letter or digital code to indicate the location on the bit surface where wear of the cutting structure oc-



Figure 3. Location of the type of wear on drill bit

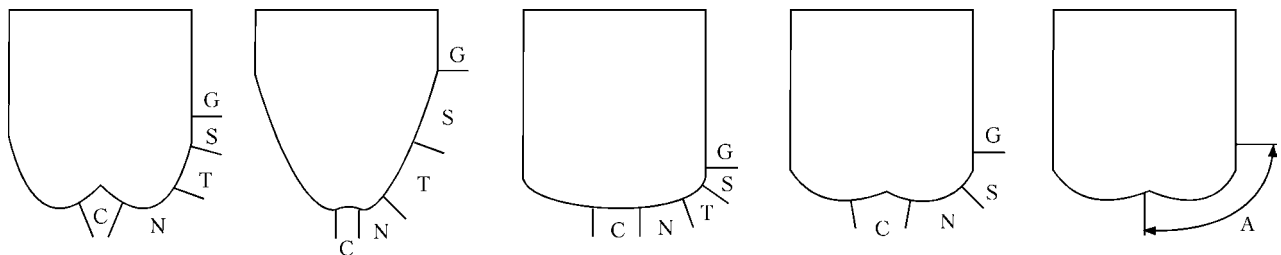


Figure 4. Schematics and codes of wear of cutting structure of bits: N – cutting structure that is closest to the bit top (middle row of bit cutters M is located between rows N and G); G – gauge row, cutting structure located on the gauge surface of bit; A – all rows (entire cutting structure of bit); C – inside cone surface; T – outside cone surface; S – shoulder

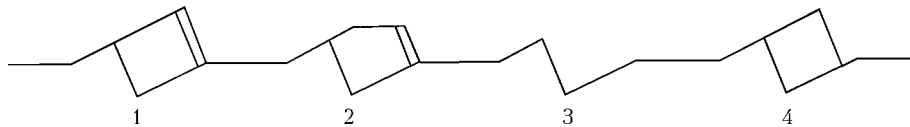


Figure 5. Schematic and codes of wear resistance of DHAC: 1 – absence of wear; 2 – worn-out cutters (WT); 3 – loss of cutter (LT); 4 – break of diamond plate (BF)

Table 2. Character of wear of bits

BC	Break of part of bit	LT	Loss of cutters
BT	Cutters are broken	NO	Absence of wear
BU	Sludging-up of bit	NR	Unfit for repeated trip-in
CC	Formation of cracks on bit	OC	Eccentric wear
CD	Bit stall	PB	Mechanical damage of bit in round-trip operations
CI	Bit bite	PN	Clogging of nozzle bushing in channel flushing
CR	Punching (wear of bit top)	RG	Wear of gauge part of cutting structure
CT	Spalling of cutter	RO	Circular wear on bit
ER	Erosion wear	RR	Bit is fit for repeated trip-in
FC	Flat wear	SD	Damage of cutter nose
HC	Thermal heating of cutters	SS	Effect of self-sharpening of cutters
JD	Operation of bit on metal	TR	Formation of ridges on bit
LC	Loss of bit	WO	Wash-out of bit body
LN	Loss of nozzle bushing of bit	WT	Wear of cutters

Table 3. Tolerances on outside diameters of drill bits

Nominal outside diameter of bit, mm	Inches	Millimetres
From 85.76 to 349.3 inclusive	From -0 to +0.313 (1/32)	From -0 to +0.794
From 355.6 to 444.5 inclusive	From -0 to +0.625 (1/16)	From -0 to +1.588
From 447.68 and more	From -0 to +0.938 (3/32)	From -0 to +2.381

curred (Figure 3). The codes used to describe the location of wear on diamond drill bits are shown in Figure 4.

The codes of wear resistance of cylindrical DHACs are shown in Figure 5.

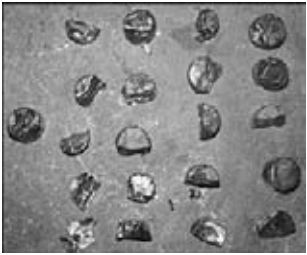
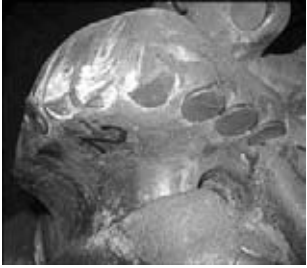
Wear of a bit on its diameter. Column 6 (G – outside diameter) defines wear of a bit by its size. For this the diameter of the bit is measured before it is lowered into the well and when it is pulled out by using a special sizing ring. Tolerances on the outside diameter of the diamond bits according to API are given in Table 3.

Column 7 (O – other types of wear) uses the same two-letter codes as in Table 2 to describe the secondary characteristic of wear of a bit, in addition to the characteristics of wear of the cutting structure listed in column 3.

Application of a new generation of oil and gas production bits fitted with PCDCs, made by the world leading companies (DDI, «Reed Hycalog», DPI, «Baker Hughes», «Smith International», «King Dream», «Security»), provides substantial advantages over the roller bits [3]: 4–5 times increase in a headway per bit and mechanical speed of drilling, decrease in the quantity of round-trip operations, substantial reduction of the cost of 1 meter headway and cost of 1 hour operation of a drilling unit, high wear resistance of cutters, possibility of the efficient reuse of repaired bits without deterioration of performance due to the absence of movable elements, high lifespan, etc.

The base for restoration of performance of the diamond drill bits is replacement of PCDCs and reconditioning of the surface layer of a die. Unbrazing of the worn-out cutters and brazing of

Table 4. Characteristics of wear of a die bit made in the USA (rock – gray sandstone, dark-gray siltstone, and dark-gray argillite)

Type of wear	Classification of wear according to IADC	Example of wear
Wear of cutting edges of PCDC	SS – wear of cutting edges WT – general wear	
General wear/fracture of PCDC	WT – general wear CT – spalled cutters BT – broken cutters	
Local wear of coating and core of bit body with fracture of PCDC seats	RO – wear of cutting structure on circumference FC – flat wear WO – washout of bit	
General wear of bit body	WO – washout of bit FC – flat wear of bit	

the new ones by using silver filler metals are the key technological processes for replacement of DHACs.

The weight of milled, welded and die bits, which differs but slightly for different types of bits, ranges from 5 to 200 kg, depending on the outside diameter (93–495 mm). Design of the blades, their quantity and schemes of location of cutters in different types of the bits differ greatly, which also requires an individual approach to selection of a source and power of heating, and of a method for transfer of the thermal energy to ensure the quality repair of each drill bit.

It is a known fact that the PCDCs of a bit wear out differently – the most worn-out cutters are the central ones, and the least worn-out cutters are the peripheral ones, i.e. the load on cutters is distributed in a statistically indeterminate way. Therefore, in visual examination of a bit it is necessary to compile a list of defects for a given type of the bit and determine the quantity and quality of the PCDCs for their complete or partial replacement.

In selection of a heating source for unbrazing of the PCDCs from the bit blade seat, it is necessary to take into account the temperature resistance of a polycrystalline diamond layer, weight and quantity of the bit blades, as well as the scheme of location of the cutters in a bit.

Analysis of the thermal energy sources [4–10] for different design types (welded, all-milled, die) of the diamond drill bits and extent of their wear (not more than 50 %) showed that the volumetric heating methods (in furnace, salt melt) do not meet requirements of monitoring of temperature-time conditions of the technological process used for replacement of DHACs. The most rational methods for brazing-in of the PCDCs in terms of maintenance of physical-chemical properties of their diamond layer are flame and induction heating.

The temperature-time conditions for unbrazing of the PCDCs from the diamond drill bits (welded steel, with die body and all-milled steel body) were determined as a result of the investigations:

- for the mass one (with the whole blade) the most suitable heating method is induction heating with a maximal capacity of up to 30 kW;
- for the selective one (one or several) – heating with one or two gas torches No.4 at a maximal capacity of the gas mixture (oxygen-propane/butane) amounting to 10 kW.

The peculiarities of repair of bits depend on the density and physical-chemical properties of the corrosion-resistant surface layer of the bits, as well as the effect on the temperature-time heating conditions, strength of the polycrystalline diamond layer and quality of the brazed joints between the PCDCs and the bit die.

The extents of wear of the diamond drill bits (welded steel, with die body and all-milled steel body) supplied to the E.O. Paton Electric Welding Institute of the NAS of Ukraine for repair were determined according to this classification. Tables of wear of the drill bits depending on the physical-chemical characteristics of rock were plotted on the basis of the investigation results. Characteristics of wear of the «Baker Hughes» (USA) die drill bit with DHAC are given as an example in Table 4. The final estimate of wear of the given bit according to IADC is as follows: 3 7 RO T 0 I (CT, BT, WT, FC) PR – subject to repair.

CONCLUSIONS

1. Tables of the peculiarities of wear of bits and defects in DHACs and hard-alloy inserts were compiled according to the IADC classification.
2. Criteria of reparability were determined for the three types of worn-out bits: steel welded bit (Ukraine), bit with an all-milled steel body (Russia), and bit with a die hard-alloy body (USA).
3. The main types of wear of PCDC bits in fields are as follows: wear of cutters (17 %), break of cutters (30 %), spalling of cutters (31 %), fallout of cutters (3 %), and absence of wear (19 %).

1. Codes of wear of diamond bits. <http://vbs-service.ru>
2. Classification of bits by wear character. <http://vbs-service.ru>
3. (2009) We sell PDC bits. Company UNITOOLS. <http://www.unitools.ru>
4. Kortés, A.R. (1999) *Welding, cutting and brazing of metals*. Moscow: Arfa SD.
5. Lindberg, R.A., Braton, N.R. (1976) *Welding and other joining processes*. Boston: Allyn & Bacon.
6. (1978) *Welding in machine-building*: Refer. Book. Vol. 1. Ed. by N.A. Olshansky. Moscow: Mashinostroenie.
7. Glizmanenko, D.L., Evseev, G.B. (1954) *Gas welding and cutting of metals*. Moscow: Mashgiz.
8. Nikolaev, G.I., Olshansky, N.A. (1974) *Special welding methods*. Moscow: Mashinostroenie.
9. Bogdanov, V.N., Ryskin, S.E. (1965) *Application of through induction heating in industry*. Moscow; Leningrad: Mashinostroenie.
10. (2007) *Handbook on brazing*. Ed. by I.E. Petrunin. Moscow: Mashinostroenie.

THERMAL SPRAYING OF COATINGS USING TIPS

A.P. MURASHOV

E.O. Paton Electric Welding Institute, NASU, Kiev, Ukraine

Application of special tips in thermal spraying reduces the number of uncontrolled factors influencing the process, increases the speed of jet outflowing, lowers the degree of its interaction with the ambient atmosphere, and reduces the opening angle. The paper gives recommendations for designing the tips, and shows their effectiveness at coating deposition.

Keywords: *thermal spraying, coatings, application of tips, high-temperature gas jet, speed distribution, average temperature of the field, sprayed particles, gas-dynamic effect*

Thermal spraying (TS) of coatings refers to unique technology which allows obtaining and applying the coatings from metals, ceramics, plastics and their combinations [1]. Such possibilities of TS predetermined the development of the process, creation of large number of spraying devices, development of spraying consumables, obtaining of the layers with multiple functional properties, i.e. from wear-resistant, antifriction, heat-resistant, insulating etc. up to coatings with the nanostructures, with specified porosity and other special properties [2–6].

Coatings in TS are formed from separate particles due to their chemical and physical activity rising in heating and acceleration. The particles in such an active state can interact with elements of the spraying jet, ambient gas atmosphere and substrate. Oxidation of the spraying consumables, the degree of which is determined by many factors including method of spraying, is possible due to its activity.

Oxidation of the coating material takes place in spraying of wire by air, during particle flight

and formation of the coating [7] in the case of application of simple electric arc metallizing. Methods of wire spraying using inert gases were developed for protection from oxidation and reduction of amount of oxygen in the coating. Methods of activating (Figure 1) and supersonic metallizing [8–11] had appeared.

Application of shielding or reducing atmosphere promotes increase of quality of coating due to reduction of oxide content in the electric arc metallizing, and decreases time of particle flight, reduces possibility of interaction of surface of heated particles with atmospheric oxygen and increases coating density in the supersonic metallizing.

High velocity oxy-fuel and detonation spraying are characterized by small interaction of the spraying material with ambient atmosphere due to application of a tip in a form of shank and supersonic speed of spraying particles. However, the application of combustion materials of fuel gases and oxygen for heating and acceleration of the particles promotes the conditions for interaction of materials with oxygen of spraying atmosphere.

Excess of gases is used for reduction of oxidation degree, a reducing medium is created, however, it can sometimes be impossible on technological reasons.

Pressure is created in a plasmatron at outflowing of high-temperature plasma jet from it to stable ambient atmosphere due to thermal contraction of arc and jet. It exceeds the pressure of environment at exit from the plasmatron. This result in jet expansion, moreover, it expands quicker at very edge of the plasmatron than at the rest of the section where pressure difference gradually decreases [12]. Turbulent mixing and viscous friction of the spraying jet leads to increase of content of ambient gases in it, areas with temperature and speed gradient appear in radial section of the jet. The heated and accelerated to different extent particles from spraying

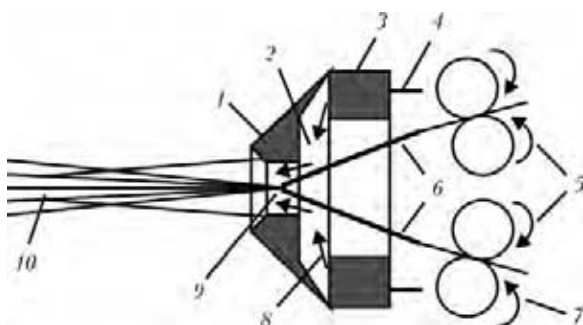


Figure 1. Scheme of activating electric arc metallizing [8]: 1 – nozzle; 2 – collector; 3 – combustion chamber; 4 – mixture of air with combustible gas; 5 – feeder; 6 – guides; 7 – wires; 8 – spraying gas; 9 – arc; 10 – jet

material, predicted synthesized combinations and phases take part in coating formation. They can have uncontrolled interaction with the gases of ambient atmosphere. Such an interaction can be referred to the uncontrolled factors having influence on content and properties of the coating obtained in free outflowing of jet (submerged).

Degree of expansion of the jet is determined by difference of pressure of flows in presence of assist gas as in the first case. The degree of mixing of gas atmosphere reduces at insignificant difference of pressures in flows, and gas shield of the main jet is formed. An intermediate layer developed at feed of the assist gas does not eliminate the possibility of admixing of ambient atmosphere in it, but limits or protects the spraying jet from interaction with the atmosphere components.

Protection of a tip from entering of ambient atmosphere in it and consequent mixing is provided at application of the tip and shielding assist gas. At that risk of formation of fields with large temperature and speed gradient is reduced. Figure 2 shows that application of the tip results in increase of average flow speed, and reduces gradient of the speed and enthalpy on cross-section of the jet in the center and on the periphery.

Possibility of interaction of the spraying jet with the ambient atmosphere determines the possibilities of coating deposition with and without tip application. Properties of the spraying jet as well as type of sprayed material are considered at that. Powders for spraying can contain particles of different size and shape or consist of particles with different density.

It is known fact that a flow force effect on particle R is determined by density ρ , flow speed v , coefficient of gas-dynamic (head) resistance C_d and effective area of influence S_p :

$$R = C_d \rho v^2 / 2 S_p.$$

Shape of the particle determines its coefficient of head resistance. A degree of nonsphericity Φ was proposed to be used for the particles of non-round shape by R. Busroid [14]. It is determined by ratio of surface area of sphere with volume, equal to particle volume V_p , to surface area of particle, increase of which promotes rise of coefficient of head resistance:

$$\Phi = \pi(6V_p/\pi)^{2/3} S_p^{-1}.$$

Gas-dynamic effect of the jet on the flake-shape particles can promote appearance the side constituents at their different orientation besides the change of their coefficient of head resistance and acceleration. As a result of that part of them get into the jet periphery. This reduces the level

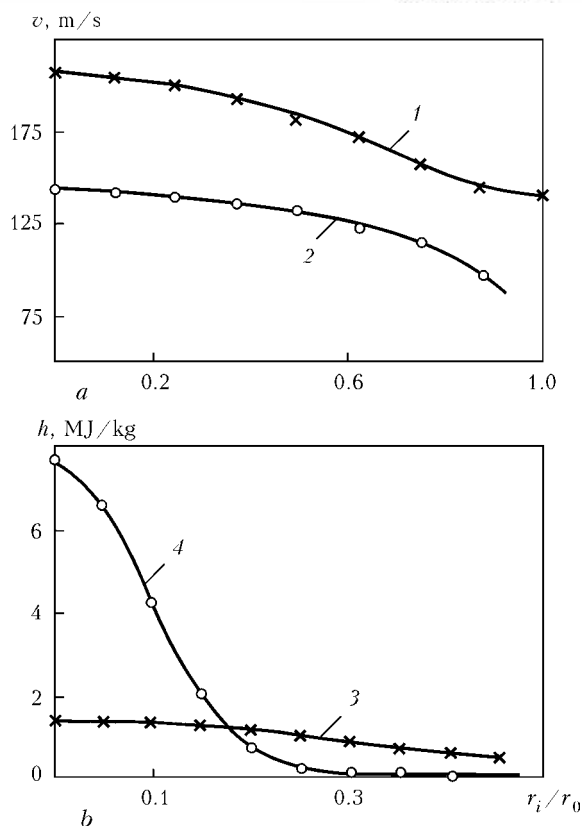


Figure 2. Distribution of speed (a) and enthalpy (b) of particles on radius of spraying spot in application of tip (1, 3) and without it (2, 4) [13]

of heating of such particles, effects their acceleration, and predetermines appearance of the cold particles in the coating structure that reduces coating quality at application of the submerged jet. If insignificant difference of heating and acceleration of the particles of different shape is provided at control of the process in coating spraying using spherical powders, then number of cold or oxidized particles has uncontrolled rise, quality of coating decreases and material utilization is reduced in use of fragment or flake-shaped particles.

Interaction of the jet with ambient gases is limited or prevented, temperature and speed of the jet on cross-section are adjusted and length of high-temperature field are increased at application of the tip and assist shielding gas. This influences the degree of heating and acceleration of the particles, in particular, the particles with large size differences, various density or irregular shape.

The negative moment of the tip equipping lies in impossibility of visual control of consumption of a transporting gas with powder on the shape of spraying jet, possibility of pickup of consumable on a side surface of the tip with formation of «accretion» and inflow of cold air inside the tip. These disadvantages result in inconvenience

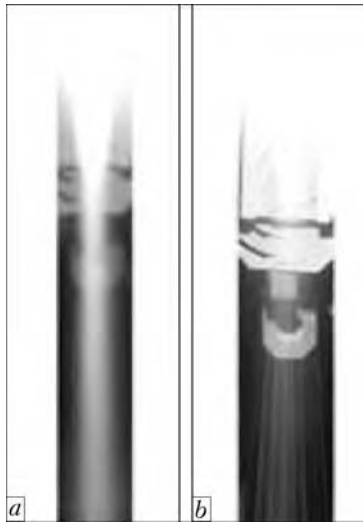


Figure 3. Appearance of plasma jet in spraying of metallic (a) and ceramic (b) powders

of operation, impair technological effectiveness of the process and limit application of the tip in industry.

Works [15, 16] show the schemes of existing tips. Consideration of structure, classification of tips on economy and technological indices and analysis of their peculiarities and efficiency of shielding were carried out.

Variant of the tips with feed of shielding gas in its lower part and extraction of gas are shown in [13]. Such a solution as well as application of «hot internal wall» reduce content of oxygen in the coating and allow increasing the average speed and temperature of sprayed particles.

Study [17] shows a tip designed for increase of outflowing speed of spraying jet and reduction of inflow of ambient atmosphere inside the tip. Larger consumption (more than $90 \text{ m}^3/\text{h}$) of periphery gas is necessary for providing its functions based on operation experience.

It is impossible to remove a deposit of the consumables on the side walls of the tips, as well as inflow of the ambient atmosphere inside the tip in the mentioned tip structures.

Thus, there are no criteria for designing of the shielding tips determining optimum structure, its capability to provide increase of coating quality through reduction of a level of material oxidation due to absence of the cold particles in its formation. An attempt was made in the present work to develop a tip, the design of which would provide quality spraying of the coatings without pickup at opening angle, equal or smaller than opening angle of spraying submerged jet, would reduce or eliminate the presence of cold particles in the coating and would decrease oxygen content in the coating. Besides, it was planned to increase the speed of jet outflowing and speed of sprayed particles.

Experience of designing of tip structures [15, 16] as well as mechanisms of outflowing of gas jets, given in the studies on gas dynamics [18, 19], was used for selection of tip shape. Inner surface of the tip should represent itself contracting and expanding cone in order to increase speed of gas outflowing. A cylinder surface with supply of assist gas can be used as a contracting one. The gas entering the cone forms a wedge at operating consumptions. At that critical section can be created and condition for jet acceleration is provided. Besides, it was assumed that feed of the assist gas would form a wall gas layer and protect inner surface of the tip from consumable pickup, and presence of excessive pressure in the layer would prevent entering of atmosphere gases inside.

Angle of expansion of the conical part was taken considering the shape of spraying jet obtained for the case of spraying of metallic and ceramic powders at free outflowing of the plasma jet. Figure 3 shows the type of spraying jet at application of PT-NA-01 (95Ni + 5Al) powders of $+(10-45) \mu\text{m}$ fraction and Al_2O_3 electrocorundum of 15A grade with $28 \mu\text{m}$ average particle size. Opening angle of the jet makes 4 and 8° , respectively. Inner diameter of the cylinder part equals 12–14 mm and length was 15 mm. Opening angle equal 6.5° was taken for the conical part. Its minimum inner diameter was 0.5 mm larger than inner diameter of the cylinder part. At that cross sizes of the cone equal the sum of jet diameter in this section and size of 1.0–1.5 mm gap for feed of the assist gas.

Length of the tip makes 90 mm that gives the possibility of process control and reduces the risk of jet interaction with the ambient medium at 100–140 mm distance normally used for spraying.

The assist gas was supplied on a circle owing to sampling at the nozzle (Figure 4) for the purpose of formation of evenly distributed wall layer.

Cylindrical part in one of the variants was made in a form of insulating insert that eliminated a possibility of formation of arc between the cathode and anode. However, application of argon or argon–nitrogen plasma forming medium provides no arc formation.

Increased consumption of the transporting gas is set at transportation of fine powder or powder with poor flowability due to possibility of formation of «clogs». The value of speed of particles, at which they can fly past central part of the jet, is achieved at outlet of the feed connection, the diameter of which significantly smaller the internal diameter of powder pipeline. The particles

can pickup to the inner surface of the tip or fly past the heating zone and take no part in coating formation entering periphery of the jet.

A feed flow at increased consumption of the transporting gas was preliminary divided into two channels for reduction of speed of powder particles at its feed in the plasmatron. Powder was introduced in the plasmatron by channels through two connections [3], symmetrically situated in one plane with jet axis. The powder was fed in a cross point of jet axis and edge line of the plasmatron at $-(6-30)^\circ$ towards the main jet in order to increase heating efficiency and eliminate particle pickup. Separate feed of the powders in different points was used in spraying of the coatings from mixture of powders having different melting temperature, for example, from metal and ceramics. Points of powder feed were preliminary determined using a program for calculation of flying path and particle temperature.

Conditions for feed of metallic (Ni) and ceramic (Al_2O_3) powders were preliminary selected based on computer model of process of plasma spraying carried out with the help of CASPSP system [20].

Path of the particles for the case of entering of metal particle at $-(6-30)^\circ$ and ceramic particle at -30° in consumption of $0.12-0.18 \text{ m}^3/\text{h}$ of transporting gas was located in the central area of the jet that corresponds with the condition of their heating from solid state up to melt. At that melting of the particles takes place at around 20 mm distance from nozzle edge.

A double feed system for ceramic and metallic powders containing two feeders and two channels with two inputs was used for obtaining of the coatings including metallic and ceramic constituents. This allows depositing the coatings from metals, ceramics and their compositions and obtaining gradient coatings with 0–100 % component content.

Testing of inner surface of the tip showed no pickup of consumables on the side wall. At that, general consumption of the transporting gas

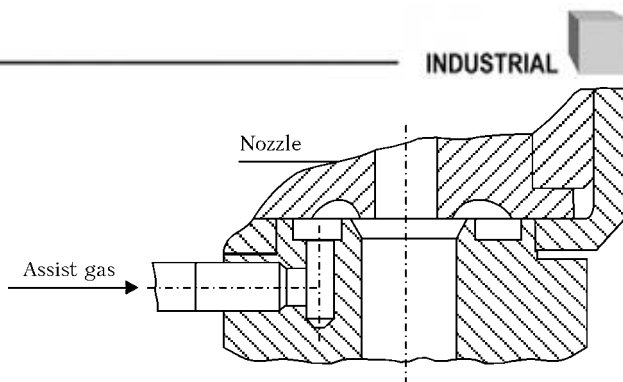


Figure 4. Scheme of feed of assist gas in a tip

made $0.168-0.270 \text{ m}^3/\text{h}$ that 2 times exceeds its value at spraying without tip with one connection. Consumption of the assist gas made $0.28-0.30 \text{ m}^3/\text{h}$.

The pickup of part of the particles takes place on inner side of the tip at consumption of assist gas not less than $0.18 \text{ m}^3/\text{h}$ and transporting gas not less than $0.12 \text{ m}^3/\text{h}$ or more than $0.36 \text{ m}^3/\text{h}$, and is observed in a contraction point where cylinder part of the tip comes into conical one (Figure 5).

It can be assumed that getting in of the part of consumables at jet periphery, where obtained speed and temperature of the particles are enough for formation of the deposit on a barrier (contraction), can be the reason of pickup. Half-molten, loose state of the deposit material proves this fact. At that the coating sprayed on the sample is dense and has little defects on the boundary with substrate.

Increase of consumption of the assist gas more than $0.48-0.60 \text{ m}^3/\text{h}$ results in «cooling» of the jet that gains number of «cold» particles and reduces of material utilization.

Figure 6 shows appearance of a spraying spot without and with tip application. The spraying spot with tip is 1.5–2 times larger than that in spraying without tip with the same material and distance. This indicates reduction of spraying angle in tip application. Level of interaction of coating material and environment characterizes the coating besides the difference of the spraying spot sizes.

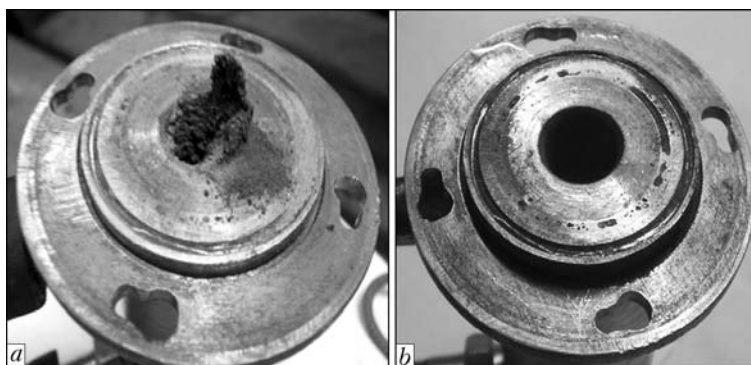


Figure 4. Appearance of lower part of tip after spraying at consumption of transporting gas 0.360 (a) and 0.264 (b) m^3/h

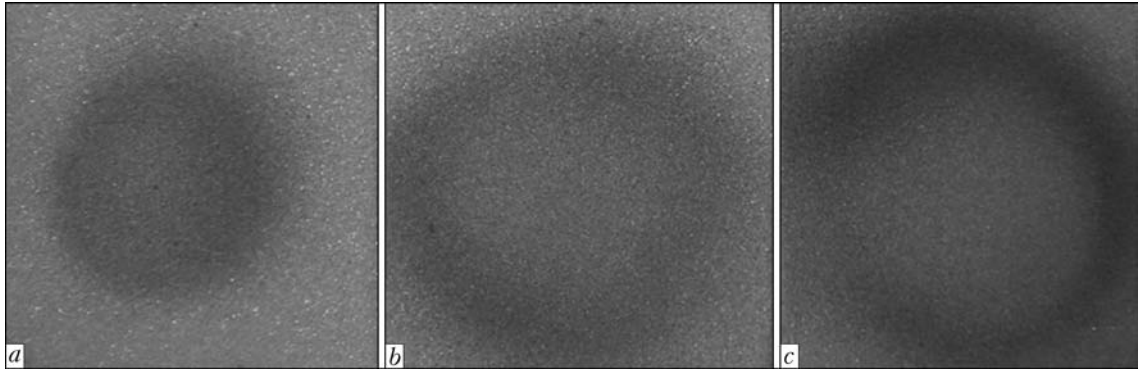


Figure 6. Spraying spot in coating with application of tip (a), cylinder part of tip (b) and without it (c)

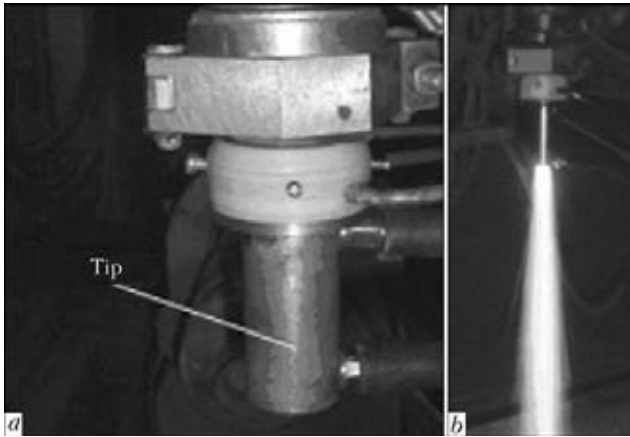


Figure 7. Appearance of tip (a) and spraying jet (b) with application of PT-NA-01 powder

Traces of powder oxidation at spot periphery are observed in the spraying spot obtained without shielding tip application. The coatings obtained with the tip application have no observable places of oxidation. This verifies absence of oxidation medium inside the tip and air inflow.

The spraying jet has cone shape with angle close to angle of tip inner surface at more than 250 mm distance from tip edge (Figure 7) in coating of metallic powder, for example, PT-NA-01 with 10–45 μm size having round shape. Jet cone in spraying of fragment-shaped aluminum oxide powder of average fraction 28 μm preserves its configuration at 50–60 mm distance from nozzle edge, after which expansion angle increases by 12° and more.

CONCLUSION

The inner surface in designing of the tip is recommended to be made in a form of expanding cone with up to 8° angle in order to increase jet outflowing.

Shape and dimensions of the tip inner surface, density of powder material, size and shape of its particles determine the opening angle of spraying jet. Angle made 4–6° and is preserved at 250 mm or more length in spraying of metallic powders

with round-shaped particles. Opening angle increases up to 8° for ceramic powders having fragment-shaped particles. At that opening angle of the jet increases after jet exit from the tip and makes 12° or more at distance of spraying more than 120 mm.

The inner geometry of the tip should be close to the shape and dimensions of the submerged jet, obtained in spraying of spherical powders, for elimination of inflow of ambient atmosphere inside the tip and interaction with the jet. Application of assist shielding gas and development of excessive pressure in the tip are recommended. Ratio of consumptions of assist and transporting gases determines the pickup of consumable on the tip inner surface. Consumption of assist gas should make not less than 0.28 m³/h for the tip with 6° opening angle.

1. Krechman, E. (1966) *Spraying of metals, ceramics and plastics*. Moscow: Mashinostroenie.
2. Hasui, A. (1967) *Technique of spraying*. Moscow: Mashinostroenie.
3. Kudinov, V.V. (1977) *Plasma coatings*. Moscow: Mashinostroenie.
4. Tsvetkov, Yu.V., Panfilov, S.A. (1980) *Low-temperature plasma in repair processes*. Moscow: Nauka.
5. Kalita, V.I. (2005) Physics, chemistry and mechanics of formation of coatings strengthened with nanosized phases. *Fizika i Khimiya Obrab. Materialov*, **4**, 46–57.
6. Suzuki, M., Sodeoka, S., Inoue, T. (2003) Study on alumina-based nanocomposite coating prepared by plasma spray. In: *Proc. of Int. Thermal Spray Conf.* (Ohio, USA, May 5–8, 2003).
7. Korobov, Yu.S., Boronenkov, V.N. (2003) Kinetics of interaction between sprayed metal and oxygen in arc metallizing. *Svaroch. Proizvodstvo*, **7**, 30–36.
8. Dorozhkin, N.N., Baranovsky, V.E., Elistratov, A.P. (1983) Activated arc metallizing process. *Vesti AN BSSR. Series Physics and Technology*, **3**, 73–78.
9. Verstak, A., Baranovski, V. (2004) HVAF arc spraying. In: *Proc. of Int. Thermal Spray Conf.* (Osaka, Japan, 10–12 May, 2004).
10. Karp, I.N., Petrov, S.V., Rudoj, A.P. (1991) Arc metallizing in high velocity flow of methane burning products. *Avtomatich. Svarka*, **1**, 62–65.
11. Buryakin, V. (2004) Improvement of thermal spraying equipment. *Svaroch. Proizvodstvo*, **5**, 30–35.
12. Dresvin, S.V., Donskoj, A.V., Goldfarb, V.M. et al. (1972) *Physics and technology of low-temperature jet*. Moscow: Atomizdat.
13. Kudinov, V.V., Kalita, V.N., Komlev, D.N. et al. (1992) Analysis of distribution of particle velocity

- and specific enthalpy on radius of spraying spot in using of conic orifice. *Fizika i Khimiya Obrab. Materialov*, **5**, 82–85.
14. Busroid, R. (1975) *Gas flow with suspended particles*. Moscow: Mir.
 15. Linnik, V.A., Pekshev, P.Yu. (1985) *Current technology of thermal spraying of coatings*. Moscow: Mashinostroenie.
 16. Kudinov, V.V., Kosolapov, A.N., Pekshev, P.Yu. (1967) Nozzles for providing of local protection in plasma spraying. *Izvestiya SO AN SSSR. Series Technical Sci.*, **21**, Issue 6, 69–75.
 17. Borisov, Yu.S., Korzhik, V.N., Chernyshov, A.V. et al. (1991) Optimization of parameters and conditions of gas-dynamic nozzle application in thermal spraying. *Avtomatich. Svarka*, **8**, 67–70.
 18. Povkh, I.L. (1974) *Aerodynamical experiment in machine-building*. Leningrad: Mashinostroenie.
 19. Abramovich, G.N. (1969) *Applied gas dynamics*. Moscow: Nauka.
 20. Borisov, Yu.S., Krivtsun, I.V., Muzhichenko, A.F. et al. (2000) Computer modeling of the plasma spraying process. *The Paton Welding J.*, **12**, 40–50.

CONTROL OF FORMATION OF WELDED JOINTS IN ESW (Review)

I.V. PROTOKOVILOV and V.B. POROKHONKO

E.O. Paton Electric Welding Institute, NASU, Kiev, Ukraine

Some technological approaches and methods for affecting the process of electroslag welding (ESW), aimed at optimisation of structure of the weld and HAZ metals, are considered. It is shown that the external magnetic fields providing the force effect on the weld pool by a contactless method are an efficient tool to control solidification of metal in ESW. The most effective schemes of electromagnetic control of the ESW process, ensuring homogenisation and refining of structure of the weld metal, are studied.

Keywords: *electroslag welding, solidification, macrostructure, weld, electromagnetic effect, hydrodynamics, magnetic field*

Electroslag welding is an efficient method for joining thick-walled pieces of alloys based on iron, titanium, aluminium, copper and other metals. One of the key advantages of ESW is its high productivity and the possibility of joining metal with thickness from 30 mm to several metres in one pass without groove preparation [1–5].

However, despite the apparent advantages, ESW is often limited in practical application because of the unfavourable effect of the thermal welding cycle and hydrodynamic processes occurring in the weld pool on formation of structure of the weld and HAZ metals. These peculiarities of ESW may lead to formation of a coarse large-grained structure of the weld metal and embrittlement of HAZ, as well as negatively affect properties of the welded joints.

As a rule, heat treatment of the welded joints eliminates heterogeneity of structure and mechanical properties of different regions of a welded joint. However, it makes the ESW process much more complicated and expensive. Moreover, it is often inapplicable for super-large parts. Different approaches are employed to decrease overheating of metal during the welding process. In a number of cases such approaches make it possible to provide the required properties of the

welded joints without postweld heat treatment. However, decrease in the extent of overheating of the weld and HAZ metals was and is one of the key problems of the ESW technology [6].

In this connection, the topical problem of ESW is development of the technological approaches and methods for affecting the welding process, which are aimed at improving structural homogeneity of the weld metal and reducing the negative effect of the thermal welding cycle on the HAZ metal (Figure 1). Such methods are based on adding different modifiers and fillers to the weld pool [3, 7], utilisation of an extra dead wire [8], application of forced cooling of the weld and HAZ metals [9], portioned energy input into the welding zone [10], increase of the electrode extension [11], concurrent heating of the weld and HAZ metals for local continuous normalising [3], introduction of ultrasonic and mechanical oscillations [12], affecting by external magnetic fields [13, 14] and other principles.

Metallurgical methods for increasing the efficiency of ESW are aimed at development of new welding consumables with special strength and thermal-physical properties, which are insensitive to the thermal welding cycle. Also, different modifiers and fillers can be added to the weld pool. Such methods are efficient enough to control properties of the weld metal. However, they exert only a slight effect on the HAZ metal.

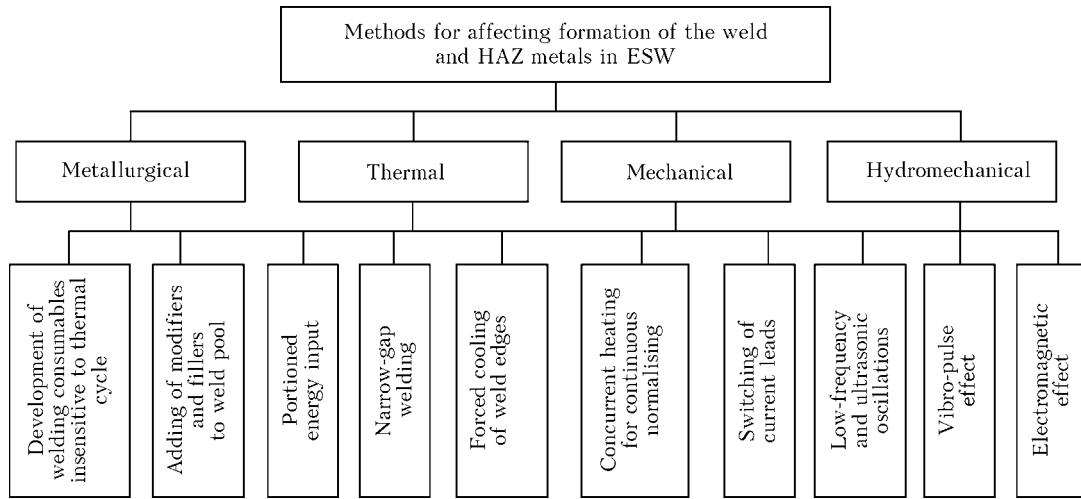


Figure 1. Schematic of technological approaches and methods used to affect formation of the weld and HAZ metals in ESW

Moreover, a change in chemical composition of the weld metal with respect to the base metal is often inadmissible.

Narrow-gap welding is one of the methods for reducing the welding heat input and narrowing the HAZ [15]. This welding method is characterised by decreased volumes of the weld pool and filler metal, and an increased welding speed. The narrow-gap welding process is similar to the standard ESW process. However, it requires the use of additional measures for prevention of short circuiting of electrodes to the weld edges and guaranteed penetration of the base metal.

Study [15] gives investigations results on development of the improved narrow-gap ESW technology to address the machine building problems. The new technology is characterised by reduction of the welding gap to 19 ± 1 mm and utilisation of the specially developed consumable

nozzle with electrical insulators, nickel-molybdenum electrode wire and neutral flux. Parameters of the suggested process and traditional ESW for 50 mm thick steel plates are given in Table 1.

It is noted that the new process is characterised by a high productivity and provides improved fatigue properties and impact toughness of the weld and HAZ metals. The said effects are achieved due to decreasing the heat input, optimising the shape of the weld pool and using the welding wire that improves metal microstructure. As a result, the high quality of the joints is achieved without extra heat treatment.

Based on the comprehensive investigations of properties of the narrow-gap welded joints, the US Department of Transportation issued a memorandum of cancellation of the moratorium on application of ESW in bridge construction [16].

The method of the vibro-pulse effect on the weld pool [12] was proposed for controlling solidification of the weld metal. The point of this method is as follows (Figure 2): the electric current pulses are formed by using the pulse current generator and the capacitor battery, these pulses being fed through the high-voltage discharger to the one-coil inductors located on the copper forming shoes on opposite sides of the workpieces welded. In electrodynamic interaction between the inductor and shoes the working walls of the

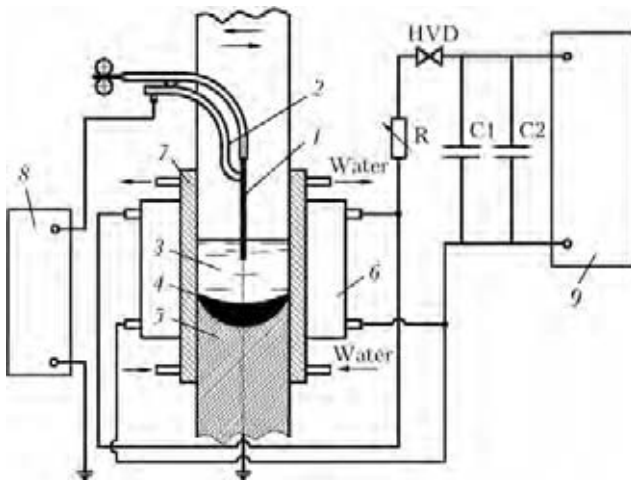


Figure 2. Scheme of ESW with concurrent electric-discharge treatment [12]: 1 – electrode; 2 – current lead; 3 – slag pool; 4 – metal pool; 5 – weld; 6 – inductor; 7 – forming straps; 8 – power supply; 9 – pulse current generator; HVD – high-voltage discharger; C1 and C2 – high-voltage capacitor batteries; R – ballast rheostat

Table 1. Parameters of ESW of 50 mm thick plates [15]

Welding method	Welding gap, mm	Current, A	Voltage, V	Welding speed, mm/min	Heat input, kJ/mm
ESW:					
conventional	32 ± 2	600 ± 100	39 ± 1	28	50
narrow-gap	19 ± 1	1000 ± 100	35 ± 0.5	55	37

latter transfer strong mechanical shocks to the molten metal, which induce periodic hydrodynamic waves in it. Intensive oscillations of the liquid phase with respect to the solid one decrease the temperature gradient at the interface between the phases, inhibit growth of crystals, and disturb periodicity and orientation of dendritic solidification.

The authors give the following explanation to the mechanism of the vibro-pulse effect on the HAZ metal. Like any liquid, the molten metal is hard to compress. Hence, with propagation of a shock wave it hits edges of the base metal, thus causing refining of structure of the HAZ metal. The fusion line loses its clearly defined shape and becomes broad.

It is apparent that in this case, in addition to the mechanical effect on the weld pool imparted by the shoes, there is also the effect exerted by the electromagnetic forces generated as a result of interaction of pulses of the magnetic field with the welding current.

The possibility of refining the weld metal structure and improving resistance of the welded joints to brittle fracture and corrosion was shown by an example of ESW of steels of the VSt3sp (killed), 09G2 and 12Kh18N10T grades with the vibro-pulse effect.

Study [17] suggests the method for high-speed ESW of thick-plate steels of the 22K, 16GNMA, 16GS and other types without subsequent normalising of the welded joints. The point of the method is a forced preset-frequency change of the location where the electric current is supplied to electrodes and weld edges (Figure 3). Switching of current leads during the welding process causes redistribution of flow lines of the current in the weld pool. Besides, this leads to a dramatic change in the character of motion of the slag-metal melt and,

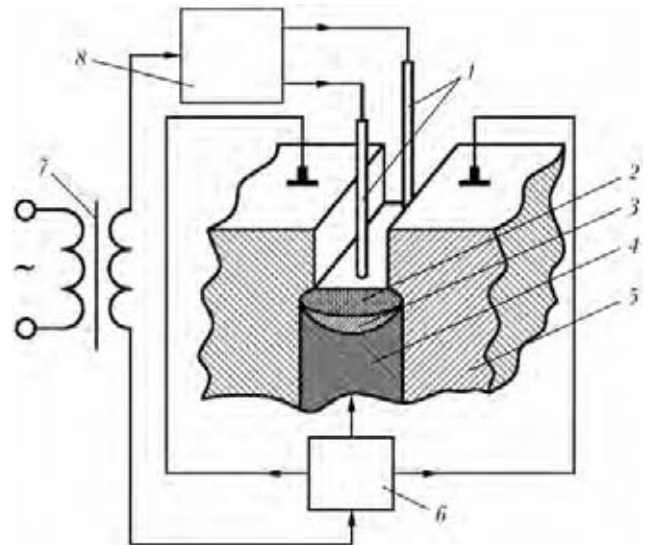


Figure 3. Scheme of high-speed ESW [17]: 1 – electrodes; 2 – slag pool; 3 – metal pool; 4 – weld; 5 – workpiece; 6 – three-channel current transducer; 7 – power supply; 8 – two-channel current switch

hence, the balance of temperatures in the pool. The larger part of the energy goes to melting of electrodes, and the smaller part is transferred to the base metal. All this increases the rate of melting of the electrodes from 3 to 4 times and minimises the extent of removal of heat to walls of the base metal. It is noted that the specific energy input of the process is 25–50 kJ/cm², which is 4–5 times lower than in conventional ESW (104–208 kJ/cm²). In addition, the thermal cycle of welding becomes close to that of the submerged-arc welding process.

Investigations of the welded joints on thick-plate steels of the 22K, 16GNMA, 16GS and other types, made by using the developed high-speed ESW process, showed improvement of macrostructure and mechanical properties of the weld and HAZ metals, which excludes the use of post-

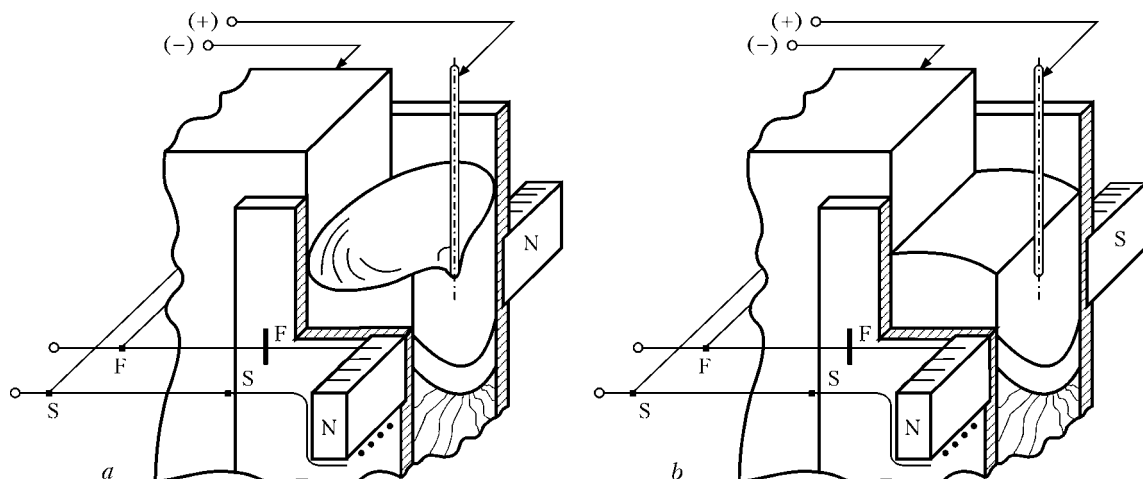


Figure 4. Schemes of ESW with electromagnets mounted on forming shoes with series (a) and opposite (b) connection of windings: S, F – start and finish of windings [14]

Table 2. Recommended parameters for ESW of steel 12Kh18N10T [14]

Welding wire	Metal thickness, mm	Parameters of welding and control magnetic field			
		I_w , A	U_w , V	B , mT	t_r , s
Sv-06Kh19N9T	23–35	550–600	Not more than 55	18–20	0.32
Sv-06Kh19N10M3T	23–35			18–20	0.32
Sv-06Kh19N10M3T	23–35			25–35	0.08
Sv-06Kh19N9T	35–45			25–35	0.32
Sv-05Kh19N10F3S2	45–60			35–45	0.32

weld high-temperature heat treatment of the welded joints.

Study [14] describes investigations of the methods of affecting the electroslag process by using the external (reversing) magnetic fields. It is noted that electromagnetic stirring of the molten pool for the ESW conditions can be provided by using the magnetic fields induced by a solenoid located on a rod electrode, by electromagnets located on the shoes, or by a welding cable passed through the gap.

It is shown that the most rational scheme of the electromagnetic effect in ESW is the use of electromagnets with a single-bar core mounted on the forming shoes (Figure 4). In this case the magnetic field penetrates the entire melt of the weld pool and affects a change in the thermal state of metal and slag.

Investigations were carried out by using carbon and austenitic steels with thickness $\delta = 20\text{--}60$ mm in the reversing magnetic field with induction $B = 5\text{--}45$ mT and reversing interval $t_r = 0.08\text{--}0.32$ s.

The welding parameters, including magnetic induction and reversing time, providing the electroslag process with no violation of its stability were developed. It was found that the reversing magnetic field tolerates a higher limiting value of induction compared to the unidirectional field.

It is noted that violation of stability of the process is promoted by formation of a paraboloid of revolution under the effect of the unidirectional magnetic field. The matter is that the metal pool becomes exposed near the apex of this paraboloid, which leads to the arc discharges induced between the electrode tip and surface of the metal pool.

The recommended parameters of the magnetic field and welding process for steel 12Kh18N10T are given in Table 2.

Metallographic analysis of the welded joints showed that structure of the welds made under conventional welding conditions differs substantially from that of the welds made by using the magnetic field. Their common property is a smaller transverse size of crystalline grains. Structural analysis of the welds on steel 09G2S showed both a change in shape of the inclination angle of crystalline grains and decrease in their cross section.

The main criterion for evaluation of properties of the weld metal was impact toughness, which was determined for different temperatures depending on the steel grade. Analysis of the obtained data allowed distinguishing the range of parameters of the control magnetic field in which the impact toughness of the weld metal can be increased 2–3 times, and its values can reach the

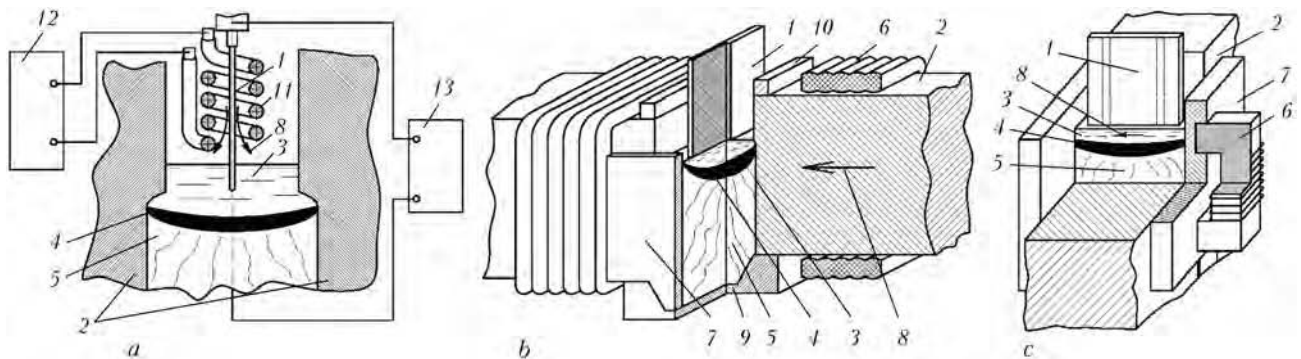


Figure 5. Scheme of ESW in longitudinal (*a*) and transverse (*b*, *c*) magnetic fields: 1 – consumable nozzle-electrode; 2 – workpieces welded; 3 – slag pool; 4 – metal pool; 5 – weld; 6 – electromagnetic device; 7 – forming straps; 8 – magnetic field lines; 9 – inlet pocket; 10 – runoff tabs; 11 – solenoid; 12 – electromagnetic system power supply; 13 – welding current power supply

level achieved in the weld as a result of high-temperature treatment.

Study [13] generalises the data on control of the hydrodynamic situation in the metal and slag pools by using the natural and external magnetic fields. It is shown that the electromagnetic forces have a decisive effect on hydrodynamics of the weld pool and formation of structure of the weld metal and properties of the welded joints. The methods for exerting the electromagnetic effect in ESW, based on inducing the electric vortex flows or vibration of the melt by using the longitudinal and transverse magnetic fields are suggested on the grounds of the conducted fundamental and applied research (Figure 5).

The effect by the longitudinal magnetic field (Figure 5, *a*) allows an efficient control of formation and detachment of the electrode metal drops. However, a drawback of the method is that it is difficult to induce in the pool the longitudinal field of a sufficient induction, which limits its application for controlling the metal structure. The transverse magnetic fields are more efficient for these purposes (Figure 5, *b*, *c*).

The welding scheme shown in Figure 5, *b* is used for welding with compact welds. In this case the electromagnet coils are mounted on the workpieces welded, which simultaneously perform the function of the magnetic cores. This makes it possible to achieve the high values of induction of the magnetic field in the welding zone. However, this scheme of affecting is hard to implement in welding of large-size parts and parts of a complex configuration.

In welding with the extended welds it is reasonable to use the magnetic system located on opposite sides of the workpieces welded, near the water-cooled shoes, and moving along the edges at a welding speed (see Figure 5, *c*). In this case, interaction of the axial component of the alternating welding current with the constant magnetic field causes vibration of the melt of the weld pool across the edges. Such reciprocating motions of the melt in a two-phase region promote homogenisation and refining of structure of the weld metal. Transverse vibration in the welding gap also adds to increase in penetration of the weld edges, thus allowing the welding energy input to be decreased. A drawback of this method is dissipation of the magnetic field because of a considerable size of the gap between the electromagnet poles determined by thickness of the workpieces welded and water-cooled shoes. Accordingly, efficiency of the electromagnetic effect decreases with increase in thickness of the workpieces.

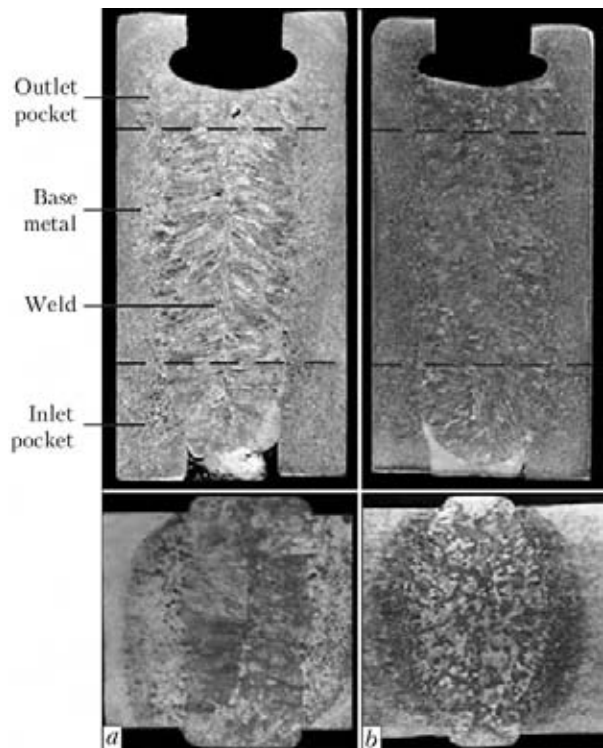


Figure 6. Macrostructure of welded joints on alloy VT1 made without (*a*) and with (*b*) the electromagnetic effect

Later investigations showed a high potential of application of the pulsed magnetic fields for affecting the melt of the weld pool [18]. In this case, coils of the electromagnets are powered by cyclic pulses of the direct current. With this scheme of the electromagnetic effect on the welding melt the possibilities of controlling its hydrodynamics substantially grow. This takes place owing to the possibility of formation of high-power pulses of the magnetic field, as well as owing to restructuring of the hydrodynamic structure of the pool while they are passing. Parameters of the pulses vary over rather wide ranges: magnetic induction of the field — 0.02–0.30 T, pulse duration — 0.3–10 s, and pause duration — 1–20 s. Implementation of this scheme and parameters makes it possible not only to affect the microstructure and chemical homogeneity of the weld metal, but also control its macrostructure (Figure 6).

CONCLUSIONS

Various technological approaches and methods for affecting formation of the weld and HAZ metals in ESW are available now. In a number of cases they are efficient and provide the required properties of the welded joints without postweld heat treatment. Nevertheless, the problems of ensuring the fine-grained, homogeneous structure of the weld metal and decreasing the negative effect of the thermal welding cycle on



the base metal remain among the key ones in the ESW technology.

The magnetic field is an efficient tool for control of hydrodynamics of the weld pool and properties of the welded joints. However, the electromagnetic effect on macrostructure of the weld in ESW requires higher power and weight-dimension parameters of sources of the external magnetic fields. This is a serious obstacle for their practical application. Apparently, the topical problems of increasing the efficiency of ESW are development of the methods for intensification of the electromagnetic effect on the weld pool, and minimisation of the devices for controlling solidification of the weld. Further investigations should be aimed at development of the comprehensive methods for controlling the ESW process based on the hydrodynamic and thermal effect mechanisms.

1. (1980) *Electroslag welding and cladding*. Ed. by B.E. Paton. Moscow: Mashinostroenie.
2. Yushchenko, K.A., Lychko, I.I., Sushchuk-Slyusarenko, I.I. (1999) Effective techniques of electroslag welding and prospects for their application in welding production. In: *Welding and Surf. Rev.*, Vol. 2, Pt 2. Amsterdam: Harwood Acad. Publ.
3. Medovar, B.I., Tsykulenko, A.K., Bogachenko, A.G. et al. (1982) *Electroslag technology abroad*. Kiev: Naukova Dumka.
4. Eregin, L.P. (1999) ESW with consumable nozzle. *Avtomatich. Svarka*, **9**, 44–46.
5. Semyonov, V.M. (2010) *Increase in efficiency of production of large-tonnage structures by electroslag welding method*: Syn. of Thesis for Dr. of Techn. Sci. Degree. Mariupol.
6. Paton, B.E., Dudko, D.A., Palti, A.M. et al. (1999) Electroslag welding (prospects of development). *Avtomatich. Svarka*, **9**, 4–6.
7. Ivochkin, I.I. (1972) Electroslag welding using powdered filler metal. *Svarochn. Proizvodstvo*, **5**, 43–45.
8. Semyonov, V.M., Gulida, V.P., Yakovleva, L.I. (1987) Electroslag welding of 09G2S steel parts 60–140 mm thick by using auxiliary filler wire. *Ibid.*, **2**, 15–18.
9. Kuzmak, E.M., Khakimov, A.N., Efimenko, L.A. et al. (1975) Application of electroslag welding with zonal control of thermal cycles for production of petrochemical equipment of 16GS and 09G2S steels. *Ibid.*, **6**, 16–19.
10. Sushchuk-Slyusarenko, I.I., Lychko, I.I. (1974) *Technique of electroslag welding*. Kiev: Naukova Dumka.
11. Sushchuk-Slyusarenko, I.I., Bryzhenko, F.G., Shabalin, N.N. et al. (1975) Electroslag welding with increased electrode stick-out. *Avtomatich. Svarka*, **5**, 71–72.
12. Dudko, D.A., Kuzmenko, A.B. (1997) Vibro-pulse action on solidified weld pool metal in ESW. *Ibid.*, **11**, 32–36.
13. Kompan, Ya.Yu., Shcherbinin, E.V. (1989) *Electroslag welding and melting with controlled MHD-processes*. Moscow: Mashinostroenie.
14. Kuznetsov, V.D., Kozakov, N.K., Shalda, L.M. (1987) *Magnetic control of electroslag process*. Kiev: Vyshcha Shkola.
15. Krishna, K. (1996) Narrow-gap improved electroslag welding of bridges. *Welding in the World*, **38(11)**, 325–335.
16. (2000) *FHWA Memorandum: Narrow-gap electroslag welding for bridges*. March 20.
17. Bondarenko, O.P., Moskalenko, A.A., Tyukalov, V.G. et al. (1999) High-speed ESW of plate metal without normalizing of welded joints. *Avtomatich. Svarka*, **9**, 28–31.
18. Protokovilov, I.V., Kompan, Ya.Yu. (2010) Electroslag technologies of melting and welding of titanium alloys with controlled hydrodynamic processes. In: *Proc. of Int. Conf. on Titanium in CIS* (16–19 May, Ekaterinburg, Russia), 154–157.

NEW BOOK

(2012) *Metallurgy of Arc Welding, and Welding Consumables* (in Russian). ISBN 978-966-360-203-5. Compiled by I.K. Pokhodnya, A.S. Kotelchuk. Kiev: Akadempriodika, 526 pp.

Book includes 120 articles of associates of Department for Study of Physical-Chemical Processes in Welding Arc at the E.O. Paton Electric Welding Institute of the NAS of Ukraine. This book generalizes the half-century experience of the Department research activity. The presented articles cover a wide scope of problems of metallurgy of the fusion arc welding and development of welding consumables.

Book can be interesting and useful for specialists and scientific-technical staff, as well as for post-graduates and students of higher education institutions, studying the problems of metallurgy of arc welding and dealing with the development of welding consumables.



Kindly send the orders for the book to the Editorial Board of «The Paton Welding Journal»

Phone / Fax: (38044) 200-82-77, e-mail: journal@paton.kiev.ua



6 YEARS ANNIVERSARY OF RUSSIAN-GERMAN REGIONAL LASER CENTRES

The 13th International Specialized Exhibition «Equipment, devices and tools for metal treatment industry» — «Metal treatment-2012» took place at the Central exponential complex «Expocentre» (Moscow, Russia) from May 28 to June 1, 2012.

More than 60 companies demonstrated equipment for laser treatment (cutting, welding, marking and other applications) at the exhibition, among them companies Amada, Bystronic Laser, Ermaksan, LaserMark, Mitsubishi Electric, PRECITEC, Prima Power, ROFIN-SINAR, SISMA, TRUMPF, VANAD, VNITEP, CJSC Laser Complexes, STA IRE-Polus, DB Bulat, OKOiS Ltd., Yunimash et al.

One of the remarkable events of the exhibition «Metal Treatment-2012» was Russian-German seminar «Regional laser innovation-technological centers as a factor of support of the process of modernization of Russian industry». The seminar was devoted to the results of the 6-year joint program of foundation of demonstration centers of laser technologies in the regions of Russia. The participants of the seminar were organizers of Russian-German program of foundation of regional centers for promoting laser technologies in Russia, participants of projects of laser innovation-technological centers (LITC) in the re-

gions, representatives of educational institutions and industrial enterprises.

As a result of project fulfillment financed by the Federal Ministry of Education and Research in Germany (BMBF) and with the support of German producers of laser equipment, 5 LITC were founded in Moscow, St.-Petersburg, Ekaterinburg, as well as in Taganrog and Obninsk.

Prof. I.B. Kovsh, the President of the LAS, presented the overview report about the role of laser technologies in the modern industry, nowadays experiment of their application at the Russian enterprises and the program of development of the system of regional centers for promoting laser technologies into wide industrial practice realized by the LAS. He outlined that mastering of laser technologies sufficiently increases flexibility of enterprises and compatibility of enterprises and gives high economical effect, therefore, such mastering has a serious governmental support in the industrialized countries. For the last 15 years the world volume of production of laser technological installations for machine building almost 10 times increased. Meantime in Russia the realization of innovation potential in the field of lasers is poor and sluggish. The delay in the field of practical use of lasers not only causes a



direct economic loss to the country but also threatens it with exclusion from international cooperation, as far as application of laser technologies and methods abroad has already been foreseen by many branch standards. I.B. Kovsh noted with regret that in the structures of federal authorities the efforts of the LAS to promote laser technologies into the practice of domestic industry as well as to develop the RLITC system, practically do not find any support as well as deficiency of proper state industrial policy does not contribute to these efforts. The laser centers of Hannover and Bavaria, working in the frames of specialized intergovernmental Russian-German agreement about research and technical cooperation in the field of laser and optical technologies, became the real partners of the LAS in the program of foundation of LITS in the regions of Russia.

K.-D. Novitsky, the German coordinator of the project «Regional laser centers in Russia» from the Laser Center of Hannover (LZH), delivered presentation «The results of 6 year cooperation in the field of regional LITS: impressions of the German party». He told about the history of development of network of joint LITS; about purposes and tasks of the project which were worked out by the German party; about the stages of project development; results and prospects of further development of cooperation.

In 1991 the first meeting of Germany and USSR took place with the purpose of cooperation in the field of laser technologies. In 1992 the Agreement between federal governments of Russia and Germany in the field of laser technologies was signed. The first 10 years of cooperation were characterized by the cooperation in the field of research and developments of fundamental character. K.-D. Novitsky characterized this stage of cooperation as «ascents and descents», but underscored that in spite of this about 100 joint research and designing projects in the field of laser technologies were carried out. The year of 2003 was a turning-point when both parties accepted the change of an old paradigm into a new one with the trend towards joint applied projects. The BMBF chose a coordinator of the project in the person of «Technological Center of the Union of German Engineers» (VDI Technologiezentrum) from the German party, which started preparation for the opening of the first Russian-German LITS and, in its turn, chose LZH as a direct performer and partner of the future RLITS.

The organization of LITC in Moscow became the «pilot» project. One of the first steps to its foundation in Russia was a decision of the United

Board on Industrial Policy of the Government of Moscow concerning wide implementation of laser technologies at the enterprises of the city accepted in 2003. In February, 2005 two ministers: A.A. Fursenko, the minister of education and science of Russia, and E. Bulman, the minister of education and research of Germany, signed agreement about «Strategic partnership in the field of education, research and innovations», which made the cooperation between two countries yet stronger. This agreement gave a significant impetus to the cooperation and already in September 12, 2005 A.A. Fursenko and E. Bulman made a solemn opening of LITC in Moscow. From the very beginning, at foundation of the center the direction was taken towards three-dimensional treatment of materials, the need in which, according to the words of K.-D. Novitsky, was and remains high in Russia. «However already by that time we encountered acute deficiency of skilled personnel in Russia working on all the levels, starting from workers and finishing by the qualified engineers and specialists. This is a grave barrier for implementation of high technologies into Russian industry». Therefore, one of the basic tasks of all five regional laser centers is preparation and enhancement of qualification of personnel, connected both directly with the service of lasers and also with management of tasks.

According to K.-D. Novitsky, it was succeeded during the last five years not only to create a real network of regional laser centers, but also to optimize a mechanism of their functioning and interaction. The model of non-profitable organizations was chosen, so-called non-commercial partnership, and the LAS of Russia, regional authorities and institutions became the founders of these LITC. The partners of the project, such companies as TRUMPH, ROFIN, Jenoptik, Scansonic, KUKA, Arnold, CAM-Service, Mars-Lasertechnik, LIMO, not only transfer laser installations proper to the LITC, but also the technologies connected with these installations, actively implement their knowledge at the enterprises of the Russian industry. Equipping of each LITC is individual and depends on needs of industry of each region. Respectively, the volume of financing for each of the LITC was individual. Thus, to found and equip the LITC in Moscow BMBF appointed about 1.16 mln Euro and about 0.4 mln Euro more were appointed from the representatives of the German industry (the contribution of Russian part had to be amounted to 0.54 mln Euro). To found the LITC in St.-Petersburg two countries invested more than



6 mln Euro in 2009 (among them BMBF invested 2 mln Euro).

All five centers are connected with each other and have the same tasks, one of which is consulting enterprises of Russian industry (from small to large ones) with the purpose of modernization of production. Consulting includes questions of practical application of laser technologies both in technical and economical aspects. The list of tasks set before the laser centers includes demonstration of capabilities of laser equipment, assistance in establishment of contacts with developers of laser technologies and manufacturers of laser equipment, development and adaptation of laser technologies for the certain industries, etc. The LITC founded one more trend of activity, i.e. retraining of specialists in the field of use of laser technologies for different fields of industry, laser safety, management in Hi-Tech. And, finally, development and adaptation of technologies of laser treatment of metals and other materials, including those on own specimens of products of the enterprises.

K.-D. Novitsky noted that a number of problems arose during organization and work of LITC in the first turn connected with «very ambitious however sluggishly realized investment promises of the Russian party»; «custom is the absolutely autonomous and difficult-to-predict brake»; difficult hierarchic relations at the enterprises and education establishments.

At the conclusion K.-D. Novitsky outlined that in the field of machine building, nano-technologies and optic technologies Russia is an important and reliable partner in the investigations and attractive market for Germany. And the realized project of creation of the network of the joint Russian-German LITC was recognized as one of the most successful in Germany, it is quite unique, as compared to many realized programs, and aimed at support not of the scientists, but small enterprises in the regions of Russia.

E.B. Kulbatsky, the Chairman of Board of Directors of the Russian-German regional laser centers, the Director General of LITC of Kaluga, stated in his report «Network of Russian-German regional laser centers. Experience in work and prospects» that the network of RLITC is a striking example of successful cooperation between Russia and Germany. He reminded that 25 years ago the USSR was one of the world leaders in developments in the field of laser technologies and equipment. In the 1990s the known reasons caused loss of this position, and now rehabilitation goes slowly. In the recent years Germany took the world leading position among the coun-

tries actively using laser technologies in industry and also supplying modern laser equipment to the market. Development of the network of innovative laser centers in Germany, rendering consultations to the enterprises being concerned and also production services by the job-shop system, organizing training of specialists, development of new technologies, played immense role in it.

According to E.B. Kulbatsky, the peculiarity of created regional LITC is the orientation to small and medium enterprises. LITC had to occupy the position which was occupied before by branch institutes, i.e. to realize the relation between fundamental science, higher establishments and definite industrial enterprises.

E.B. Kulbatsky outlined that the decisive role in foundation of the LITC in the certain regions of Russia lies in the joint work of regional administration namely (but not by federal) and the LAS. Having presented the short review of state of the art of the modern industry of Kaluga region, its innovative potential, E.B. Kulbatsky stated that foundation of the LITC of Kaluga is an economically grounded and prospective project. 40 % of the whole industry of Kaluga region belongs to machine building and metal treatment. Many enterprises of the region were interested in mastering and application of laser technologies.

The Center of implementation of laser and innovative technologies of Kaluga region was founded in October, 2007 in Obninsk. Since November, 2007 it started active cooperation with the enterprises of Kaluga region. Before that time the initiative group conducted active work with the Authorities of Kaluga region, LAS of Russia, LZH, education establishments of Obninsk, the result of which were agreements about the support of activity of the founded Center. Since November, 2008 the enterprise was registered as the «Non-commercial partnership «Kaluga LITC» and included into the network of Russian-German regional laser centers, i.e. infrastructure promoting practical mastering of laser technologies by domestic enterprises. The partners of Kaluga LITC are RASTR-technology (Obninsk), Moscow LITC, LAS, LZH, and also a number of German companies, supplying high-quality laser equipment to the world market. The foundation of Kaluga LITC should help the development of small and medium innovative business of the region.

The Russian-German Laser Center «Non-commercial partnership «UralLITC» was opened in Ekaterinburg in October, 2008. V.T. Komarov, the technical director of UralLITC (Ekaterin-

burg), in his presentation «Programs of improvement of qualification of teachers» made emphasizes not only on the subject of the report, but also on the history of foundation and all kinds of activity of the UralLITC.

The premises for the opening of the center lied in several factors. The investigations, carried out by the Government of Sverdlovsk region showed that (at the moment of opening of UralLITC) about 60 enterprises of Sverdlovsk region have already used laser equipment in their production, about another more 100 enterprises needed it. The RTsL Company, the regional center of metal sheet treatment, equipped with the modern laser technological installations, successfully works in Ekaterinburg. The decision to found a regional LITC in Ekaterinburg was taken in the Ministry of Industrial Energy of Sverdlovsk region which was succeeded by negotiations between the directorship of the LAS and LZH. The guarantees of these organizations as to the support of the project «UralLITC in Ekaterinburg» were a very important argument for the ministry during taking the decision about including of this project into the regional program of foundation of centers of new technologies. The founders of the project were UralNITI, CJSC «Regional center of sheet treatment» (Ekaterinburg) and Moscow LITC. The German party transferred to UralLITC the multi-functional five-axial laser installation TRUMPF LASERCELL-1005 of the cost of several hundreds thousand Euro for temporary use. Then, when it turned out that the project of foundation of the center in Ekaterinburg was carried out successfully, LZH in May, 2009 transferred this installation to irrevocable use as the technical support. On the order of the region enterprises the UralLITC is developing the new technologies of volume laser treatment for use in production of aircraft engines and mine-rescue equipment, in transport, chemical and heavy ma-

chine building, in power engineering, processing industry, construction. When necessary, these technologies are accompanied by manufacture of pilot batches of products. Among the partners of UralLITC were OJSCs Aviadvigatel, Permsky motorny zavod, DB Novator, Ural plant of transport machine building, Ural mine-metallurgy company and many other.

In conclusion of work of the seminar, Prof. I.B. Kovsh noted that the experience of work of regional LITC clearly evidence about high efficiency of these centers in stimulating practical mastering of laser technologies in their regions, definite assistance to the enterprises implementing these technologies. Without substitution of the existing specialized research institutes, labs of higher educational establishments and operating areas of laser processing, the regional LITC facilitate the use of their potential, provide access of enterprises also to the laser technologies, which are in deficiency in the region, and become bases for the preparation of modern personnel. Small and medium enterprises in particular feel acute need in such centers. I.B. Kovsh outlined that key moment for foundation of the regional LITC is the purchase of modern laser equipment for it. Relatively high cost of such equipment (about 500,000 Euro for technological complex) requires purposeful financial assistance for the laser center. As the experience showed, after mastering of laser technologies and considerable widening of their industrial capabilities, the increase of volume of taxes paid by enterprises of the region will compensate budget costs with a high profit. Therefore, the use of budget funds for financial assistance for foundation of regional LITC is completely justified.

Eng. A.V. Bernatsky, PWI



INTERNATIONAL SEMINAR «MATERIALS SCIENCE IN EU PROJECTS»

International Seminar «Materials Science in EU Projects» was held on September 6, 2012 at the E.O. Paton Electric Welding Institute. Organisation of this Seminar is a result of cooperation of the European Commission, Ukrainian State Agency for Science, Innovations and Informatisation (USASII), and the E.O. Paton Electric Welding Institute of the NAS of Ukraine (PWI).

The Seminar was attended by representatives of a number of research institutes of the NAS of Ukraine, as well as Dr. A. Stalios, the expert of the European Commission, and E.P. Dubinsky, the First Secretary of the European Commission in Ukraine. The Seminar had the form of presentations and sharing of opinions between the participants on each presentation.

By opening of the Seminar, Prof. B.V. Grinyov, the first Vice-Chairman of the USASII, academician of the NAS of Ukraine, noted that the topicality of the Seminar was caused by the need to inform Ukrainian scientists of the results and prospects of development of the 7th Framework Program of the EU for the scientific and technical cooperation (FP7). Also topical is rendering the information support in the field of preparation of project materials to obtain funding under FP7 in 2013–2020.

In his paper «Development of Science, Technology and Innovations in Ukraine», Prof. Grinyov presented the data on structure of investigations and financial aspects of activities of the research institutions of Ukraine, as well as the dynamics of innovation indicators during a period from 2000 till 2011, and briefly described the priority areas of development of science and technology in Ukraine for a period of up to 2020.

The information on PWI achievements in the field of fundamental research and development of advanced welding and special metallurgy technologies was presented by Prof. K.A. Yushchenko, academician of the NAS of Ukraine. In his paper he noted the topicality of development of the mutually beneficial cooperation of scientists of Ukraine and EU in FP7 collaborative projects.

Presentation «The 2012 SICA results. The NMP 2013 Framework Programme & the Horizon 2020» by Dr. Stalios caused the highest interest. The presentation comprised the information on

organisational structure of FP7, results of accomplishment of the Specific International Cooperation Actions (SICA) projects in 2012, as well as prospects for funding the projects in a period of 2013–2020. Dr. Stalios noted that Ukraine belongs to a category of the «International Cooperation Partner Countries» (ICPC), for which two mechanisms of participation in FP7 are applicable.

The first mechanism implies participation of Ukrainian scientific teams in a competition of collaborative projects together with organisations of the EU member-countries or associated countries (minimum three freelance legal entities from different member-countries or candidates to EU). To participate in the competitions, in the majority of cases it is necessary to form a consortium or join an existing consortium.

The second mechanism implies involvement in SICA. SICA are intended to solve the problems facing Ukraine or other ICPC or have the global significance. Addressing these problems should be of mutual interest and benefit both for the EU countries and for Ukraine. The minimal quantity of participants to form a consortium is four freelance legal entities, out of which two should be from the EU member-countries or associated countries, and two – from Ukraine (or other ICPC).

5 main programmes are distinguished in the FP7 structure: Cooperation, Ideas, People, Capacities, and Nuclear Research. About two-thirds of the total FP7 budget is allocated for the «Cooperation» programme.

The speaker briefly dwelt on the main types of projects used to implement FP7. There are six types of the projects or funding schemes:

- collaborative projects providing for funding of two types of the projects – large-scale integrating projects and small- or medium-scale focused research projects;
- collaborative projects for SICA dedicated to ICPC;
- research for the benefit of specific groups, such as small or medium enterprises;
- coordination and support actions;
- network of excellence (NoE);
- support for training and career development of researchers.

Dr. A. Stalios presented the data on organisational and financial aspects of performance of the work in 2012 under SICA. Out of the ten main themes of international cooperation under SICA, the speaker dwelt in detail on a theme that is of interest to the materials scientists – «Nanosciences, Nanotechnologies, Materials and New Production Technologies» (NMP).

In 2012, 13,752 Million Euro were allocated to perform the work under the SICA NMP.2012.2.2-3 programme. Out of 23 projects submitted for competition only four projects that involve 13 research and production teams from the ICPC (Ukraine, Armenia, Georgia, Belarus) successfully passed all the stages of selection.

The given indicators make it possible to estimate substantial difficulties which the submitted projects have to overcome to pass all the stages of the competitive selection. Most of the submitted projects are estimated by the 2-stage procedure. At the first stage the eligibility is estimated in the remote mode, i.e. the estimation is made by limited criteria (scientific and technological quality, expected results). At the second stage the complete forms of the submitted proposals are subjected to the comprehensive analysis by experts, members of the programme committee

and funding commission, and after consultations, reconciliations and discussions a decision is made on funding or rejection of the projects.

In 2013, to realise the «Integration» action projects NMP.2013.4.0-5 «Deployment of socially beneficial nano-and/or materials technologies in ICPC» that provide for involvement of the East-European Partnership countries it is planned to allocate about 13.9 Million Euro, out of which approximately 4 Million Euro will be allocated to fund the projects corresponding to the «Materials» action NMP.2013 2.1-1.

By analysing the prospects of development of the FP7 «Horizon 2020» programme, Dr. Stalios noted three priorities which the projects submitted to the competition should correspond to – excellent science, industrial leadership, and social challenges. The planned scope of funding to realise the projects in 2014–2020 is about 80 Million Euro.

By summarising results of the Seminar, Prof. B.V. Grinyov marked its topicality and usefulness for further development of cooperation of the Ukrainian and EU scientists in collaborative projects under the SICA.

Prof. I.V. Zyakhov, PWI

MODIFICATION OF WELD METAL ON STEELS 14KhN3A AND 20KhN3A TO IMPROVE SERVICE PROPERTIES OF DRILL BITS

The research work on the above subject was completed in 2011 at the E.O. Paton Electric Welding Institute (supervisor – Prof. O.K. Nazarenko)

Conventional steels 14KhN3A and 20KhN3A used in structures of rolling drill bits have limited weldability, and properties of metal of the welded joints on these steels in a number of cases do not meet the high-speed drilling conditions. If design of the diamond bits requires a combination of steels 40KhN and 14KhN3A, this makes the process of manufacture of the bits much more complicated. Increase in sizes of the bits and, at the same time, thicknesses welded raises the probability of formation of fine cracks in the welded joints, thus leading to violation of their hydraulic tightness and decrease in service life.

Technologies were developed for EBW with modification of metal of the welded joints to improve their performance. Offered was the design of insert modifiers which does not violate the quality of assembly of bit components, has no effect on accuracy of operation of the seam tracking system and, at the same time, provides formation of the welds containing no solidification cracks. The most optimal material for modification of the welds on the rolling drill bits was stainless austenitic steel 10Kh18N10T with a thickness of 0.2 mm, and for the welds on the diamond bits – zirconium foil inserts, also 0.2 mm thick. Width and length of the plate modifiers depends on the type of the bits welded and may vary from 15 to 20 mm in width and from 45 to 70 mm in length.

The research and development work was performed to design the specialised fixture to fit the units for EBW of drill bits in accordance with the developed technologies. Software for EBW of the bits with modification of the welds was worked out.

Comprehensive investigations of the quality and properties of the EB welded joints on the drill bits, including the use of modification elements, were conducted to improve strength and prevent solidification cracking of the joints, tensile strength of the joints being 95–98 % of that of the base metal. All technological and design developments were verified in manufacture of an experimental batch of the full-scale parts, which were passed to tests to be conducted in real service environment of the drill bits.